# The role of *Bartonella* adhesin A and fibronectin in adherence of *Bartonella henselae* to endothelial cells

Dissertation
zur Erlangung des Doktorgrades
der Naturwissenschaften

vorgelegt beim Fachbereich Biowissenschaften
der Johann Wolfgang Goethe-Universität
in Frankfurt am Main

von
**Diana Jaqueline Vaca Llerena**
aus Quito, Ecuador

Frankfurt am Main, 2023

D 30

Vom Fachbereich Biowissenschaften der

**Johann Wolfgang Goethe - Universität als Dissertation angenommen.**

Dekan: Prof. Dr. Sven Klimpel

Gutachter: Prof. Dr. Volker Müller

Prof. Dr. Volkhard Kempf

Datum der Disputation:

# TABLE OF CONTENTS

## LIST OF FIGURES

## LIST OF TABLES

## ABBREVIATIONS

| | |
|---|---|
| µg | microgram |
| µm | micrometre |
| µM | micromolar |
| °C | degree Celsius |
| AGC | automatic gain control |
| ATP | adenosine 5′-triphosphate |
| BadA | *Bartonella* adhesin A |
| BI | binding inhibitor |
| BSA | bovine serum albumin |
| cDNA | complementary DNA |
| $CO_2$ | carbon dioxide |
| cPCR | conventional PCR |
| CRISPR | Clustered Regularly Interspaced Short Palindromic Repeats |
| CSD | cat scratch disease |
| Da | dalton |
| DAPI | 4′,6-diamidino-2-phenylindole |
| DDA | data dependent adquisition |
| DIA | data independent adquisition |
| DMSO | dimethyl sulfoxide |
| DNA | deoxyribonucleic acid |
| DSS | disuccinimidylsuberate |
| DTT | dithiothreitol |
| EC | endothelial cell |
| ECGM | endothelial cell growth medium |
| ELISA | Enzyme-Linked-Immunosorbent-Assay |
| FCS | fetal calf serum |
| FDR | false discovery rate |
| Fn | fibronectin |
| g | gravity |
| gRNA | guide RNA |
| GAPDH | glyceraldehyde-3-phosphate dehydrogenase |
| h | hour |
| HCD | higher-energy collisional-induced dissociation |
| HCl | hydrochloric acid |
| HEK 293T | human embryonic kidney cell line |
| Hep | heparin domain in fibronectin |
| HMEC-1 | dermal microvascular endothelial cell |
| HRP | horseradish peroxidase |
| HUVEC | human umbilical vein endothelial cells |
| IFM | immunofluorescence microscopy |
| IEM | immunoelectron microscopy |

| | |
|---|---|
| M | molar |
| ml | millilitre |
| MOI | multiplicity of infection |
| MS | mass spectrometry |
| MS1 | mass spectrometric analysis of non-fragmented precursor ions |
| MS/MS | mass spectrometric analysis of fragment ions generated by gas-phase dissociation of precursor ions |
| ng | nanogram |
| nm | nanometer |
| min | minute |
| qPCR | quantitative PCR |
| OD | optical density |
| PCR | polymerase chain reaction |
| RNA | ribonucleic acid |
| ppm | parts per million |
| RPM | revolutions per minute |
| RT | room temperature |
| s | second |
| SDS PAGE | sodium dodecyl sulfate polyacrylamide gel electrophoresis |
| TAE | tris-acetate-EDTA |
| TCEP | tris(2-carboxyethyl) phosphine hydrochloride |
| TMB | 3,3',5,5'-tetramethylbenzidine |
| TRITC | tetramethylrhodamine |
| U | unit |
| WB | Western blotting |
| WT | wildtype |
| XL-MS | crosslinking mass spectrometry |
| XLs | crosslinks |

# 1 INTRODUCTION

Adhesion to the host cell is the most decisive step in bacterial infections. The bacterial capacity to adhere to host cells and avoid clearance by the host defence systems (e.g. via peristalsis, fluid flow or innate immunity) is a determinant for successful colonisation. Adhesion to the host cells enables the translocation of pathogenic bacteria across cellular and tissue barriers by generating a stable starting point on which the microorganism can persist, replicate, internalise into cellular compartments, and express virulence factors enabling subsequent steps of infections.

On the pathogen's side, a group of proteins exposed on the surface called “adhesins” are the molecular basis for bacterial adherence to host molecules. From the host side, the extracellular matrix (ECM), a widely distributed proteinaceous tissue component, has been postulated as a potential target for bacterial adhesion [1]. Adhesins with affinities to ECM proteins have been described as key factors for host cell adherence in Gram-positive and Gram-negative bacteria [1, 2]. In Gram-negative bacteria, the family of trimeric autotransporter adhesins (TAAs) are important virulence factors. The prototypic TAA *Bartonella* adhesin A (BadA) from human pathogenic *Bartonella henselae* is a crucial determinant for bacterial adherence to endothelial cells (ECs) and ECM proteins such as fibronectin (Fn). The relevance of the interaction between TAAs and ECM proteins in the context of bacterial adhesion has not been clarified. Still, it might represent a critical step for the adherence of human-pathogenic Gram-negative bacteria to the host cells.

Describing the mechanisms of bacterial host cell adhesion is a clue for preventing infections. Identifying the molecular mechanisms involved in bacterial adherence might provide a basis for developing novel antivirulence therapeutic alternatives for drug-resistant bacteria.

## 1.1 *Bartonella henselae*

### 1.1.1 The genus *Bartonella*

The genus *Bartonella* includes about 45 species of facultative intracellular Gram-negative bacteria [3]. The clinically most important species are *B. bacilliformis*, causative of "Carrion´s disease"; the zoonotic cat-transmitted species *B. henselae*, causative of "cat scratch disease" (CSD); and the human-restricted *B. quintana,* causative of "trench fever". *Bartonella* spp. share a unique infection strategy targeting persistence in an intraerythrocytic niche, thus enabling continuous transmission by bloodsucking arthropods. Some *Bartonella* spp. are geographically restrained due to the vector distribution, as in the case of *B. bacilliformis* transmitted by the sandfly *Lutzomyia verrucarum*, only described in South America, contrary to the worldwide dissemination of *B. henselae* and *B. quintana* vectors, the cat flea *Ctenocephalides felis* and human lice *Pediculus humanus corporis*, respectively [4].

### 1.1.2 Life cycle of *Bartonella*

The two primary habitats used by *B. henselae* are the gut of obligate bloodsucking arthropod vectors (i.e. fleas) and the bloodstream of mammalian hosts, where they induce acute or persistent intravascular infections [3]. The cat is the natural reservoir host of *B. henselae*, causing asymptomatic bacteraemia [5]. Cat-to-cat transmission occurs mainly by cat fleas [6]. Human transmission takes place indirectly by the cat flea or directly by a cat scratch or bite [7]. Once in humans, the incidental host species, the pathogen can cause a variety of clinical manifestations; the individual's immune status is critical for disease progression in *B. henselae* infection [8].

### 1.1.3 Disease manifestations and diagnosis

In immunocompetent individuals, *B. henselae* infection manifests as CSD with lymphadenopathy (i.e. inflammatory enlarged lymph nodes) accompanied by prolonged fever. *B. henselae* infection induces a self-limiting response, with spontaneous regression usually after one to two months. If complications occur, antibiotic treatment can be given,

e.g. with azithromycin for five days [8]. Severe manifestations of *B. henselae* infection occur primarily in patients with impaired cellular immunity, likely due to the ability of the pathogen to persist intracellularly [4, 9]. In immunocompromised individuals (e.g. HIV-positive patients), infections can manifest as bacillary angiomatosis with vasoproliferative skin lesions or bacillary peliosis with vascular proliferation in inner organs (e.g. liver or spleen) resulting in the formation of blood-filled cysts [10].

Clinical laboratory diagnosis of *B. henselae* infections is based on serology and PCR. Immunofluorescence assays and ELISA-based approaches have become the standard method due to their reproducibility and improved sensitivity [11, 12]. Moreover, PCR-based detection has proven high specificity for the detection of *B. henselae* infections (e.g. via amplification of 16S-rRNA and riboflavin synthase *ribC*) [13, 14]. Pathogen isolation from blood and tissue specimens (e.g. from lymph nodes) is not considered an effective and reproducible diagnostic method due to the fastidious and slow-growing nature of the bacteria (doubling time ~24 h), and the relatively low bacteraemia level in patients [15, 16].

### 1.1.4 Infection biology of *B. henselae*

Limited *in vivo* evidence is available to draw the precise picture of the infection process from the inoculation of *B. henselae* into the skin (e.g. from the faeces of arthropod vectors) and the bacteremic stage of the infection. *B. henselae* infection strategy involves complex interactions between nucleated host cells (e.g. ECs, epithelial cells) and possibly erythrocytes (mainly described in cats). Migratory cells may play a role in establishing and disseminating *B. henselae* infections from typical intradermal inoculation to other organs. The frequent affliction of lymph nodes during *B. henselae* infections may indicate that such transport might occur via the lymphatic system, using lymphocytes or mononuclear phagocytes as vehicles for bacterial transport [17]. Therefore, after inoculation, *B. henselae* could target these migratory cells to reach locations where they would persist and multiply, most probably in the microvasculature. Clinical evidence and *in vitro* assays suggest that ECs are the primary niche of *B. henselae,* as vascular proliferative disorders are found in association with proliferating ECs [4].

### 1.1.5 Interaction with ECs and angiogeneic reprogramming

The interaction of *B. henselae* with ECs reveals a set of distinct mechanisms which may act synergistically: cellular invasion, angiogenic reprogramming, apoptosis inhibition, cellular proliferation, and mitogenic stimulation. Several virulence factors of *B. henselae*, such as the TAA or the VirB/D4 type IV secretion system (T4SS), have been shown to participate in the interaction with ECs, not only contributing to specific steps of infection but also co-manipulating a set of cellular responses. The *B. henselae*-triggered proliferation of the endothelia and interference with host cell metabolism has been speculated as bacterial promotion of its own niche: the ECs [18, 19].

The initial step in the infection of ECs represents bacterial adherence. Such interactions involve bacterial surface proteins (**Table 1**) mediating contact with EC surfaces, of which the TAA from *B. henselae*, BadA, has been described as one of the principal contributors [20]. Subsequently, cellular invasion of *B. henselae* into ECs occurs using two mutually exclusive pathways, either as single bacteria using a zipper-like mechanism in *Bartonella*-containing vacuoles (BCVs) [18] or in the form of large aggregates or invasome [21].

The angiogenic reprogramming of host cells seems to be promoted by BadA and VirB/D4 T4SS interaction. BadA induces the activation of hypoxia-inducible factor 1 (HIF-1) and secretion of angiogenic cytokines (e.g. vascular endothelial growth factor, VEGF) [20, 22], while *Bartonella* effector proteins (Beps), secreted by the VirB/D4 T4SS, mediate a proinflammatory host cell response, cytoskeletal rearrangements, and the inhibition of apoptosis [23]. Activation of HIF-1 and secretion of VEGF have been observed *in vitro* from cultured host cells with *B. henselae* and *in vivo* from patient's bacillary angiomatosis tissue lesions [20, 22, 24].

**Table 1.** Adhesins from *B. henselae* and interaction with ECs

| Protein | Accession no. (NCBI) | Functions | Reference |
|---|---|---|---|
| BadA | AAT69970/ KY88514 | adhesin, induces auto-aggregation and biofilm formation, binds multiple ECM components, mediates cell adhesion, required for colonisation of ECs | [20, 25] |
| Omps (28, 32, 52, 58 kDa) | - | putative adhesins, interaction with ECs | [26] |
| Omp43 | AAF27661 | adhesin, recombinant Omp43 binds ECs and Fn | [26, 27] |
| Omp89 | AF461795 | adhesin, recombinant Omp89 binds Fn | [27] |
| Pap31 (HpbA) | JC6528 | adhesin, hemin binding protein, recombinant Pap31 binds ECs and Fn | [27–29] |

### 1.2 Trimeric Autotransporter Adhesins

The group of Trimeric Autotransporter Adhesins (TAAs) are a class of adhesins widely represented in α-, β-, and γ-proteobacteria, with similar roles in pathogenesis affecting a broad range of hosts. All the described TAAs have been functionally associated with adhesion roles [30]. TAAs form a characteristic, trimeric, lollipop-like surface structure and share a modular and repetitive domain organisation. Among the TAA family, *Yersinia* adhesin A (YadA) from *Y. enterocolitica* is the best-characterised adhesin [31]. Other representatives of the TAA family include *Acinetobacter* trimeric autotransporter (Ata), from *A. baumannii* [32]; BadA from *B. henselae* [20]*; Haemophilus influenzae* adhesin (Hia) and *Haemophilus* adhesin A (HadA) from *H. influenzae* [33, 34]; *Neisseria* adhesin A (NadA) from *N. meningitidis*, an antigen present in the meningococcal vaccine [35]; ubiquitous surface protein A1 and A2 (UspA1, UspA2) from *Moraxella catarrhalis* [36]; and variably expressed outer membrane proteins (Vomps A-D) from *B. quintana* [37].

### 1.2.1 Architecture, domain organisation and structure of TAAs

These obligate homotrimeric proteins show a conserved "membrane anchor domain" at the C-terminus and a modular "passenger domain" at the N-terminus, which includes an often highly repetitive "neck/stalk domain" and a "head domain". TAAs are secreted via the type Vc pathway: the C-terminal membrane anchor domain interacts with the β-barrel assembly machinery (BAM) to be inserted into the outer membrane, and the N-terminal long passenger domain is translocated through the barrel guided by a signal peptide on the bacterial surface [38, 39].

The membrane anchor is the only homologous domain throughout TAAs and, as such, defines the family. It contains four heptads of a coiled-coil followed by four transmembrane β-strands, which presumably assemble into a 12-stranded β-barrel in the trimeric conformation [36]. The stalk of TAAs is rich in heptad coiled coils with polar interactions stabilizing the three α-helices. The neck is highly conserved in TAAs and structurally is composed of two β-strands which function as an adaptor between the head and stalk. The head domain is a trimer of β-helices forming a globular structure [40]. The neck/stalk domain is extremely variable in length and acts as a spacer to expose the head away from the bacterial cell surface and towards its eukaryotic binding partners [30].

### 1.2.2 *Bartonella* adhesin A

*Bartonella* adhesin A (BadA) is a prototypic and one of the largest described TAA. By the use of long-read sequencing technologies, it was recently identified that *badA* gene holds about 11,922 bp, resulting in a molecule of 417 kDa per monomer and BadA fibre lengths of about 243 nm long [41]. The expression of *badA* is crucial for *B. henselae* adhesion to ECs and ECM host components (i.e. collagen I, III and IV, laminin and Fn) and a critical factor for the induction of a proangiogenic host cell response in diverse host cells [20].

The genetic modifications driving the expression of *badA* seem to be influenced by the extracellular environment correlating with frequently alternating host conditions (e.g. temperature, iron source, and pH) [42]. Phase variation in *badA* expression has been

observed during *in vitro* growth of *B. henselae* [43]. The mechanism of gene regulation for this phase variation is still unknown, but it is speculated that due to the enormous size of *badA*, the expression should be a highly energy-consuming process; therefore, loss of *badA* expression might be promoted without ecological pressure [44]. Until now, no correlation between the expression of *badA* and the source of the pathogen (human or cat host) or geographic region of first isolation has been observed. However, it is known that recombination events or single-base deletions or insertions affect *bada* expression [41].

BadA is a prominent protein present in the outer membrane of *B. henselae*. Structurally, BadA shows a modular arrangement. N-terminally, BadA exhibits a signal sequence followed by the head domain composed of three distinct subdomains: a YadA-like head, a neck, and a Hia-like head [45]. The central part of BadA, or stalk/neck region, is a long and highly repetitive structure and consists of 30 stalk motifs of coiled-coil segments separated by neck sequences [41]. The stalk/neck domain is elemental to the great length of BadA. C-terminally, there is a membrane anchor domain, homologous to YadA, with four transmembrane β-helices (**Figure 1**).

The biological function of each BadA domain has been elucidated in detail. The head is primarily responsible for bacterial autoagglutination, adhesion to collagen and activation of HIF-1 in host cells [46]. Sequence analyses of different *B. henselae* isolates showed a high degree of similarity of the head within the different strains [44]. The long stalk/neck domains have been primarily associated with Fn binding [47]. *B. henselae* isolates have demonstrated different *badA* gene sizes correlating with length variation in the stalk/neck sequences [41, 44]. It was postulated that a shuffling mechanism might use the extensive number of repeats in *badA* gene as a “toolbox” for TAA evolution [41, 48]. Finally, the membrane anchor domain is responsible for the protein´s autotransporter activity and is highly conserved among different *B. henselae* isolates [40, 44].

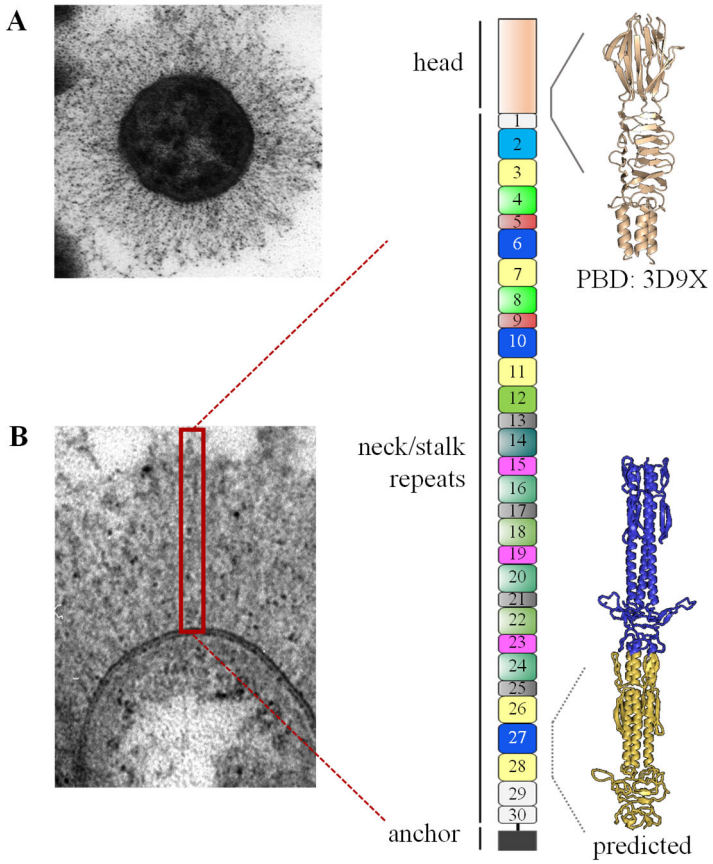


**Figure 1. *Bartonella* adhesin A (BadA) from *B. henselae*.** **(A)** Electron microscopy from *B henselae,* the abundant surface presence of BadA is visible in the image (length per fibre ~240nm) [49]. **(B)** Enlarged electron microscopy from *B. henselae*, the trimeric BadA fibres are displayed in a rectangle. Next to it, the monomeric representation of BadA with each region is depicted. N-terminally, the head domain is shown as the most exposed region. The next/stalk repeats region is the longest part of BadA, including 30 highly repetitive domains. Similar domains are colour coded. At the C-terminus, the anchor domain is the most conserved region among all trimeric autotransporter adhesins (TAAs) and is anchored to the outer membrane. The crystal structure for a portion of the head domain (PBD: 3D9X) [45] is the only part of BadA that has been resolved; the structure for domains 27 and 28 was predicted using AlphaFold2 [50].

### 1.3 Extracellular matrix proteins

The extracellular matrix (ECM) is in charge of the structural support and scaffolding of cellular barriers and the regulation of physiological processes and cellular signalling. The ECM is a highly dynamic structure comprising proteoglycans and glycoproteins secreted locally and brought together into an organised network. The proteoglycans are composed of glycosaminoglycan (GAG) chains linked to a specific core protein and fill most of the

extracellular interstitial space within the tissue [51]. The main fibrous proteins forming parts of the ECM are collagen, elastin, Fn, laminin, and vitronectin [51].

### 1.3.1 Collagens

Collagens are crucial for maintaining tissue structure, cell adhesion, embryonic development, and many other functions. A total of 28 collagen types have been described and are distributed in body tissue and organs [52]. Collagens are secreted by fibroblasts and some epithelial cells, indicating a broad distribution of the molecule in the human body. The collagen family is present in the skin (collagen type I in association with collagen types III, V, VII, XII, XIII and XIV), in bones (collagen type I in association with collagen types XXIV), in cartilage (collagen type II in association with IX, X, XI and XIII), and in basement membranes (collagen type IV in association with collagen type XVIII) [52]. Structurally, collagen consists of α-chains and the variability in the number of α-chains present in the molecule defines the different collagen types distributed in the human body. Despite the presence of multiple isoforms, all the different types of collagen share common structures [53, 54].

### 1.3.2 Laminins

Laminins are in charge of maintaining the structural scaffold, cell migration, and signalling. A total of 15 isoforms have been described and are distributed in basement membranes, connective tissue, cell surface, skin, and blood vessels [55]. Structurally, laminins are heterotrimeric molecules consisting of α-(400 kDa), β-(200 kDa), and γ-(200 kDa) chains, independently expressed and interconnected via disulphide bonds at their C-terminal regions. Laminin trimerises before its extracellular secretion and then forms networks cooperating with other ECM proteins [56, 57].

### 1.3.3 Fibronectin

Fibronectin (Fn) is present in body fluids and on cell surfaces with the principal function of connecting the cell to the exterior ECM. Fn is encoded by an 8-kb mRNA yielding Fn subunits that range in size from 230–270 kDa, depending on alternative splicing [58]. Two major forms of Fn are present in the body: a soluble or globular form (plasma Fn) and an insoluble or fibrillar form (cellular Fn). Plasma Fn is produced by hepatocytes and is present in blood, saliva, and other fluids, playing important roles in blood clotting [59]. Cellular Fn is secreted by fibroblasts and ECs and is incorporated on the cell surface into a fibrillar-type matrix [60]. Structurally, Fn is a heterodimer composed of two splice variants of 230 and 270 kDa connected by a C-terminal disulphide bond. In general, the Fn molecule is organised into 12 type I repeats (FnI), two type II repeats (FnII), and a variable number (between 16 and 18) of type III repeats (FnIII) (**Figure 2**). Differences in splicing variants modify the number of modules in FnIII [58, 60, 61]. Cellular Fn can include the EIIIA and EIIIB domains, which are not present in plasma Fn [62, 63]. Domains in Fn interact with other ECM proteins, cell surface receptors, GAGs, and other Fn molecules. This combination of domains allows Fn to bind simultaneously to cells and molecules within the surrounding matrix

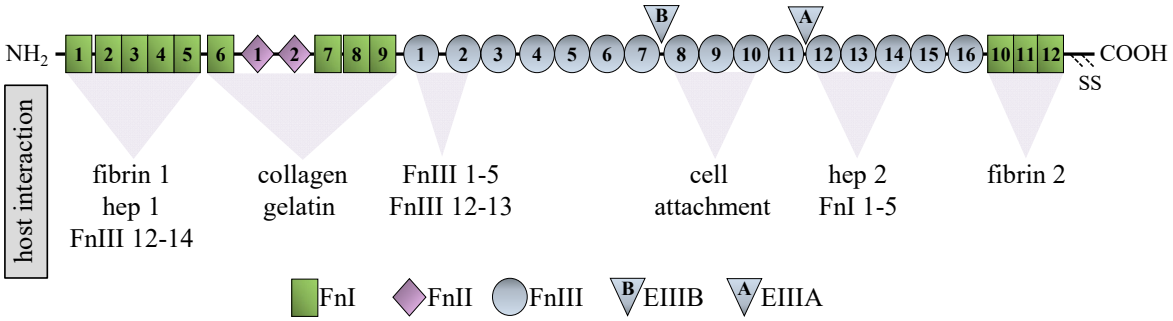


**Figure 2. Schematic representation of fibronectin (Fn) molecule (monomer).** Fn is a heterodimer composed of two splice variants connected by a C-terminal disulfide bond. The molecule contains Fn type I repeats (12), Fn type II repeats (2), and Fn type III repeats (between 16 and 18). In cellular Fn, EIIIA (A) and EIIIB (B) domains are present due to alternative splicing. Fn interactions with other host-cell components and with Fn molecules are depicted. Figure adapted from [64].

#### 1.3.3.1 Interaction of Fn with other ECM components

Fn is intimately involved in directing the organisation of the interstitial ECM and has a crucial role in mediating cell attachment and function. Fn mediates important human protein-protein and protein–proteoglycans interactions during the formation of the ECM [2]. Fn has several binding sites to other Fn dimers, collagen, heparin/heparan sulfate, fibril, and cell-surface integrin receptors [61] (**Figure 2**). The FnI 1-5 components are the most conserved Fn region across vertebrates. This domain is required for the proper assembly of the ECM and binds to heparin (lower affinity) and fibrin (stronger affinity). The interaction between Fn and fibrin is important for cell adhesion, cell migration into fibrin clots, and for macrophage removal from circulation after a trauma or in the case of inflammation. Another region consisting of FnI 6, FnII 1–2, and FnI 7–9, promotes collagen binding. This interaction has been suggested to occur either to mediate cell adhesion or to favour clearance of denatured collagenous material from blood and tissue. The FnIII domain mediates cell attachment via integrins (cell-surface heterodimeric receptors) in the RGD loop located at the FnIII 8–10 area. The interaction via integrins allows the linkage of ECM with the intracellular cytoskeleton. The FnIII 12–14 modules contain the strongest interaction site necessary for heparin binding. It has been proposed that this region facilitates the formation of protein interactions for insoluble fibril assembly. A second fibrin-binding site is located at the C-terminal FnI 10–12 modules [61, 65, 66].

#### 1.3.3.2 Fn matrix assembly

In solution, Fn is present as a compact dimer that does not form fibrils *per se*, even at extremely high concentrations. This is important, as uncontrolled fibril formation in the blood would have life-threatening consequences, e.g. clot formation [66]. Intramolecular self-interaction sites in the molecule are responsible for Fn conformation in soluble form. Interactions between FnIII 2-3 and FnIII 12-14 stabilise the compact conformation [67]. These regions overlap with Fn-binding sites, which suggests that disrupting these interactions to extend compact Fn dimers frees these sites to participate in intermolecular interactions. Other intramolecular interactions might, however, also contribute to the compact conformation [60].

The assembly of Fn into fibrils is an essential cell-mediated process [66]. Integrins tether Fn dimers to initiate Fn-Fn interactions mediated by the N-terminal assembly domain. Conformational changes expose additional Fn-binding sites to promote further Fn interactions, associations between fibrils, and matrix insolubility. For fibrillogenesis, integrin α5β1 is the only cellular receptor able to bind native soluble Fn, and it is known as the classical "Fn receptor" [68]. This receptor recognises the Arg-Gly-Asp (RGD) motif in FnIII 10 assisted by the neighbouring sites in FnIII 9, enhancing the binding affinity. Downstream signalling leads to clustering and changes in the conformation of Fn. First, end-to-end association of Fn dimers is mediated by the N-terminal 70 kDa domain (FnI 1-9). Next, cryptic self-association sites in the Fn molecule are exposed and accessible for interacting with other Fn binding sites (e.g. FnI 1-5, FnIII 1-2, FnIII 2-3, and FnIII 12-14). These intramolecular interactions form Fn fibrils and are converted into a detergent-insoluble matrix. Insolubility is a critical property to provide tissues with stability, rigidity and shape [60, 69].

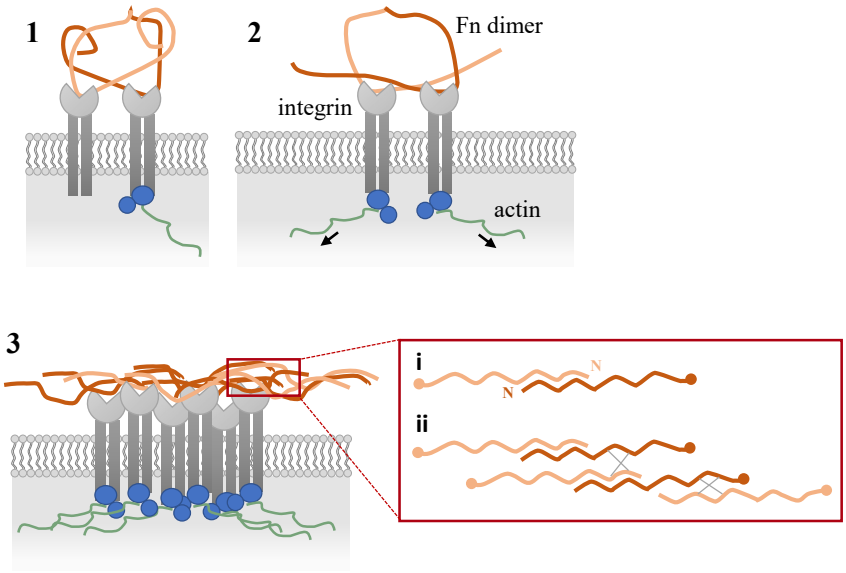


**Figure 3. Steps in Fn matrix assembly**. **(1)** Compact soluble Fn binds integrin (grey), Fn heterodimer is shown in shades of orange. **(2)** Intracellular proteins (blue) are recruited to the cytoplasmic domains of integrins and are connected to the actin cytoskeleton (green). Cytoskeletal connections increase cell contractility (arrows), which induces conformational changes in Fn. **(3)** These events trigger the formation of a stable insoluble fibrillar matrix. The red box shows interactions between single subunits of Fn dimers. Fibrils are formed through **(i)** N-terminus – N-terminus association of Fn dimers, followed by **(ii)** lateral associations between fibrils that involve the other Fn-binding sites in FnIII 1−2, FnIII 4−5, and FnIII 12−14. Interactions within fibrils are depicted with X. Figure adapted from [66].

### 1.4 Bacterial adhesins and ECM proteins interaction

Adhesion to the host cells facilitates bacterial persistence, replication and internalisation into host cellular compartments enabling subsequent steps of infections. On the bacterial side, adhesins mediate host-cell adhesion and interaction with ECM proteins. Adhesins are involved in biofilm formation and have proven to undermine host responses for pathogen clearance [70, 71]. On the host side, targeting the ECM has been postulated as one of the major strategies for bacterial colonisation and host invasion [2, 64, 72, 73].

Adhesins interacting with ECM proteins in Gram-positive bacteria are classified in covalently surface-anchored proteins known as MSCRAMMs (microbial surface components recognising adhesive matrix molecules) and non-covalent surface-associated proteins (e.g, proteins of the secretable expanded repertoire adhesive molecules, SERAM) [74]. The adhesin repertoire in Gram-negative bacteria includes pili and non-pilus structures such as TAAs, other secretion systems as monomeric autotransporter adhesins, and surface-expose lipoproteins N-terminally linked to the membrane by fatty acids [74] (**Table 2**).

**Table 2.** Adhesins from selected bacterial species and interactions with ECM proteins. Adapted from [64].

| Bacterial species | Adhesin | Class of adhesin | Binding to ECM | Reference |
|---|---|---|---|---|
| *Acinetobacter baumannii* | Ata | TAA | collagen I, III, IV, V<br>Fn (lower binding) | [32, 75] |
| | | | Ln | [32] |
| | OmpA (Omp38) | porin | Fn | [76] |
| | Omp33 (Omp33-36) | porin | Fn | [76, 77] |
| *Bartonella henselae* | BadA | TAA | Fn<br>collagen I, III, IV<br>Ln | [20, 78] |

**Table 2.** Adhesins from selected bacterial species and interactions with ECM proteins. Adapted from [64] (*continuation*).

| Bacterial species | Adhesin | Class of adhesin | Binding to ECM | Reference |
|---|---|---|---|---|
| *Bartonella henselae* (continuation) | Pap31 | porin | Fn | [28] |
| | Omp43 | porin | Fn | [27] |
| | Omp89 | porin | Fn | |
| *Borrelia burgdorferi* | BBK32 | surface-exposed lipoprotein | Fn | [79, 80] |
| | BBA33 | surface-exposed lipoprotein | collagen IV, VI | [81] |
| | BB0347 | surface-exposed protein | Fn | [82] |
| | BmpA-D | surface-exposed lipoprotein | Ln | [83] |
| | CspA | surface-exposed lipoprotein | collagen I, III, IV<br>Fn<br>Ln | [84] |
| | CspZ | surface-exposed lipoprotein | Fn<br>Ln | |
| | ErpX | surface-exposed lipoprotein | Ln | [85, 86] |
| | RevA | surface-exposed protein | Fn | [85, 87] |
| | RevB | surface-exposed protein | Fn | [85, 88] |
| *Staphylococcus aureus* | Cna | MSCRAMMs | collagen | [89] |
| | Eap | SERAM | collagen I, IV, VI<br>Fn | [90] |

**Table 2.** Adhesins from selected bacterial species and interactions with ECM proteins. Adapted from [64] (*continuation*).

| Bacterial species | Adhesin | Class of adhesin | Binding to ECM | Reference |
|---|---|---|---|---|
| *Staphylococcus aureus* (continuation) | Emp | SERAM | collagen I<br>Fn | [91] |
| | FnBPA | MSCRAMMs | Fn<br>fibrinogen<br>elastin | [92] |
| | FnBPB | MSCRAMMs | Fn,<br>elastin | |

The presence of bacterial adhesins binding Fn (Fn-binding proteins, FnBPs) has been demonstrated by the inactivation of the respective FnBP gene and the observation of reduced bacterial adhesive characteristics. A canonical binding site for adhesins in the Fn molecule is located in the FnI 2-5 region [72, 93], but other non-canonical bacterial binding sites have also been described (**Figure 4**). The molecular interactions and functional consequences of FnBPs in Gram-positive bacteria have been extensively studied in several bacterial species, particularly for *S. aureus* (85–87).

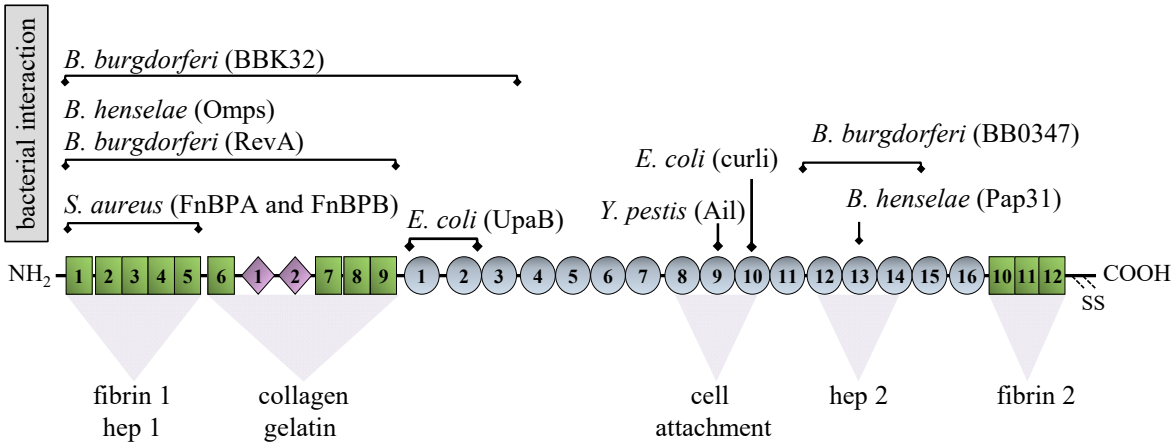


**Figure 4. Schematic representation of reported bacterial interaction with specific domains of Fn.** Fn domains are depicted according to their affinities with other host-cell components: fibrin, heparin [hep], collagen/gelatin, and cell attachment. The region of Fn interaction with the bacteria (*B. burgdorferi*, *B. henselae*, *Escherichia coli*, *Y. pestis* and *S. aureus*) and their specific adhesin (shown in parenthesis) are depicted in the upper part of the figure. Figure adapted from [64].

The presence of collagen- and laminin-binding proteins in pathogenic bacteria is presumed to have evolved because of the broad distribution of this ECM protein in organs and tissue. The majority of adhesin–collagen interactions observed in bacteria have been associated with collagen type I, III, IV, and V [1]. Laminin-binding adhesins have been demonstrated in many pathogenic agents with affinity to the respiratory tract and central nervous system, such as *E. coli*, *H. influenzae*, *Klebsiella pneumoniae, Mycobacterium tuberculosis, N. meningitidis*, *Streptococcus pneumoniae*, among others [94–99].

## 1.5 Aim of the study

Adhesins are the basis for bacterial adherence to host structures. *Bartonella* adhesin A (BadA) is a key factor for *B. henselae* interaction with extracellular matrix proteins such as fibronectin (Fn). This research aimed to dissect BadA-Fn interaction and to evaluate the role of Fn as a host target for bacterial adherence. The following aspects should be addressed:

1. Apart from BadA, outer membrane proteins (OMPs) from *B. henselae* have reported Fn binding affinity, raising questions about the individual role of BadA in Fn binding. As whole cells (WT and BadA deficient bacteria) have been used to study Fn interaction, it should be first established that these OMPs are present in the strains used for this research and that BadA presence is crucial for Fn binding. This should be evaluated by protein abundance quantification and binding assays.
2. The interaction with plasma or cellular Fn has been described for many bacterial adhesins, with preferable adhesion to one or the other. BadA interaction with plasma Fn has been identified; however, information about BadA interaction with cellular Fn should be evaluated using binding assays and mass spectrometry.
3. The neck/stalk region of BadA was described as important for Fn binding. The molecular interactions and Fn regions supporting bacterial binding should be clarified by combining mass spectrometry and binding assays.
4. The intervention of adhesins and cell receptors supports bacterial adherence to host cells. In this context, the specific role of Fn as the endothelial cell (EC) target for bacterial adherence should be clarified. This should be done by generating an EC model using CRISPR Cas to be applied in infection experiments for loss-of-function assays.
5. Many bacterial adhesins from pathogenic bacteria have reported binding affinities to Fn. The role of Fn in bacterial adhesion as a general principle in infections should be tested using the generated ECs in infection experiments with *Acinetobacter baumannii*, *B. henselae*, *Borrelia burgdorferi*, and *Staphylococcus aureus*.

Results from these experiments should reveal the molecular mechanisms underlying BadA-Fn interactions and, more generally, to which extent bacterial adherence to Fn represents a conserved biological principle of bacteria-host cell interactions.

# 2 MATERIAL AND METHODS

## 2.1 Bacterial strains and culture

### 2.1.1 Bacterial strains

The bacterial strains used in this research are listed in **Table 3**.

**Table 3.** List of bacterial strains.

| Bacteria | Description | References/ provider |
|---|---|---|
| *B. henselae* wildtype (WT) | Patient isolate from Marseille, early passage | [100] |
| *B. henselae* BadA$^-$ | *B. henselae* WT, EZ::TN<KAN2>-transposon mutant, BadA-negative, Km$^r$ | [20] |
| **Other bacterial genera** | | |
| *A. baumannii* 1372 | carbapenem-resistant clinical isolate (sequence type 2) | * |
| *B. burgdorferi* B31-e2 | derivative of *B. burgdorferi* type strain B31 | [101] |
| *S. aureus* 8325-4 | laboratory strain, derivative of 8325 strain and parent strain of SH1000 | [102] |
| *E. coli* NEB 5 alpha | competent (high efficiency) | C2987H, NEB |

* kindly provided by Dr. Stephan Göttig (Johann Wolfgang Goethe University Frankfurt, Germany)

### 2.1.2 Bacterial culture

The media used for bacterial cultures are given in **Table 4**. *B. henselae* WT and BadA$^-$ were cultured for three days at 37 °C, 5% $CO_2$. *B. henselae* strains were grown in *Bartonella* liquid (BaLi) medium [103], supplemented with 2.5% Fn-depleted fetal calf serum (FCS) (see **Section 2.9.1**), and constant shaking at 120 RPM. *B. henselae* strains were grown on a

solid medium using Columbia blood agar plates supplemented with human blood (hCBA). For *B. henselae* BadA$^-$ strain culture, 30 µg/ml kanamycin was supplemented to the medium. *E. coli* were cultured on solid or liquid LB (180 RPM) at 37 °C overnight. *A. baumannii* and *S. aureus* were cultured on CBA plates overnight at 37 °C. A colony was selected for an overnight culture in liquid LB at 37°C, 180 RPM. All bacterial centrifugation steps were performed at 3,800 g for 10 min at 4 °C. *B. burgdorferi* was cultured in Barbour-Stoenner-Kelly medium by Prof. Peter Kraiczy (Johann Wolfgang Goethe University Frankfurt, Germany) and provided fresh for the experiments.

**Table 4**. List of media used for bacterial culture.

| **Medium** | **Description** |
|---|---|
| liquid LB | 25 g LB base<br>to 1,000 ml dH2O<br>autoclave at 121°C for 15 min |
| solid LB | 40 g LB agar base<br>to 1,000 ml dH2O<br>autoclave at 121°C for 15 min |
| bacterial freezing medium | 20% glycerol in LB-medium<br>autoclave at 121°C for 15 min |
| hCBA plates | 42.5 g Columbia agar base<br>950 ml dH2O<br>autoclave at 121°C for 15 min<br>50 ml defibrinated human donor blood |
| BaLi | 24.45 g Schneider's *Drosophila* medium in 850 ml H2O<br>50 g sucrose<br>0.79 g CaCl2 x 2H2O in 10 ml<br>0.4 g NaHCO3 in 10 ml<br>13 ml 1M NaOH<br>to 1,000 ml dH2O, pH 6.5<br>filter sterilize |
| 2xYT-Medium | 16 g tryptone<br>10 g yeast extract<br>5 g NaCl<br>to 1,000 ml dH2O, pH 7.0<br>autoclave at 121°C for 15 min |

### 2.1.3 Quantification of bacteria

Optical density 600 ($OD_{600}$) was used to estimate the density of bacterial cells using the factor 1 $OD_{600} = 5x10^8$ cell/ml. The colony-forming units (CFU) method was used to estimate the number of viable bacterial cells. Bacteria were grown in CBA plates.

### 2.1.4 Cryopreservation of bacteria

Bacteria in liquid media were centrifuged and resuspended to a known $OD_{600}$ using ice-cold bacterial freezing medium. Bacterial cells were aliquoted in cryogenic storage vials and stored for long-term preservation at -80 °C. CFU was performed for each bacterial stock.

## 2.2 Human cells and culture

### 2.2.1 Human cells

The human cells used in this research are listed in **Table 5**.

**Table 5.** List of human cells.

| Cell type | Characteristics | Provider |
|---|---|---|
| HUVEC | primary human umbilical vein endothelial cells isolated from the vein of the umbilical cord of pooled or individual donors (ethical approval: 4/12, University Hospital Frankfurt am Main, Germany). | C-12203, PromoCell/ *in house* isolated from single donor |
| HMEC-1 | dermal microvascular endothelial cell. Isolated from human foreskins and transfected with pSVT vector. | 98247, CDC, USA |
| HEK 293T | highly transfectable subclone of transformed human embryonic kidney cell line (Lenti-X™ 293T) | 632180, Takara |

### 2.2.2 Human cells culture

The media used for human cell cultures are listed in **Table 6**. For HUVEC and HMEC-1 cultures, the respective media and supplement mix was used with 10% FCS and 1% penicillin-streptomycin. The flasks, dishes, and plates used for the culture of both cell types were precoated with 1:40 collagen G before use. For HEK 293T culture, DMEM with glutamax was used with 10% FCS and 1 % penicillin-streptomycin. Human cells were incubated at 37 °C and 5% $CO_2$. Fresh cell medium was added every three days. All the media and solutions were preheated to 37 °C before use.

**Table 6.** List of media used for human cells culture.

| Cell type | Characteristics | Provider |
|---|---|---|
| HUVEC | endothelial cell growth medium (ECGM) basal and supplement mix | C-22110, C-39215, PromoCell |
| HMEC-1 | ECGM with supplement mix | PB-MH-100-2199, PELOBiotech |
| HEK 293T | Dulbecco's Modified Eagle Medium (DMEM) | 10566016, Gibco |

### 2.2.3 Subculture

Human cells subculture was performed when cells reached 80-90% confluency. Cells were briefly washed with 1X DPBS to remove non-adherent cells. Subsequently, cells were incubated with 40 µl/cm$^2$ of trypsin/EDTA for 4 min. After the cells detached, the trypsinization was stopped by adding twice the volume of the culture medium. Cells were passed in a 1:10 dilution to a new flask with the respective growth medium. The passage number of cells was registered.

### 2.2.4 Thawing human cells from liquid nitrogen

Human cells were collected from liquid nitrogen and incubated in a water bath at 37 °C until thawed. Cells were transferred to a new tube and centrifuged at 200 g for 5 min at 4 °C. The supernatant was discarded, and the sediment was resuspended in preheated growth medium. Finally, cells were transferred to a tissue culture flask (collagen precoated for HUVEC and HMEC-1) containing the respective medium. Cells were incubated at 37 °C and 5% $CO_2$ until they reached confluency.

### 2.2.5 Determination of live human cell count

Live human cell count was performed using trypan blue to identify dead or damaged cells (blue-stained). The cell suspension was prepared in a dilution of 1:3 using trypan blue and incubated for 2 min at RT (room temperature). The live cell count was performed under a light microscope using a Neubauer counting chamber.

### 2.2.6 Cryopreservation of human cells

Human cells at 80% confluency were detached following the protocol described in **Section 2.2.3** and centrifuged at 200 g for 10 min at RT. Human cells were resuspended in ice-cold freezing media containing FCS supplemented with 10% DMSO with a known cell concentration ($2x10^6$ cells/ml for HUVEC or $5x10^6$ cells/ml HMEC). Cells were aliquoted in cryogenic storage vials and stored overnight at -80 °C under controlled rate freezing conditions. Vials were transferred frozen to liquid nitrogen for long-term preservation. The passage number for the stored cells was registered.

## 2.3 Molecular methods

### 2.3.1 Oligonucleotides and plasmids

Oligonucleotides and plasmids used are listed in **Table 7**.

**Table 7.** List of oligonucleotides and plasmids.

| **Guide RNA (gRNA)** | **Oligonucleotides sequence (5′-3′)** | **References** |
|---|---|---|
| gRNA_A | AAT CGG CGC GCG GTC GGC TG | this study [104] |
| gRNA_B | GAC CGT CCC ATA TAA GCC C | |
| gRNA_C | CCG GGA GCC GGG GCT TAT AT | |
| gRNA_D | CAA GCG TGA GTA CTG ACC GC | |
| gRNA_E | CAA GCG TGA GTA CTG ACC G | |
| gRNA_F | AAT CTC TTC CTT ACT TGC GA | |

| **Primers** | | **Oligonucleotide sequence (5′-3′)** | **Annealing** |
|---|---|---|---|
| Fn cDNA | fn_fwd<br>fn_rev | AAG ACC AGC AGA GGC ATA AG<br>AAA GCA CGA GTC ATC CGT AG | 55 °C |
| actin cDNA | actin_fwd<br>actin_rev | AAA GAC CTG TAC GCC AAC AC<br>GTC ATA CTC CTG CTT GCT GAT | 55 °C |
| *B. henselae* DNA quantification | glyA_fwd<br>glyA_rev | GAC AGG AAA ATG TGC CGA AT<br>GCA GGT GAA CCA AGA CGA AT | 57 °C |
| *A. baumannii* DNA quantification | rpoB(Ab)_fwd<br>rpoB(Ab)_rev | GAG TCT AAT GGC GGT GGT TC<br>ATT GCT TCA TCT GCT GGT TG | 57 °C |
| *B. burgdorferi DNA quantification* | 16S_fwd<br>16S_rev | GCT TCG CTT GTA GAT GAG TCT GC<br>TTC CAG TGT GAC CGT TCA CC | 57 °C |
| *S. aureus* DNA quantification | rpoB(Sa)_fwd<br>rpoB(Sa)_rev | TGC GAA CAT GCA ACG TCA AG<br>CGA CCT CTG TGC TTA GCT GT | 57 °C |
| endothelial cells DNA quantification | hmbs_fwd<br>hmbs_rev | TTC CTT CCC TGA AGG GAT TCA CTC AG<br>TTA AGC CCA GCA GCC TAT CTG ACA CCC | 57 °C |

**Table 7.** List of oligonucleotides and plasmids (*continuation*).

| Plasmids | Characteristics | References |
|---|---|---|
| lentiCRISPR v2 | lentiviral transfer plasmid (no. 52961). $Amp^r$ & $Pur^r$ | Addgene |
| pMD2.G | envelope expressing plasmid (no. 12259), vesicular stomatitis virus G glycoprotein (VSV-G). $Amp^r$ | Addgene |
| psPAX2 | packaging plasmid (no. 12260). $Amp^r$ | Addgene |
| lentiCRISPR-gRNA_A | lentiviral transfer plasmid including gRNA_A | this study [104] |
| lentiCRISPR-gRNA_B | lentiviral transfer plasmid including gRNA_B | |
| lentiCRISPR-gRNA_C | lentiviral transfer plasmid including gRNA_C | |
| lentiCRISPR-gRNA_D | lentiviral transfer plasmid including gRNA_D | |
| lentiCRISPR-gRNA_E | lentiviral transfer plasmid including gRNA_E | |
| lentiCRISPR-gRNA_F | lentiviral transfer plasmid including gRNA_F | |
| pCR 2.1-TOPO vector | standard cloning vector for TA-overhangs. $Kan^r$ & $Amp^r$ | Invitrogen |
| pCR 2.1-TOPO_glyA | pCR 2.1-TOPO with *B. henselae glyA* fragment. $Kan^r$ & $Amp^r$ | this study [104] |
| pCR 2.1-TOPO_hmbs | pCR 2.1-TOPO with human *hmbs* fragment. $Kan^r$ & $Amp^r$ | |
| pCR 2.1-TOPO_rpoB(Ab) | pCR 2.1-TOPO with *A. baumannii rpoB* fragment. $Kan^r$ & $Amp^r$ | this study |
| pCR 2.1-TOPO_rpoB(Sa) | pCR 2.1-TOPO with *S. aureus rpoB* fragment. $Kan^r$ & $Amp^r$ | this study |
| pCR 2.1-TOPO_16S | pCR 2.1-TOPO with *B. burgdorferi* 16S fragment. $Kan^r$ & $Amp^r$ | this study |

### 2.3.2 Conventional polymerase chain reaction and electrophoresis

DNA amplification via conventional polymerase chain reaction (cPCR) was performed using PCR master mix 2X and primers listed in **Table 7,** using an end-point thermocycler instrument. For amplification, 1X PCR master mix, 0.3 µM forward and reverse primers, and 1 µl DNA. For colony PCR the volume was completed with $H_20$. The conditions used for DNA amplification are detailed in **Table 8**.

**Table 8.** Cycling conditions for cPCR.

| Step | Temperature (°C) | Time | Cycle |
|---|---|---|---|
| initial denaturation | 98 | 1 min | 1 |
| denaturation | 98 | 10 s | |
| annealing | variable | 30 s | 35 |
| extension | 72 | 60 s | |
| final extension | 72 | 10 min | 1 |

Amplified DNA was separated using agarose gel electrophoresis. Agarose gels at 1.5% (w/v) were prepared in 1X TAE buffer (2 M Tris,1 M acetic acid, 100 mM EDTA pH 8.1). DNA ladder 100 bp was used as a reference and Midori green for nucleic acid staining and loading dye. Electrophoresis was carried out at 100 V for about 40 min. DNA was visualized under UV light using a gel documentation system.

### 2.3.3 Quantitative polymerase chain reaction

Amplification of DNA or cDNA via quantitative polymerase chain reaction (qPCR) was performed using Luna® Universal qPCR Master Mix and the primers listed in **Table 7** using a LightCycler® 480 instrument. For amplification, 1X Luna Universal qPCR Master Mix, 0.25 µM forward and reverse primers, and 1 µl DNA or cDNA. The conditions used for amplification are detailed in **Table 9**.

**Table 9**. Cycling conditions for qPCR.

| Step | Temperature (°C) | Time | Cycle |
|---|---|---|---|
| initial denaturation | 95 | 60 s | 1 |
| denaturation | 95 | 15 s | |
| annealing | variable | 20 s | 35 |
| extension | 60 | 30 s | |
| melt curve | 40-97 | | 1 |

### 2.3.4 Preparation of standard vector for absolute quantification

A standard vector was prepared for absolute quantification of adherent bacteria (*A. baumannii*, *B. henselae, B. burgdorferi, S. aureus*) onto HUVECs using the Topo™ TA Cloning™ kit. For ligation, the linearized vector was mixed with 4 µl of Taq-amplified PCR product (**Section 2.3.2**) using the DNA quantification primers (**Table 7**). The ligation mix was incubated at RT for 15 min. For transformation, *E. coli* NEB 5 alpha were incubated with 2.5 µl of ligated plasmid on ice for 30 min. Heat shock was performed in a water bath at 42 °C for 30 s, followed by incubation on ice for 5 min. For recovery, bacteria were incubated with SOC outgrowth media at 37 °C for 60 min and 350 RPM. *E. coli* were spread into LB plates supplemented with 50 µg/ml kanamycin for selection. Colony PCR was performed to evaluate transformed clones (**Section 2.3.2**). Positive clones were grown overnight in LB liquid with 50 µg/ml kanamycin.

Plasmid DNA extraction was done using NucleoSpin Plasmid, following the manufacturer´s recommendations for high-copy plasmid DNA. The extracted plasmid was verified by sequencing by GATC Biotech (Eurofins). Confirmed colonies were cryopreserved at -80 °C (**Section 2.1.4**).

### 2.3.5 Preparation of *FN1* knockout ECs

The experimental design was done in collaboration with Dr. Matthias Leisegang (Cardiovascular Department, Goethe University, Germany). Single or dual gRNA combinations were tested for efficient *FN1* knockout. The human February 2009 (GRCh37/hg19) assembly from UCSC Genome Browser was used for the evaluation of *FN1* gene.

#### 2.3.5.1 Guide RNA design and plasmid preparation

Sequences that included the 5′ untranslated region (UTR), transcription starting site (TSS), and introns 1 and 3 were used as templates for the guide RNA (gRNA) sequences with lower predicted off-targets were retrieved from the CRISPOR interface. The specificity of gRNAs

was analyzed against the human genome using BLAST. The selected gRNA sequences (**Table 7**) were ordered, including overhands for matching the LentiCRISPR v2 plasmid (CACCG).

Plasmid preparation was done as described before [105] with some modifications. Oligos were phosphorylated and annealed using 100 ng sense and antisense oligos and 5 U of T4 polynucleotide kinase at 37 °C for 30 min and 95 °C for 5 min. For plasmid digestion and ligation, a single-step reaction was performed using 100 ng LentiCRISPR v2, 1X FastDigest buffer, 2500-fold annealed oligos, 0.5 mM DTT, 0.5 mM ATP, 1 µl FastDigest Esp3I, and 1500 U T7 DNA ligase. The ligation reaction was incubated at 37 °C and 23 °C each for 5 min; this was repeated for six cycling steps. To remove contaminating DNA from the plasmid preparation, linear DNA was digested using 11 µl ligation reaction, 1X buffer, 10 U Plasmid-Safe DNase, and 1 mM ATP. The reaction was incubated at 37 °C for 30 min.

#### 2.3.5.2 Cloning and plasmid DNA isolation

For cloning, 15 µl of ligation (**Section 2.3.5.1**) were transformed into DH5α cells with 100 µl of transformation buffer. The mixture was incubated on ice for 20 min before heat shock at 42 °C for 90 sec, followed by incubation on ice for 5 min. Cells were recovered in 450 µl of 2xYT medium for 45 min at 37 °C with 650 RPM. Cells were concentrated by centrifugation at 6,000 g for 5 min, and 250 µl were grown overnight in LB plates with 100 µg/ml ampicillin for selection. Colonies were selected and grown overnight in LB medium for plasmid DNA isolation.

A protocol for alkaline lysis was used for plasmid DNA isolation. The solutions used for plasmid DNA isolation are shown in **Table 10**. Overnight cultures were centrifuged at full speed for 1 min; bacterial pellet was collected and resuspended in 300 µl solution P1. To achieve cell lysis, 300 µl solution P2 was used, inverting the tube several times. Finally, 300 µl solution P3 was used to neutralize the solution. For cleaning and concentration of plasmid, chloroform purification was used in combination with isopropanol and 70% ethanol precipitation. Centrifugation at maximum speed for 15 min and 4 °C was used for the last

steps. The pellet was resuspended in 30 µl $H_2O$. Plasmids containing the expected gRNAs were confirmed by sequencing.

**Table 10.** Solutions for cloning and plasmid extraction.

| Solutions | Description |
|---|---|
| transformation buffer | 100 nM CaCl $2H_2O$<br>50 mM $MgCl_2$ |
| solution P1 | 25 mM Tris<br>10 mM EDTA<br>15% glucose |
| solution P2 | 0.2M NaOH<br>1% SDS |
| solution P3 | 5 M potassium acetate<br>11.5% acetic acid<br>adjust with HCl to pH 5 |

Positive clones were grown overnight in 150 ml LB media with 100 µg/ml ampicillin. Maxiprep plasmid extraction was performed using GenElute™ kit, following the manufacturer's recommendations for vacuum protocol.

#### 2.3.5.3 Lentivirus production

For lentivirus production, HEK 293T cells were seeded on a 10 cm dish using DMEN growth media until they reached 80% confluency. A transfection mixture was prepared for each gRNA; the solutions are shown in **Table 11**. An empty LentiCRISPR v2 plasmid was used for one treatment to maintain the WT phenotype. The mixture was briefly vortexed and incubated for 20 min at RT. The transfection mixture was transferred dropwise to HEK 293T cells and incubated at 37 °C. After 48 h and 72 h of incubation, the supernatant was collected, centrifuged at 170 g for 4 min to remove cell debris, and passed through a 0.22 µm filter. Samples were tested for viral presence using Lenti-X™ GoStix™ following the manufacturer's recommendations. Aliquots were stored at -80 °C for transduction.

**Table 11.** Transfection mix.

| Solutions | Description |
|---|---|
| solution A | 700 µl DMEN<br>4.1 µg LentiCRISPR v2_gRNA<br>3.8 µg psPAX2<br>2.1 µg pMD2.G |
| solution B | 650 µl DMEN<br>50 µg PEI |

#### 2.3.5.4 Transduction of ECs

The treatments used for single or dual lentiviral *FN1* knockout are shown in **Table 12**; a treatment including lentivirus with empty LentiCRISPR v2 vector was used to maintain the WT phenotype. HUVEC isolated *in house* (passage 3), HUVEC Promocell (passage 1) or HMEC-1 (passage 3) were cultured on a 6 cm dish until they reached 70% confluency. For transduction, 1 ml DMEN growth medium and 1 ml of single/dual lentiviral were used in combination with 8 µg of polybrene to enhance retroviral infection efficiency. The lentiviral transduction was allowed for 24 h. After this time, transduced cells were selected with 2 µg/ml puromycin for four days. Cells were expanded and saved in liquid nitrogen following the protocol described in **Section 2.2.6**. Passage number was recorded, passage 6 for HUVEC isolated *in house*, passage 3 for HUVEC Promocell, and passage 6 for HMEC-1 were stored.

**Table 12.** Treatments used for single or dual lentiviral *FN1* knockout.

| Treatment | Lentivirus 1 | Lentivirus 2 | Target |
|---|---|---|---|
| vector | empty* | none | NTC1 |
| 1 | gRNA_A | gRNA_D | promoter to end of exon 1 |
| 2 | gRNA_A | gRNA_E | promoter to end of exon 1 |

* empty LentiCRISPR v2 for WT phenotype

**Table 12.** Treatments used for single or dual lentiviral *FN1* knockout (*continuation*).

| Treatment | Lentivirus 1 | Lentivirus 2 | Target |
|---|---|---|---|
| 3 | gRNA_A | gRNA_F | promoter to end of exon 1 |
| 4 | gRNA_B | gRNA_D | TSS to end of exon 1 |
| 5 | gRNA_B | gRNA_E | TSS to end of exon 1 |
| 6 | gRNA_B | gRNA_F | TSS to end of exon 1 |
| 7 | gRNA_C | gRNA_D | TSS to end of exon 1 |
| 8 | gRNA_D | none | splicing exon 1 / intron 1 border |
| 9 | gRNA_H | none | splicing exon 3 / intron 3 border |

#### 2.3.5.5 Knockout evaluation

The different treatments for *FN1* knockout were evaluated using relative quantification of *FN1* RNA, Western blot and immunofluorescence microscopy. For RNA evaluation, $5x10^5$ cells were seeded on six-well plates (**Section 2.3.6**); for protein evaluation via western blot, $1x10^6$ cells were seeded on 6 cm dishes (**Section 2.4**); and for immunofluorescence microscopy, $1.5x10^5$ cells were seeded on coverslips (**Section 2.8.2**).

### 2.3.6 RNA isolation from human cells

HUVECs and HMEC-1 were seeded on six-well plates and cultured until they reached 80% confluency. RNA extraction was performed using RNeasy Mini kit following the protocol for "Purification of total RNA from animal cells using spin technology". After cell lysis, samples were homogenized using QIAshredder. DNase digestion was performed on-column using RNase-Free DNase Set. RNA was eluted in 30 µl of RNase-free $H_2O$.

### 2.3.7 Relative quantification of *FN1* mRNA levels

Extracted RNA was used for reverse transcription with LunaScript® RT SuperMix. The protocol suggested by the manufacturer was followed using 500 ng of extracted RNA for the generation of cDNA; a non-RT sample was included as a control. Amplification of DNA was performed following the protocol described in **Section 2.3.3** using primers for *FN1* gene (fn_fwd and fn_rev) and primers for *beta-actin* (actin_fwd and actin_rev) as a housekeeping gene (**Table 7**).

The analysis of relative quantification was done following the average normalized fold expression method [106]. Ct values from *FN1* and *beta-actin* were used to calculate the average normalized fold expression ($2^{-\Delta\Delta Ct}$). The $\Delta Ct$ value was calculated for the knockout treatments (test) and the empty vector (control) as described below:

$\Delta Ct = Ct(FN1) - Ct(beta - actin)$.
$\Delta\Delta Ct = \Delta Ct(test) - \Delta Ct(control)$
converted to normalized fold expression following: $2^{-\Delta\Delta Ct}$

## 2.4 Protein methods and Western blotting

Buffers and solutions for this section are given in **Table 13**.

**Table 13.** List of buffers and solutions for protein methods.

| **Buffers and solutions** | **Description** |
|---|---|
| digestion buffer trypsin | 50 mM HEPES<br>150 mM NaCl<br>adjust with NaOH to pH 8.0 |
| digestion buffer factor Xa | 20 mM TrisHCl pH 6.5<br>50 mM NaCl<br>1 mM $CaCl_2$ |
| digestion buffer caspase I | 50 mM HEPES adjust with KOH to pH 7.2<br>0.1% CHAPS<br>2mM EDTA<br>10% glycerol<br>10 mM DTT |
| digestion buffer thrombin | 50 mM TrisHCl pH 8.3<br>0.1 NaCl |
| protein extraction buffer | 7 M Urea<br>1% SDS<br>10% glycerol<br>10 mM Tris-HCl pH 6.8<br>5 mM DTT<br>1X proteinase inhibitor cocktail |
| Laemmli buffer (6X) | 10 mM Tris-HCl pH 6.8<br>10% glycerol<br>5 mM DTT<br>7M urea<br>1% SDS<br>1X proteinase inhibitor cocktail |
| SDS running buffer | 50 mM Tris<br>384 mM glycine<br>0.1% SDS |
| solution for stacking gel (1X)<br>2.157 ml | 5% acrylamide<br>380 µl of 0.5 M Tris-HCl pH 6.8<br>0.1 % SDS<br>0.1 % ammonium persulfate<br>2 µl TEMED<br>1.4 ml dH2O |

**Table 13.** List of buffers and solutions for protein methods (*continuation*)

| Buffers and solutions | Description |
|---|---|
| solution for resolving 10 % gel (1X)<br>5.02 ml | 10% acrylamide<br>1.3 ml of 1.5 M Tris-HCl pH 8.8<br>0.1 % SDS<br>0.1 % ammonium persulfate<br>2 µl TEMED<br>1.9 ml dH2O |
| blotting buffer (1X) | 25 mM Tris<br>192 mM glycine<br>10% ml methanol |
| washing buffer (1X) | 10 mM Tris/HCl pH 7.4<br>150 mM NaCl<br>0.5% Tween 20 |
| blocking buffer (1X) | 5% skimmed milk in 1X washing buffer<br>10% ROTI®Block in dH2O (used for human proteins) |

### 2.4.1 Enzymatic digestion of Fn

Enzymatic digest of Fn was performed using 10 µg of Fn with 100 µl of the specific enzyme digestion buffer (**Table 13**). The reaction was started by the addition of enzyme using specific enzyme : substrate ratios [2 U of Caspase I (1:125); 0.2 U of Factor Xa (1:10); 2 U of thrombin (1:25); 5 U trypsin 1:20]. Incubation was performed at 37 °C using different time points. The enzymatic reaction was stopped with Pefablock at a final concentration of 1 mM. Samples were analysed using SDS PAGE (**Section 2.4.5**), and selected time points were used for bacterial binding assays (**Section 2.5.1**).

### 2.4.2 Determination of protein concentration

The protein concentration was evaluated using a micro-BCA protein assay kit. The manufacturer´s recommendations were followed for the "Microplate protocol". BSA was used as a protein standard for a working range from 2 to 40 µg/ml. The plate was incubated at 37 °C for 2 h. The absorbance was measured using a multifunction plate reader Infinite M200 Pro spectrophotometer at 562 nm. The protein concentration in the sample was estimated using a calibration curve.

### 2.4.3 Protein cell extracts from ECs

ECs lysates were prepared from $1x10^6$ cells seeded on 6 cm dish and incubated overnight. ECs were washed once with 1X DPBS and lysed using 250 µl of protein extraction buffer. Lysed cells were transferred to a microtube on ice and homogenised using an Ultra-Turrax instrument. Samples were centrifuged at 4 °C for 12 min at 12,000 g. The supernatant was transferred to a new tube, and protein concentration was determined following the protocol described in **Section 2.4.2**. ECs lysate samples were stored at -80 °C until they were used for analysis.

### 2.4.4 Protein cell extracts from *B. henselae*

*B. henselae* cell lysates were produced by resuspending $OD_{600}$ = 1 of *B. henselae* into 250 µl of protein extraction buffer. Samples were homogenised by passing cells through a 21-gauge needle to shear the DNA. Samples were centrifuged at 4 °C for 10 min at 10,000 g. The supernatant was transferred to a new tube, and the protein concentration was determined following the protocol described in **Section 2.4.2.** Bacterial lysate samples were stored at -20 °C until they analysis.

### 2.4.5 SDS polyacrylamide gel electrophoresis

A discontinuous Tris-glycine-system was used for SDS polyacrylamide gel electrophoresis (PAGE). For samples with a known protein concentration, 10 µg of protein was used with

6X Laemmli sample buffer for denaturation. For samples with purified protein (i.e. Fn-fragments and purified Fn), 1 µg of protein was used with 6X Laemmli sample buffer for denaturation. Bacterial samples without protein quantification were prepared by resuspending $OD_{600}$ = 1 of bacteria with 2X Laemmli sample buffer. All samples with Laemmli buffer were boiled at 95 °C for 4 min and subjected to electrophoresis. Pre-stained protein ladder was used to estimate the molecular weight; when more precise fragment discrimination was required (i.e. Fn fragments), an additional ladder was included (Spectra multicolor broad range). For 10% gels, the running conditions were set at 15 mA during stacking and 25 mA for separation. For gradient gels, running conditions were set at 25 mA for 15 min and 15 mA for 45 min.

### 2.4.6 Staining of proteins in polyacrylamide gels

Proteins separated by SDS PAGE were visualised by incubation with InstantBlue protein gel stain for 1 h, followed by incubation with $H_2O$ for 1 h. All steps were applied under constant shaking at RT. Gels were analysed using ChemiDOC XRS+ system equipped with ImageLab software.

### 2.4.7 Western blotting

Proteins separated by SDS PAGE were transferred ("blotted") to nitrocellulose membranes using a tank blotting system. Briefly, two filter papers and the membrane were soaked in blotting buffer. The proteins were transferred at 300 mA constant for 1 h. After the transference, the membrane was incubated with blocking buffer (skimmed milk for bacterial proteins or ROTI block for mammalian proteins) for 1 h at RT. The membrane was incubated with the primary antibody overnight at 4 °C and the respective secondary antibody for 1 h at RT. Both antibodies were prepared in a blocking solution. After each incubation step, the membranes were washed with washing buffer three times for 5 min. For detection, blots were developed using SuperSignal West Pico PLUS Chemiluminescent Substrate and detected using ChemiDOC XRS+ system equipped with ImageLab software.

## 2.5 Bacterial binding assays

Buffers and solutions for this section are given in **Table 14**.

**Table 14.** List of buffers and solutions for ELISA.

| Buffers and solutions | Description |
|---|---|
| washing buffer (1X) | 0.05% v/v Tween 20<br>in 1X DPBS |
| blocking buffer I (1X) | 2% w/v BSA<br>in 1X washing buffer |
| blocking buffer II (1X) | 3% w/v BSA<br>in 1X washing buffer |

### 2.5.1 *B. henselae* binding assays in a suspension format

For *B. henselae* binding assays, *B. henselae* strains were grown in BaLi medium. *B. henselae* ($OD_{600}$ = 1) binding to plasma, cellular, or recombinant Fn was analyzed using 7.5 µg/ml Fn in 1X DPBS. For competition experiments, bacteria, plasma Fn, and 0, 0.5, or 5 µg/µl heparin were added simultaneously. Samples were incubated at 37 °C and mixed using a rotator Intelli Mixer (program 2, 20 RPM); the incubation time was adjusted to the application (binding and competition assays: 2 h; crosslinking assays: 30 min). After each incubation step, cells were centrifuged and washed three times with 1X DPBS. *B. henselae* binding to Fn in solution was subsequently evaluated using Western blot (**Section 2.4**).

### 2.5.2 *B. henselae* binding assays in an ELISA format

*B. henselae* adherence to immobilized Fn or heparin was identified using a whole cell-ELISA. For binding assays to full-length Fn and fragments, 1 µg was coated onto Nunc Maxisorp 96-wells (unless mentioned otherwise). For *B. henselae* binding assays to heparin, 0, 0.5, 5, or 50 µg/µl of heparin was used for coating. Plates were coated at 4 °C overnight and incubated with blocking buffer I at 37 °C for 2 h. *B. henselae* ($OD_{600}$ = 0.3; 100 µl) was

added to the wells and incubated for 2 h at 37 °C. For the identification of adhered bacteria, the plate was incubated with rabbit anti-*B. henselae* IgG antibodies, followed by HRP-conjugated anti-rabbit IgG antibodies, both in blocking buffer I and incubated for 1 h. After each step, three washes were performed using washing buffer. The plate was incubated with TMB solution for 1 min, and the reaction was stopped using 1 M HCl. The absorbance was spectrophotometrically measured at 450 nm using an ELISA plate reader Sunrise.

For binding competition assays, after the blocking step, the plate was incubated with heparin and bacteria simultaneously. *B. henselae* and 0, 0.5, 5, or 50 µg/µl of heparin in 1X DPBS were incubated at 37 °C for 2 h. For inhibition assays, after the blocking step, the plate was incubated with Fn-directed monoclonal antibodies for 1 h, followed by incubation with bacteria for 1 h. The identification of bond bacteria in binding competition and inhibition assays was performed as described before.

### 2.5.3 Analysis of Fn binding to immobilised bacteria in an ELISA format

*A. baumannii*, *B. henselae*, *B. burgdorferi*, and *S. aureus* interaction with Fn was evaluated using bacterial-coated microtiter wells exposed to increasing amounts of Fn in an ELISA format. Bacteria were resuspended in 1X DPBS and adjusted to specific concentrations ($OD_{600} = 0.6$ for *A. baumannii*, *B. henselae*, and *S. aureus*; and $5x10^8$ cells/ml for *B. burgdorferi*). Aliquots (100 µl) of the respective bacterial suspensions were coated onto Nunc Maxisorp flat-bottom 96-wells and incubated overnight at 4 °C. Plates were incubated with blocking buffer II at 37 °C for 2 h. Increasing amounts of plasma Fn were added to the wells (0, 0.2, 0.4, 0.8, 1.5, 3.0, or 6.0 µg) and incubated for 2 h at 37 °C. A subsequent step for incubation with 20% v/v rabbit serum in 1X DPBS was added to prevent unspecific antibody recognition. Fn interaction with bacteria was examined using mouse anti-Fn IgG antibodies, followed by HRP-conjugated anti-mouse IgG antibodies, both in blocking buffer and incubated for 1 h. After each step, three washes were performed using washing buffer. The assay was developed using TMB solution for 2 min, and the reaction was stopped using 1 M HCl. The absorbance was spectrophotometrically measured at 450 nm using an ELISA plate reader Sunrise.

## 2.6 Evaluation of bacterial adherence to HUVECs

Evaluation of *A. baumannii*, *B. henselae*, *B. burgdorferi*, and *S. aureus* adherence to HUVECs was performed using *in vitro* infection experiments. HUVECs were plated overnight using seeding medium (ECGM basal, supplement mix, and 10% Fn depleted FCS). Two hours before infection, HUVECs were incubated in pre-infection medium (ECGM basal and 2% Fn depleted FCS). Infection was performed for 60 min at 37 °C. For infection, HUVECs were incubated with bacteria using specific multiplicity of infection (MOI) values (*B. henselae* and *S. aureus*: MOI 200; *A. baumannii* and *B. burgdorferi*: MOI 500). After infection, three washes with ECGM were performed to remove unbound bacteria.

### 2.6.1 Absolute quantification of adherent bacteria

Adherent bacteria to HUVECs were evaluated by quantification of gene copy equivalents using qPCR. HUVECs ($5x10^5$ cells) were seeded on six-well plates and infected as described above. Infected cells were scraped off and transferred to microtubes, pelleted at 20,000 g for 3 min, and washed once with 1X DPBS.

The DNA extraction was performed using the alkaline lysis method. The cell pellet was resuspended in 22 µl alkaline lysis buffer (25 mM NaOH, 0.2 mM EDTA) and boiled at 95 °C for 30 min. The sample was cooled at 4 °C for 5 min and mixed with 22 µl of neutralization buffer (40 mM Tris HCl, pH 7.8). After this, the sample was centrifuged at 10,000 g for 10 min to remove cell debris. The supernatant containing DNA was transferred to a new tube for absolute quantification.

The supernatant containing DNA was used as a template to amplify via qPCR (**Section 2.3.3**). Species-specific genes (**Table 15**) were used for the identification of bacterial and HUVECs gene copy numbers [107] using oligos described in **Table 7**.

**Table 15.** List of species-specific genes for absolute quantification of bacteria.

| DNA quantification | Primers | Target gene | Amplicon size |
|---|---|---|---|
| *A. baumannii* | rpoB(Ab)_fwd<br>rpoB(Ab)_rev | β subunit of bacterial RNA polymerase (*rpoB*) | 110 bp |
| *B. henselae* | glyA_fwd<br>glyA_rev | serine hydroxymethyltransferase (*glyA*) | 120 bp |
| *B. burgdorferi* | 16S_fwd<br>16S_rev | 16S ribosomal RNA | 107 bp |
| *S. aureus* | rpoB(Sa)_fwd<br>rpoB(Sa)_rev | *rpoB* | 123 bp |
| ECs | hmbs_fwd<br>hmbs_rev | hydroxymethylbilane synthase (*hmbs*) | 207 bp |

The standard vector controls pCR 2.1-TOPO_glyA, pCR 2.1-TOPO_rpoB(Ab), pCR 2.1-TOPO_rpoB(Sa), pCR 2.1-TOPO_16S, and pCR 2.1-TOPO_hmbs were used for absolute quantification of each gene. The copy numbers of the resulting standard plasmids were estimated following the formula:

copy numbers $= (N_A \times n/M)$, where $N_A$ is Avogadro constant number ($6.02 \times 10^{23} mol^{-1}$),
n is plasmid concentration,
M is plasmid molecular mass.

For each qPCR, a standard with the estimated gene copy numbers was included. For absolute quantification of adherent bacteria per HUVEC, the following formula was used:

$binding\ ratio = bacterial\ gene\ equivalent / 0.5\ hmbs\ gene\ equivalent.$

### 2.6.2 Evaluation of adherent bacteria using immunofluorescence microscopy

HUVECs ($1.5x10^5$ cells) were seeded on collagenised coverslips placed into 24-well plates. Infection was performed as previously described. After the infection, cells were fixed using 3.75% PFA at 4 °C for 10 min and washed three times using ECGM basal. Cells were stored in ECGM basal at 4 °C until immunofluorescence staining (**Section 2.8.2**).

## 2.7 Mass spectrometry methods

The mass spectrometry (MS) analysis was done in collaboration with Dr. Lotta Happonen (Lund University) as part of the Marie Sklodowska-Curie program from the European Union. MS and crosslinking methods, including bioinformatics analysis, were performed as previously described [108] with some modifications as described below.

### 2.7.1 Crosslinking sample preparation

*B. henselae* binding to Fn in solution was performed as described in **Section 2.5.1**. After binding, samples were resuspended in 1X DPBS and heavy/light disuccinimidylsuberate (DSS) crosslinker was added to a final concentration of either 500 or 2,000 μM. Samples were subsequently incubated for 60 min at 37 °C and shaking. The crosslinking reaction was quenched with 50 mM ammonium bicarbonate for 15 min at 37 °C and shaking. Crosslinked samples were split into two treatments: surface-attached proteins and whole-cell proteins. The surface-attached proteins were recovered by limited proteolysis using 2 μg of sequencing grade trypsin for 2 h at 37 °C with shaking, the cell debris was removed by centrifugation at 3,800 g for 10 min and the supernatant was recovered to a new tube. Surface-attached and whole-cell protein samples were heat-inactivated at 85 °C for 5 min and used for MS sample preparation. All the shaking steps were performed at 800 RPM.

### 2.7.2 MS sample preparation

Samples for MS analysis were prepared by denaturing the proteins using 8 M urea / 100 mM ammonium bicarbonate solution. For surface-attached protein samples, protein concentration was measured (**Section 2.4.2**) and 5 µg were used for denaturation. For whole-cell protein samples, the cell pellet was resuspended for denaturation, cells were mechanically disrupted, and samples were centrifuged at maximum speed for 10 min at 4 °C; 50 µl of the supernatant was collected to a new tube and was used in the following steps. For all samples, cysteine bonds were reduced using 5 mM Tris(2-carboxyethyl) phosphine hydrochloride (TCEP) for 60 min at 37 °C and alkylated using 10 mM 2-iodoacetamide for 30 min at 22 °C. For initial digestion of crosslinked samples, 1 µg lysyl endopeptidase was added to samples and incubated for 2 h at 37 °C. Samples were diluted with 100 mM ammonium bicarbonate to a final urea concentration of 1.5 M. For complete protein digestion, 1 µg sequencing grade trypsin was added and incubated for 18 h at 37 °C. The digested samples were acidified with 10% formic acid to a pH 3.0.

Peptides were purified and desalted using SOLAµ reverse phase extraction plates following the manufacturer's recommendations. Dried peptides were reconstituted in a solution containing 2% acetonitrile and 0.1% formic acid before MS analysis.

### 2.7.3 Liquid chromatography MS

MS data were collected using data-dependent acquisition (DDA) and data-independent acquisition (DIA) analysis. In DDA analysis, theoretical m/z values for fragments of crosslinked peptides are selected, and then they are fragmented and analysed in a second stage of tandem MS (MS/MS). In DIA, several peptides are fragmented at a time, increasing the capacity and complexity of the data. All peptides were analysed on a Q Exactive HFX mass spectrometer connected to an EASY-nLC 1,200 liquid chromatography instrument. The peptides were separated by C18 reverse-phase chromatography using a 25-cm EASY-Spray column (50 cm column, temperature 45 °C) operated at a maximum pressure of 800 bar. For both DDA and DIA analysis, a linear gradient of 4% to 45% acetonitrile in aqueous 0.1% formic acid was run for 50 min.

For DDA, the 15 most intense precursor ions from an MS1 scan (resolution 60,000 for a mass range of 350-1,600 m/z) were fragmented and measured from a MS/MS scan (resolution 15,000). The precursor ions with 2 m/z isolation width were isolated and fragmented using higher-energy collisional-induced dissociation (HCD) at a normalised collision energy of 30. The automatic gain control (AGC) was set as 3e6 for full MS1 scan and 1e5 for MS/MS; and the dynamic exclusion was set to 10 s. For DIA, one MS1 scan (resolution 60,000 for a mass range of 390-1,210 m/z) was followed by 32 MS/MS full fragmentation scans (resolution 30,000) using an isolation window of 26 m/z (including 0.5 m/z overlap between consecutive windows). The precursor ions within each isolation window were fragmented using HCD at a normalised collision energy of 30. The AGC was set to 3e6 for MS1 and 1e6 for MS/MS.

Quantitative MS data were stored and managed using openBIS [109]. All MS raw data were converted to gzipped and Numpressed mzML (standard rich XML) [110] using the tool MSconvert from the ProteoWizard, v3.0.5930 suite [111]. Data analysis was performed as described below.

### 2.7.4 Generation of protein library for human and *B. henselae* proteome using DDA

The library preparation was done by Dr. Lotta Happonen. An *in house* compiled database was prepared with the *Homo sapiens* reviewed proteome (UniProt ID: UP000005640) and the *B. henselae* unreviewed proteome (UniProt ID: UP000000421), yielding a total of 21,846 proteins. DDA-acquired spectra (**Section 2.7.3)** were analysed using the search engine X! Tandem (2013.06.15.1-LabKey, Insilicos, ISB), OMSSA (version 2.1.8), and COMET (version 2014.02 rev.2) [112–114]. Trypsin digestion was selected, allowing two missed cleavages. Modifications were set to static for carbamidomethylation (C) and variable for oxidation (M). Mass tolerance for precursor ions was set to 0.2 Da, and for fragment ions was set to 0.02 Da. The identified peptides were analysed through the Trans-Proteomic Pipeline (TPP v4.7 POLAR VORTEX rev 0, Build 201403121010) using PeptideProphet [115]. The false discovery rate (FDR) was set to 1% resulting in a peptide FDR < 1%.

### 2.7.5 Identification of protein abundance using DIA

For comparison of protein abundance between *B. henselae* strains, the DIA acquired data (**Section 2.7.3)** were processed using the OpenSWATH pipeline (version 2.0.1 revision: c23217e) [116]. Spectral libraries from the DDA-generated dataset (**Section 2.7.4)** were managed in openBIS. The retention time extraction was calibrated using iRT peptides. Peptide precursors were identified by OpenSWATH (2.0.1), and PyProphet (2.0.1) was used to control the FDR of 1% at peptide precursor and protein levels. The resulting DIA data sets were analysed using Jupyter Notebooks (version 3.1.1).

### 2.7.6 Analysis of sequence coverage for Fn-fragments and isoform abundance in cellular

The peptide sequence coverage of the proteolytic Fn fragments and the Fn isoform distribution were analysed from the DDA-acquired spectra (**Section 2.7.3)** using PEAKS (version X), referring to the UniProt *H. sapiens* proteome. Tryptic digestion was selected, allowing for two missed cleavages. Carbamidomethylation (C) was set to static modification, while oxidation (M) and deamination (N and Q) were set to variable modifications. Mass tolerance for precursor ions was set to 5 ppm, and for fragment ions to 0.02 Da. The search results were filtered using 1% FDR.

### 2.7.7 Crosslinking data analysis

DDA-acquired spectra (**Section 2.7.3**) were analysed for crosslinking data analysis using pLink 2 (version 2.3.9). The program default settings for conventional DSS-H12/D12 crosslinking were used, including trypsin as a protease and an allowance of up to three missed cleavages. Peptides with a mass range of 35-8,000 m/z were selected. The fragment tolerance was set to 10 ppm, and the precursor tolerance was set to 20 ppm. The protein database provided to the program contained the BadA (GenBank: MK993576.1) and human Fn (UniProt: P02751-1 and P02751-14) amino acid sequences. The results were processed using a filter tolerance of 20 ppm and an FDR of 1%. All crosslinked peptides were filtered based on an E-value <1.

### 2.7.8 Analysis of BadA and FnI 11 structures

The structures from BadA head domain crystal structure (PDB: 3D9X) [45] and FnI 11 NMR structure (PDB: 2EC3), deposited at RCSB Protein data bank (RCSB PDB), were retrieved and analysed using PyMOL V2.5 (The PyMOL Molecular Graphics System, Schrödinger, LLC.). Both structures were rendered next to the other, and the location of the interacting peptides from each sequence was highlighted, including the crosslinked lysine residues.

## 2.8 Immunofluorescence microscopy

The protocol used for immunofluorescence staining is described below. Mounted samples were examined using a Zeiss Axio Imager 2 microscope equipped with a Spot RT3 microscope camera and operated by the VisiView V.2.0.5 program.

### 2.8.1 Immunofluorescence staining for *B. henselae*

*B. henselae* (OD = 0.2) in 1X DPBS were placed on glass microscopy slides and airdried. Cells were fixed using 40 µl of 3.75% PFA for 10 min at 4 °C. Fixed bacteria were stained using rabbit anti-BadA antibodies and subsequently incubated with Alexa 488 conjugated anti-rabbit IgG antibodies, both for 1 h at RT. Bacterial DNA was stained with 4′,6-diamidino-2-phenylindole (DAPI) for 10 min at 4°C. All incubation steps were performed in a humid chamber and were followed by three washes with 1X DPBS. Slides were mounted using a fluorescence mounting medium and saved at 4 °C until examination.

### 2.8.2 Immunofluorescence staining for *B. henselae* infected human cell cultures

Fixed cells were permeabilised with 0.1% Triton X 100 for 15 min and blocked with 1% BSA for 1 h (both dissolved in 1X DPBS and incubated at RT). Samples were incubated with primary and secondary IgG-antibodies (rabbit anti-*B. henselae*, mouse anti-cellular Fn, Cy5 conjugated anti-mouse, Alexa 488 conjugated anti-mouse, Alexa 488 conjugated anti-rabbit, Alexa 488 conjugated rabbit anti-laminin, Alexa 647 conjugated rabbit anti-collagen

V). Actin cytoskeleton was stained with tetramethylrhodamine (TRITC) phalloidin. Incubation with antibodies was performed for 1 h at RT in a dark chamber. Bacterial and human DNA were stained with DAPI for 10 min at 4 °C. Three washes with 1X DPBS followed each incubation step. Coverslips were mounted using fluorescence mounting medium and saved at 4 °C until examination.

### 2.8.3 Immunoelectron microscopy

*B. henselae* bound to Fn in solution (**Section 2.5.1**) were used for immunoelectron microscopy. Cells were fixed using 3% PFA and 0.02% glutaraldehyde for 3 h at 4 °C. Fixed cells were washed once with 1X DPBS and kept at 4 °C for 18 h. The protocol for immunoelectron microscopy was performed by Ms. Birgit Fehrenbacher and Prof. Martin Schaller (Eberhard Karls-University of Tübingen, Germany). Samples were centrifuged for 10 min at 3,800 g at 4 °C; the sediment was embedded in 4% agarose (Sigma-Aldrich) at 37 °C and then cooled on ice. Agarose blocks were embedded in Lowicryl (Polysciences Ltd.). Ultra-thin sections of 50 nm were mounted on formvar-coated nickel grids and incubated with rabbit anti-Fn (Abcam), followed by 6 nm gold-conjugated goat anti-rabbit IgG (Jackson ImmunoResearch). Grids were examined using a transmission electron microscope (Zeiss LIBRA 120).

## 2.9 Supportive methods

### 2.9.1 Preparation of Fn-depleted FCS

The FCS supplemented to BaLi or ECGM used for *B. henselae,* or ECs culture was pretreated to remove Fn background. Fn-depleted FCS was prepared by adding 5 ml of gelatin Sepharose-4B to 42 ml of heat-inactivated FCS (56 °C for 30 min). The mixture was incubated at 4 °C in a roller mixer overnight. The gelatin-Sepharose was separated from FCS using polypropylene columns. The FCS was filter-sterilised, and aliquots were stored at -20 °C. Fn removal was confirmed via Western blotting (**Section 2.4.7**) using anti-Fn antibodies.

### 2.9.2 Preparation of defibrinated human blood

Human blood from donors was collected without anticoagulant and transferred to a sterile bottle containing autoclaved glass pearls. Blood and pearls were manually mixed for 5 min. Defibrinated blood was recovered under sterile conditions and used fresh for the preparation of hCBA plates.

## 2.10 Statistical analysis

Statistical analysis was performed using Prism V6 (GraphPad Software, San Diego, CA, USA). For the analysis, data parametric distribution was assumed. A value of $p < 0.01$ was considered statistically significant unless otherwise specified. The figure legend describes the specific test for each analysis and P-value.

## 2.11 Antibodies, staining chemicals, enzymes and Fn fragments

### 2.11.1 Antibodies and staining chemicals

The antibodies and staining chemicals used in this research are listed in **Table 16**.

**Table 16.** List of antibodies and staining chemicals.

| Description | Concentration/ application | Provider/ reference |
|---|---|---|
| **Primary antibodies** | | |
| mouse anti-cellular Fn | 1:100 (IFM) | MAB1940, Sigma-Aldrich |
| mouse anti-Fn | 1:10,000 (WB); 1:100 (BI) | 610077, Becton Dickinson |
| mouse anti-Fn TA803784 | 1:100 (BI) | TA803784, Origene |
| mouse anti-Fn SC18827 | 1:100 (BI) | SC18827, Santa Cruz |

**Table 16.** List of antibodies and staining chemicals (*continuation*).

| Description | Concentration/ application | Provider/ reference |
|---|---|---|
| **Primary antibodies** (*continuation*) | | |
| rabbit anti-Fn | 1:2,000 (WB) | F3648, Sigma-Aldrich |
| rabbit anti-GAPDH | 1:2,000 (WB) | PA1-16777, Thermo Fischer |
| rabbit anti-*B. henselae* | 1:1,000 (ELISA); 1:1,1000 (IFM) | [18] |
| rabbit anti-BadA | 1:2,000 (WB); 1:250 (IFM) | [20] |
| Alexa 488 conjugated rabbit anti-laminin | 1:100 (IFM) | NB300-144AF488, NOVUS |
| Alexa 647 conjugated rabbit anti-collagen V | 1:100 (IFM) | SC-166155AF647, Santa Cruz |
| **Secondary antibodies** | | |
| HRP conjugated anti-rabbit IgG | 1:2,000 (ELISA); 1:1,000 (WB) | P0217, Dako |
| HRP conjugated anti-mouse IgG | 1:1,000 (WB) | P0260, Dako |
| Alexa 488 conjugated anti-rabbit IgG | 1:200 (IFM) | 111-545-045, Dianova |
| Alexa 488 conjugated anti-mouse IgG | 1:400 (IFM) | 115-546-062, Dianova |
| Cy5 conjugated anti-mouse IgG | 1:80 (IFM) | 115-175-062, Dianova |
| Cy5 conjugated anti-rabbit IgG | 1:80 (IFM) | 111-175-144, Dianova |
| **Staining chemicals** | | |
| DAPI | 1 µg/ml (IFM) | 1.24653, Merk |
| TRITC conjugated phalloidin | 2.5 µg/ml (IFM) | 1951, Sigma-Aldrich |

WB: Western blotting, IFM: immunofluorescence microscopy; BI: binding inhibitor

### 2.11.2 Enzymes

The enzymes used in this research are listed in **Table 17**.

**Table 17**. List of enzymes.

| Enzyme | Application | Provider |
|---|---|---|
| caspase 1 human | Fn proteolysis for BadA binding side | C5482, Sigma-Aldrich |
| factor X activated (Xa) from bovine plasma | Fn proteolysis for BadA binding side | F9302, Sigma-Aldrich |
| FastDigest Esp3I | DNA digestion | FD0454, Thermo Fisher |
| Luna® Universal qPCR Master Mix | DNA and cDNA amplification using quantitative PCR | M3003, NEB |
| LunaScript® RT SuperMix | reverse transcription of RNA | E3010, NEB |
| lysyl endopeptidase | protein digestion for MS analysis | 125-05061, Wako Chemicals |
| Plasmid-Safe DNase | removal of contaminating linear DNA from plasmid preparations | E3110K, Epicentre |
| PCR master mix 2X | DNA amplification using conventional PCR | K0171, Thermo Fischer Scientific |
| T4 polynucleotide kinase | phosphorylation and annealing of oligonucleotides | M0201, NEB |
| T7 DNA ligase | DNA ligation | M0318, NEB |
| thrombin from bovine plasma | Fn proteolysis for BadA binding side | T6634, Sigma-Aldrich |
| trypsin from bovine pancreas | Fn proteolysis for BadA binding side | T1426, Sigma-Aldrich |
| trypsin sequencing grade | protein digestion for MS analysis | V511A, Promega |

### 2.11.3 Fn and Fn fragments

The proteins were obtained from Sigma-Aldrich/Merck Millipore and are described in **Table 18**.

**Table 18.** List of types of Fn and Fn fragments.

| Protein | Characteristic | Reference |
|---|---|---|
| plasma Fn | Fn purified from human plasma | F2006 |
| cellular Fn | Fn purified from human foreskin fibroblasts | F2518 |
| recombinant Fn | HEK 293 cells recombinantly expressing *FN1* | ECM001 |
| Hep I/gelatin fragment | 70 kDa Fn fragment obtained by cathepsin D digestion. Binds to gelatin and heparin | F0287 |
| Hep I fragment | N-terminal 30 kDa Fn fragment obtained by tryptic digestion of 70 kDa fragment. Binds to heparin | F9911 |
| gelatin fragment | 45 kDa Fn fragment obtained by tryptic digestion of 70 kDa fragment. Binds to gelatin. | F0162 |
| cell-binding fragment | 120 kDa Fn fragment obtained by chymotryptic. Contains the cell attachment region. | F1904 |
| Hep II fragment | 40 kDa Fn fragment obtained by chymotryptic digestion. Contains CS-1 and heparin-binding regions. | F1903 |

## 2.12 Commercial kits

The list of commercial kits used in this research are described in **Table 19**.

**Table 19.** List of commercial kits.

| Kit | Application | Provider/ reference |
|---|---|---|
| GenElute™ HP Endotoxin-Free Plasmid Maxiprep Kit | plasmid extraction for lentiviral production | NA0410, Sigma-Aldrich |
| Lenti-X™ GoStix™ Plus | identification of lentivirus packaging in cell supernatants | 631280, Takara |
| Micro BCA protein assay | determination of protein concentration | 23235, Thermo Fischer Scientific |
| NucleoSpin Plasmid | mini kit for plasmid DNA extraction | 740588.50, Macherey-Nagel |
| QIAshredder | cell-lysate homogenizer for RNA extraction | 79656, QIAGEN |
| QIAamp DNA Mini kit | DNA extraction | 51306, QIAGEN |
| RNeasy Mini kit | RNA extraction | 74104, QIAGEN |
| RNase-Free DNase Set | digestion of DNA during RNA purification | 79254, QIAGEN |
| SuperSignal West Pico PLUS Chemiluminescent Substrate | development of membranes | 34577, Thermo Fischer Scientific |
| Topo™ TA Cloning™ kit | preparation of standard plasmid for absolute quantification | 451641, Invitrogen |

## 2.13 Chemicals, equipment, and consumables

### 2.13.1 Chemicals and reagents

The list of commercial kits used in this research are described in **Table 20**.

**Table 20.** List of chemicals and reagents.

| Chemical | Provider | Catalogue number |
|---|---|---|
| **A** | | |
| acetonitrile | Sigma-Aldrich | 34998 |
| acetic acid ($CH_3COOH$) | Fisher Chemical | A/0400/PB15 |
| acrylamide and bisacrylamide solution | Roth | 3029.1 |
| agarose | Sigma-Aldrich | A9539 |
| ammonium bicarbonate | Sigma-Aldrich | A6141 |
| ammonium persulfate | BioRad | 131-0700 |
| ampicillin | Sigma-Aldrich | A9518 |
| **B** | | |
| bovine serum albumin (BSA) | Sigma-Aldrich | A7030 |
| β-Mercaptoethanol | AppliChem | A1108 |
| **C** | | |
| calcium chloride dihydrate ($CaCl\ 2H_2O$) | AppliChem | A3587.0500 |
| CHAPS | Sigma-Aldrich | 75621-03-3 |
| collagen G | Biochrom | L7216 |
| Columbia agar base | Becton Dickinson | 211124 |
| Columbia blood agar plates | Becton Dickinson | 254005 |
| cOmplete Protease Inhibitor Cocktail | Roche | 11697498001 |
| **D** | | |
| dimethyl sulfoxide (DMSO) | Roth | A994.2 |
| disuccinimidylsuberate (DSS-H12/D12) | Creative Molecules Inc. | 001S |
| dithiothreitol (DTT) | Thermo Fischer Scientific | 20290 |
| DNA ladder 100 bp | NEB | N0551 |
| Dulbecco's phosphate-buffered saline (DPBS) | Gibco | 14190-169 |

**Table 20.** List of chemicals and reagents (*continuation*).

| Chemical | Provider | Catalogue number |
|---|---|---|
| **E** | | |
| EDTA disodium salt | J.T. Baker | 1073 |
| ethanol (absolute) | Sigma-Aldrich | 32221 |
| **F** | | |
| fetal Bovine Serum (FCS) | Sigma-Aldrich | F7524 |
| fluorescence mounting medium | Dako | S3023 |
| formic acid | Sigma-Aldrich | 5.33002 |
| **G** | | |
| gelatin sepharose-4B | GE Healthcare | 17095601 |
| glycerol | Sigma-Aldrich | G-6279 |
| glycine | Roth | 3783.2 |
| glucose | Sigma-Aldrich | G8270 |
| glutamax supplement | Thermo Fischer Scientific | 35050061 |
| glutaraldehyde | Sigma-Aldrich | G6257 |
| **H** | | |
| heparin sodium salt | Sigma-Aldrich | H4784 |
| HEPES | Roth | 9105.2 |
| hydrochloric acid (HCl) | Roth | T134.1 |
| **I** | | |
| Instant blue | Expedeon | ISB1L |
| 2-Iodoacetamide | Sigma-Aldrich | I6125 |
| **K** | | |
| kanamycin monosulfate | MP | 150029 |
| **L** | | |
| Laemmli sample buffer (2X) | Sigma-Aldrich | S3401 |
| Luria/Miller broth (LB) base liquid | Roth | X968.1 |
| Luria/Miller broth (LB) base agar | Roth | X969.1 |
| **M** | | |
| magnesium chloride ($MgCl_2$) | Sigma-Aldrich | M8266 |
| methanol | Sigma-Aldrich | 32213 |

**Table 20.** List of chemicals and reagents (*continuation*).

| Chemical | Provider | Catalogue number |
|---|---|---|
| **M** *(continuation)* | | |
| Midori Green | Biozym | 617004 |
| **P** | | |
| paraformaldehyde (PFA) | Electron Microscopy Science | 15710 |
| PBS (1X) cell culture | Gibco | 14190-169 |
| pefablock | Sigma-Aldrich | 76307 |
| penicillin/streptomycin Mix | Gibco | 15140-122 |
| polybrene | Sigma-Aldrich | TR-1003-G |
| polyethylenamine (PEI) | Sigma-Aldrich | 408727 |
| potassium acetate ($CH_3CO_2K$) | Sigma-Aldrich | P1190 |
| pre-stained protein ladder | Thermo Fischer Scientific | 26619 |
| puromycin | Sigma-Aldrich | P9620 |
| **R** | | |
| rabbit serum | Sigma-Aldrich | R4505 |
| ROTI®Block | Roth Carl | A151.1 |
| **S** | | |
| sodium chloride (NaCl) | Sigma-Aldrich | 31434 |
| sodium dodecyl sulfate (SDS) | Sigma-Aldrich | L5750 |
| sodium hydroxide (NaOH) | VWR | 31627.290 |
| Schneider's *Drosophila* medium | SERVA | 47521 |
| spectra multicolor broad range | Thermo Fischer Scientific | 26634 |
| **T** | | |
| TEMED | Roth | 2367.3 |
| 3,3′,5,5′-Tetramethylbenzidine (TMB) | Sigma-Aldrich | T4444 |
| tris | AppliChem | A1086.1000 |
| tris(2-carboxyethyl) phosphine hydrochloride (TCEP) | Sigma-Aldrich | 646547 |
| Triton X 100 | AppliChem | A1388.0500 |
| trypan blue solution 0.4% | Gibco | 15250061 |
| trypsin/EDTA 1X | Gibco | 25300054 |
| Tween 20 | Roth | 9127.1 |
| **U** | | |
| urea | Riedel-de Haen | 33247 |

### 2.13.2 Consumables

The list of consumables used in this research are described in **Table 21**.

**Table 21.** List of consumables.

| Consumable | Provider |
|---|---|
| inserts/ cell retainer | 352340, Becton Dickinson |
| Mini-PROTEAN TGX (Tris-glycine extended) gradient 4 -15% | 4568086, BioRad |
| Neubauer counting chamber | Optik Labor |
| Nunc Maxisorp flat-bottom 96-wells | 468667, Thermo Fischer Scientific |
| Poly-Prep® chromatography columns | 731-1550, BioRad |
| filter 0.22 µm Syringe | 726-2520, Thermo Fischer Scientific |
| SOLAµ reverse phase extraction plates | 60509-001, Thermo Fischer Scientific |
| Thermo EASY-Spray column | ES803, Thermo Fischer Scientific |

### 2.13.3 Equipment

The equipment used in this research is described in **Table 22**.

**Table 22.** List of equipment.

| Equipment | Provider |
|---|---|
| **Microscopes and cameras** | |
| Zeiss Axio Imager 2 microscope | Zeiss |
| Spot RT3 microscope camera | Diagnostic Instruments Inc |

**Table 22.** List of equipment (*continuation*).

| Equipment | Provider |
|---|---|
| **Microscopes and cameras** (*continuation*) | |
| Light microscope Primostar | Zeiss |
| **Centrifuges** | |
| Centrifuge Biofuge Stratos | ThermoFisher |
| Centrifuge Multifuge 3SR+ | Thermo Fischer Scientific |
| Microcentrifuge | Eppendorf |
| Minispin centrifuge | Eppendorf |
| **Pipettes** | |
| Micropipettes | Eppendorf |
| Multichannel pipettes | Eppendorf |
| **Mass spectrometry** | |
| Q Exactive HF-X Hybrid Quadrupole-Orbitrap Mass Spectrometer | Thermo Fischer Scientific |
| EASY-nLC™ 1200 liquid chromatography instrument | Thermo Fischer Scientific |
| **Incubators** | |
| CO2 incubator Series 3 Water Jacketed | Thermo Fischer Scientific |
| CO2, shaker incubator Minitron | INFORS HT |
| Shaker incubator Novotron | INFORS HT |
| Incubator Heraeus | Thermo Fischer Scientific |
| **Thermocyclers** | |
| Thermocycler trio 48 | Biometra |
| TProfessional Basic Gradient | Biometra |
| LightCycler® 480 | Roche |

**Table 22.** List of equipment (*continuation*).

| Equipment | Provider |
|---|---|
| **Spectrophotometer/ plate readers** | |
| ELISA plate reader Sunrise | Tecan |
| Multifunction plate reader Infinite M200 Pro | Tecan |
| Nanophotometer Pearl P-31 | Implen |
| **Electrophoresis and imaging systems** | |
| Trans-Blot Turbo transference system | BioRad |
| Power supply electrophoresis | BioRad |
| ChemiDOC XRS+ system | BioRad |
| Gel documentation system | Peqlab |
| **Other equipment** | |
| Biosafety cabinet class II Herasafe KS | ThermoFisher |
| Rotator roller mixer SRT9D | Stuart |
| Rotator Intelli-Mixer RM-2M | ELMI |
| Water bath WNB14 | Memmert |
| Thermomixer Comfort 5355 | Thermo Fischer Scientific |
| pH-meter 654 | Metrohm |
| Orbital shaker Unimax 2010 | Heidolph |
| Ultra-Turrax homogenizer | IKA |

## 2.14 Software

The software used in this research is described in **Table 23**.

**Table 23.** List of software.

| Software | Reference/ provider |
|---|---|
| GraphPad Prism V 6 | Graphstats Technologies |
| ExPasy-PeptideCutter | https://web.expasy.org/peptide_cutter/ |
| ImageLab V 6.0.1. | BioRad |
| pLink 2 version 2.3.9 | [117] |
| PyMOL V2.5 | Schrödinger, Inc. |
| CRISPOR interface | http://crispor.tefor.net/ |
| VisiView V.2.0.5 | Visitron Systems |
| RCSB Protein data bank (RCSB PDB) | https://www.rcsb.org/ |
| SnapGene v6.1.1 | Dotmatics |
| UniProt | https://www.uniprot.org/ |
| MSconverter v3.0.5930 ProteoWizard | https://proteowizard.sourceforge.io/ |
| UCSC Genome Browser | https://genome.ucsc.edu/ |
| BLAST: Basic Local Alignment Search Tool - NCBI | https://blast.ncbi.nlm.nih.gov/Blast.cgi |

# 3 RESULTS

## 3.1 Analysis of the role of BadA in *B. henselae* binding to Fn

The experiments performed in this section aimed to evaluate the importance of BadA presence for adherence of *B. henselae* to Fn. Two bacterial strains were used for these assays, *B. henselae badA* expressing strain (WT strain) and *B. henselae* BadA transposon mutant with a BadA deficient phenotype (BadA$^-$ strain). Bacterial binding (WT or BadA$^-$ strains) to human plasma Fn or cellular Fn were qualitatively and quantitatively evaluated.

### 3.1.1 Analysis of BadA binding to plasma Fn

Bacteria cultivated on hCBA (human Columbia blood agar) plates were used to assess *B. henselae* WT and BadA$^-$ binding to human plasma Fn. Cultivated bacteria were washed twice in 1X DPBS and tested for BadA and Fn presence via Western blotting and protein abundance using MS (**Figure 5**). Western blotting of cell lysates using rabbit anti-BadA and mouse anti-Fn antibodies revealed the presence of Fn only in WT bacteria (**Figure 5A**). Furthermore, the differing proteins between both strains (WT and BadA$^-$) were analysed by magnitude and significance using crosslinking mass spectrometry (XL-MS). The proteome analysis identified Fn as the only protein in human blood that bound *B. henselae* in a BadA-dependent manner (**Figure 5B**). These data were used as quality control to demonstrate that BadA is the only different bacterial protein between WT and BadA$^-$ strains and that Fn binding to *B. henselae* depends on the presence of BadA protein.

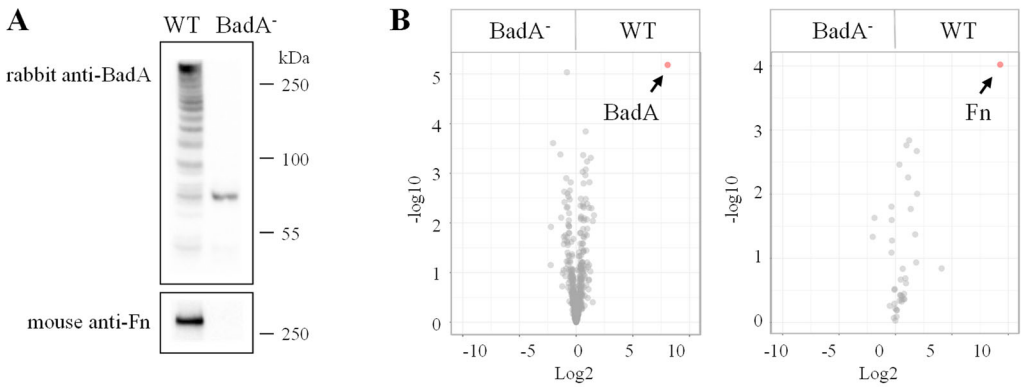


**Figure 5. Evaluation of *B. henselae* grown on human Columbia blood agar (hCBA) plates. (A)** Western blot evaluation of bacterial lysates demonstrating Fn bound to *B. henselae* WT. BadA (417 kDa monomer) and Fn (260 kDa monomer) proteins are shown in resolving gel. For BadA protein, WT strain shows a ladder-like structure resulting from incomplete denaturation of the trimeric BadA. For a complete image of the membranes, please refer to supplementary information (**Section 6.4**). **(B)** Volcano plot from data-independent acquisition MS-based proteomics (DIA-MS) demonstrating magnitude and significance of differing proteins identified in *B. henselae* WT and BadA$^-$ strains grown on hCBA. Arrows indicate proteins differing by log2 > 2-fold and P-value = 0.01 for the bacterial (left) and human (right) proteome. The volcano plot analysis was performed in collaboration with Dr Lotta Happonen, while a visit to Lund University (Sweden). The figures were adapted from [104].

As *B. henselae* WT has proven to bind plasma Fn from other species [20, 46] and to avoid a mixture of Fn from different species in further analysis, the presence of Fn in all bacterial stocks was tested to set up working conditions. Bacteria cultivated under various growth media were pelleted down and assessed for Fn presence using Western blotting. The assay demonstrated bacterial binding to Fn obtained from sheep blood (CBA plates) and calf serum (BaLi supplemented with FCS). Additionally, it was confirmed that bacteria cultivated using Fn-depleted FCS (BaLi supplemented with Fn-depleted FCS) effectively reduced the presence of background Fn (**Figure 6**). Based on this analysis, Fn-depleted FCS was used to supplement the liquid media for bacteria culture and bacterial stocks (**Section 2.9.1**).

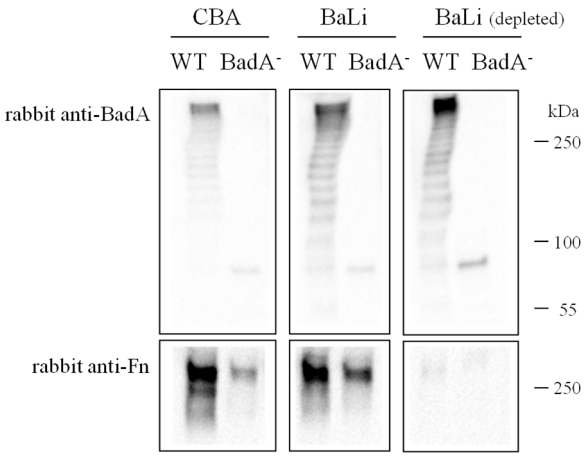


**Figure 6. Evaluation of Fn presence in *B. henselae* stocks**. Evaluation of Fn presence in bacterial stocks cultivated on Columbia blood agar plates (CBA) containing sheep blood, BaLi media containing fetal calf serum (FCS), and BaLi (depleted) containing FCS treated for Fn depletion. The analysis aimed to set up working conditions to reduce background Fn from different species. Western blotting was used to evaluate BadA and Fn presence in pelleted bacteria. BadA (417 kDa monomer) and Fn (260 kDa monomer) proteins were identified using rabbit anti-BadA and rabbit anti-Fn antibodies and are shown in resolving gel. For BadA protein, WT strain shows a ladder-like structure resulting from incomplete denaturation of the trimeric BadA. Please refer to supplementary information for a complete image of the membranes (**Section 6.4**).

Furthermore, bacteria and Fn interaction was quantitatively analysed using an ELISA format (**Figure 7**). ELISA-based titrations using different optical densities ($OD_{600}$) of *B. henselae* WT and µg of Fn were tested to identify working conditions. Bacteria binding to Fn were detected using rabbit anti-*B. henselae* antibodies. This assay revealed bacterial saturation above $OD_{600} = 0.3$ and 1 µg of Fn; these settings were used for further evaluation (**Figure 7A**). Increasing amounts of Fn were assessed against *B. henselae* WT and BadA$^-$ strains ($OD_{600} = 0.3$) to evaluate bacterial adherence to Fn. The assay revealed a dose-dependent *B. henselae* WT adherence, with a saturation of Fn reached at 1.0 µg per well, and a strongly reduced binding of *B. henselae* BadA$^-$ (**Figure 7B**).

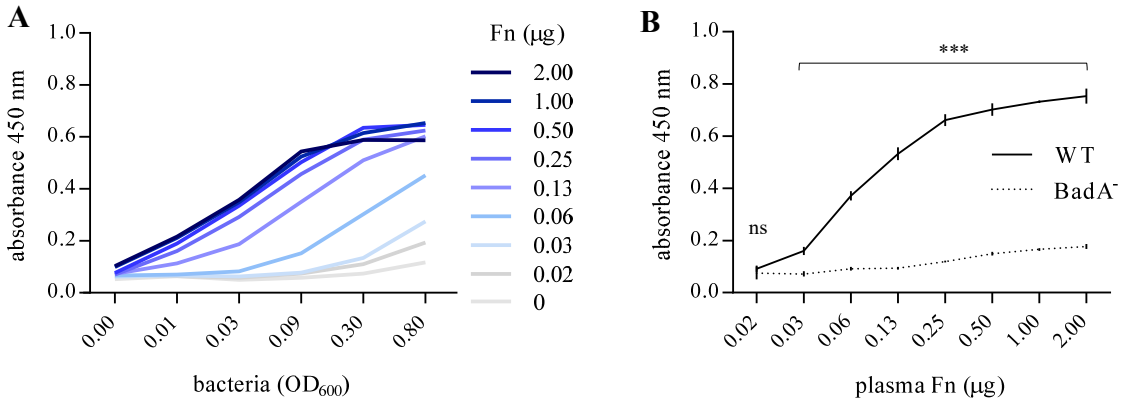


**Figure 7. ELISA-based titrations and dose-dependent binding of *B. henselae* to Fn-coated wells. (A)** Saturation conditions of bacteria and Fn were evaluated using microtiter wells coated with increasing amounts of Fn (µg) and exposed to increasing optical densities ($OD_{600}$) of *B. henselae* WT. Bacterial adherence was detected using rabbit anti-*B. henselae* antibodies. This assay was performed in two separate experiments with similar results. **(B)** Binding of *B. henselae* WT and BadA$^-$ ($OD_{600}$ = 0.3) to increasing amounts of immobilised Fn. Adherent bacteria were detected using rabbit anti-*B. henselae* antibodies. The mean and SD of quadruplicates are depicted. Statistical significance was determined using a two-way ANOVA with Šídák's multiple comparisons test between WT and BadA$^-$ (ns: not significant, *** P-value < 0.0001). Figure 7B was adapted from [104].

Finally, the interaction of BadA with Fn was documented using immunoelectron microscopy of bacteria pre-adsorbed with purified human plasma Fn in solution. Fn was identified using rabbit anti-Fn and gold-labelled antibodies. Results indicated the Fn deposition at the BadA-layer with nearly no Fn presence on the surface of *B. henselae* BadA$^-$ (**Figure 8**). These results were in congruence with the other observations in this section, demonstrating lesser Fn binding in the BadA$^-$ strain.

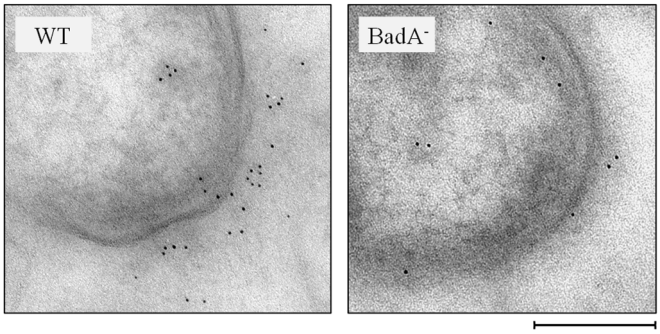


**Figure 8. Immunoelectron microscopy (IEM) of Fn bound to *B. henselae* WT and BadA$^-$.** Bacteria were incubated in solution with purified human plasma Fn and washed to remove any unbound protein. Fn (black dots) was detected using rabbit anti-Fn (primary) and gold-labelled (secondary) antibodies (scale bar: 200 nm). The IEM pictures were generated in collaboration with Ms. Birgit Fehrenbacher and Prof. Martin Schaller (Eberhard Karls-University of Tübingen, Germany). The figure was adapted from [104].

### 3.1.2 Analysis of BadA binding to cellular Fn

*B. henselae* binding to cellular Fn was evaluated using purified Fn from human foreskins (**Figure 9**). Cellular Fn was first analysed using SDS PAGE (**Figure 9A**), revealing the presence of several fragments, contrasting the one predominant fragment observed in plasma Fn. The presence of several fragments in cellular Fn was expected due to the description of different cellular Fn isoforms. Furthermore, *B. henselae* binding to cellular Fn was evaluated in dose-dependent (**Figure 9B**). Different amounts of cellular Fn were coated in microtiter wells and assessed for *B. henselae* WT and BadA$^-$ adherence. Dose-dependent *B. henselae* WT binding to cellular Fn was observed; however, a higher amount of cellular Fn was required to identify bacterial adherence, in contrast with plasma Fn (**Figure 7B**). The possibility of lesser binding due to less affinity to certain cellular Fn isoforms might be responsible for this reduced bacterial binding.

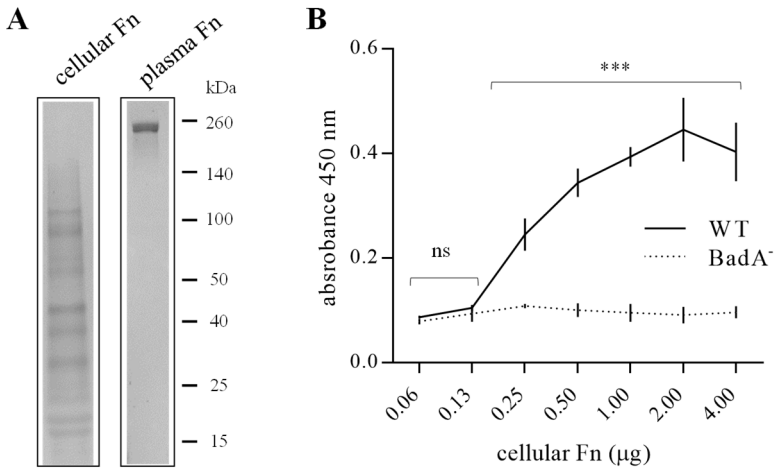


**Figure 9. Cellular Fn interaction with *B. henselae* WT and BadA$^-$. (A)** SDS PAGE of purified cellular and plasma Fn. Purified proteins were denatured, separated via SDS PAGE, and stained using Instantblue. Note the presence of several fragments in cellular Fn and one define fragment in plasma Fn. **(B)** Binding of *B. henselae* WT and BadA$^-$ (OD600 = 0.3) to increasing amounts of immobilised cellular Fn. Adherent bacteria were detected using rabbit anti-*B. henselae* antibodies. The mean and SD of triplicates are depicted. Statistical significance was determined using a two-way ANOVA with Šídák's multiple comparisons test between WT and BadA$^-$ (ns: not significant, *** $p<0.0001$). Figure 9B was adapted from [104].

### 3.1.3 Analysis of Fn binding outer membrane proteins of *B. henselae*

The relevance of the presence of BadA for Fn binding has been discussed in the previous sections, but other outer membrane proteins (OMP) such as OMP 43, OMP 89 and Pap 31 have also been reported to bind Fn [27, 28]. Therefore, the aim was to identify the presence of these proteins in the strains used in this research. For this, lysates of *B. henselae* WT and BadA$^-$ grown in hCBA plates were processed for MS analysis; data were collected using data-independent acquisition (DIA) and further analysed against the DDA library for *B. henselae* proteome. The analysis demonstrated the presence of Omp 43, Omp 89 and Pap 31 proteins in both *B. henselae* strains, with no difference in abundance (**Figure 10**). This assay demonstrated the presence of OMP 43, OMP 89 and Pap 31 in both bacterial strains used in this research. This result suggests that the "background" Fn-binding observed when using the BadA$^-$ strain might be related to the presence of these proteins but with lesser importance than BadA

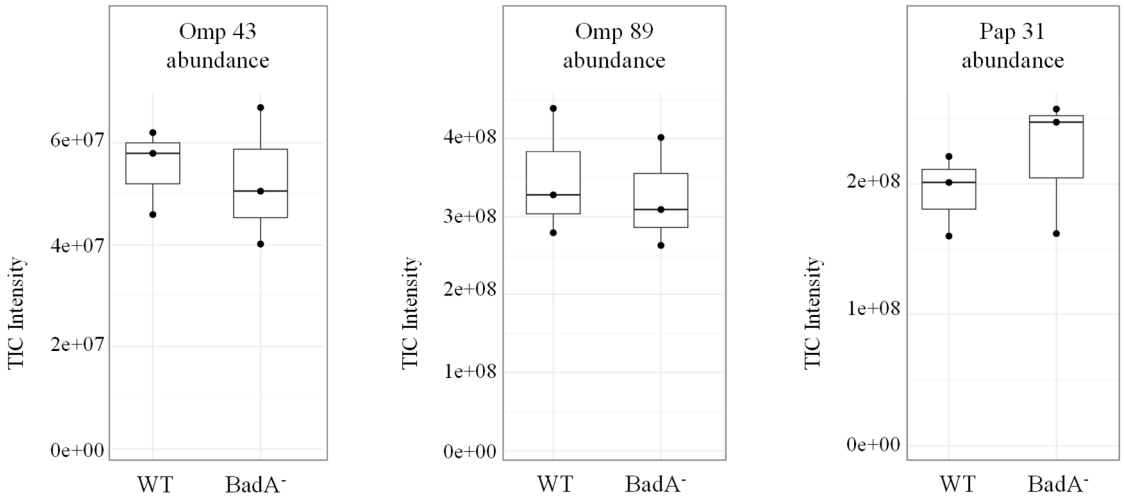


**Figure 10. Abundance of outer membrane Fn binding proteins in *B. henselae* WT and BadA$^-$.** Whole-cell bacteria growth on hCBA were processed for mass spectrometry (MS). Data-independent acquisition (DIA-MS) was used for the detection of outer membrane proteins (OMP) from *B. henselae* described as Fn binding proteins (FnBPs) [27]. Omp43 (UniProt accession number A0A0R4J8D0), Omp89 (UniProt accession number A0A0R4J719), and Pap31 (UniProt accession number A0A0R4J7W6). Note that all three proteins were present in both strains of *B. henselae* (WT and BadA$^-$) used in this study. The analysis was performed in collaboration with Dr Lotta Happonen, while a visit to Lund University (Sweden). This figure was adapted from [104].

## 3.2 Functional analysis of the BadA binding sites in Fn

As described, the presence of BadA is the primary determinant for *B. henselae* WT binding to cellular and plasma Fn. This interaction was verified by Western blotting, ELISA, MS and electron microscopy. To further analyse BadA-Fn interaction, two approaches were tested to localise Fn regions important for BadA binding: (i) proteolysis of Fn followed by bacterial binding assays and (ii) usage of commercially available Fn fragments for bacterial binding.

### 3.2.1 Analysis of BadA binding sites in Fn using a proteolysis approach

Proteolysis of Fn was pursued as an initial approach to identify the Fn regions important for BadA interaction. For this, full-length Fn was digested and subsequently incubated with *B. henselae* WT, followed by the identification of bacterial bond Fn-fragments using anti-Fn antibodies.

First, limited proteolysis using trypsin enzyme was tested. According to *in silico* digestion with trypsin using ExPasy-PeptideCutter program, human Fn canonical sequence (FINC_HUMAN P02751) includes 178 potential cleavage sites in Fn. Full-length Fn was digested with trypsin using specific time points and assessed via SDS PAGE (**Figure 11A**). Western blotting of trypsinised Fn was performed to evaluate Fn-fragments detection using rabbit anti-Fn antibodies. This assay revealed that polyclonal Fn antibody failed to detect all the trypsin-digested fragments observed in the SDS PAGE (**Figure 11B**). Furthermore, Fn digested for 45 s was selected for *B. henselae* binding to minimise the presence of full-length Fn (see **Figure 11B**). Trypsinized Fn was incubated with *B. henselae* WT in solution and assessed via Western blotting. Bacterial-bond Fn was identified after a longer exposure time only in a fragment corresponding to the full-length Fn; no other fragment (smaller size) was detected (**Figure 11C**).

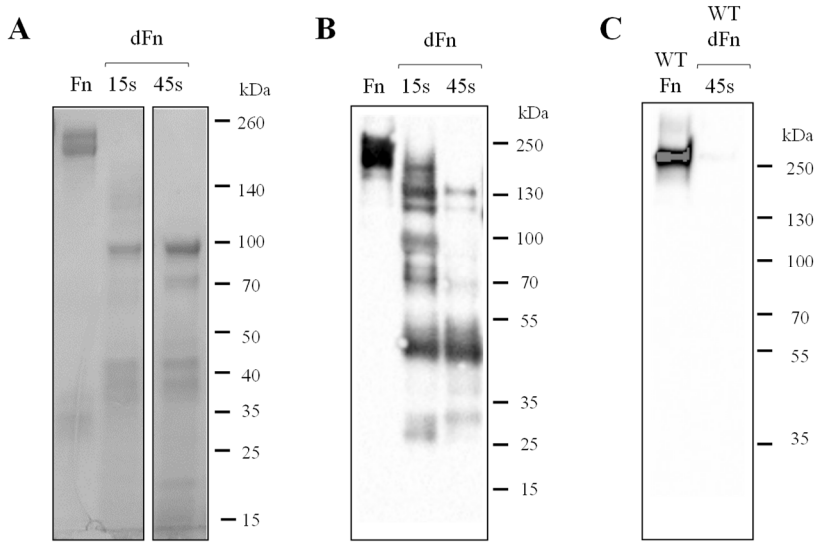


**Figure 11. BadA binding site in Fn using trypsin limited proteolysis approach.** Purified plasma Fn was digested with trypsin for selected time points and incubated with *B. henselae* WT to identify bacterial-bond Fn fragments. **(A)** SDS PAGE evaluation of full-length Fn (Fn) and digested Fn (dFn) using specific time points for digestion. **(B)** Western blot analysis of Fn and dFn for antibody detection using rabbit anti-Fn antibodies. Note the antibody detection of full-length Fn before 15 s digestion and the undetected antibody Fn-fragments compared to SDS PAGE. **(C)** Western blot evaluation of bacterial-bond Fn, rabbit anti-Fn antibodies were used for Fn detection.

Subsequently, an approach using enzymes with more restricted cleavage sites was proposed to aim the antibody detection of all Fn-fragments identified in SDS PAGE. *In silico* digestion

using Fn sequence and enzymes available in ExPasy-PeptideCutter database was performed. The enzymes thrombin, caspase I and factor Xa were selected based on their restricted number of cleavage sites.

Eight potential cleavage sites were obtained after *in silico* digestion using thrombin resulting in nine Fn-fragments after full Fn digestion. For *in vitro* digestion, two-time points were tested, and the result was evaluated via SDS PAGE. After 24 h of digestion, complete digestion was not achieved; this test was repeated using different buffer solutions and substrate-enzyme concentrations without successful results (**Figure 12A**). Western blotting using anti-Fn antibodies demonstrated that only high molecular weight fragments were detected by rabbit anti-Fn antibodies (**Figure 12B**). Digested Fn (dFn) was incubated with bacteria and assessed using rabbit anti-Fn antibodies for Fn identification. The assay revealed bacterial-bond Fn corresponding to full-length Fn size (**Figure 12C**).

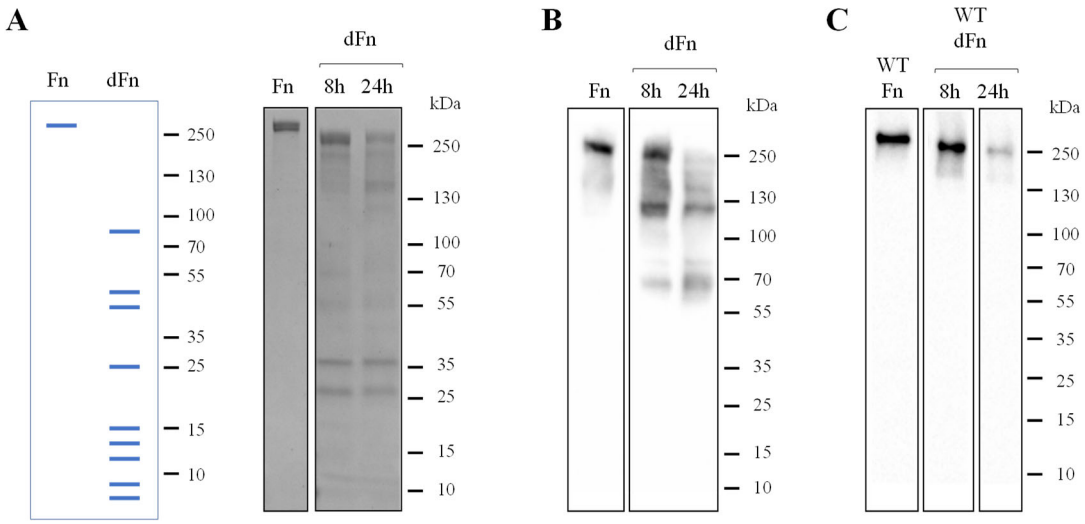


**Figure 12. BadA binding site in Fn using thrombin proteolysis approach.** Purified plasma Fn was digested with thrombin for selected time points and incubated with *B. henselae* WT to identify bacterial-bond Fn fragments. **(A)** *In silico* digestion (left) of full-length Fn (Fn) predicted nine digested Fn fragments (dFn) after full digestion (kDa: 5, 5.5, 14.2, 15.1, 15.4, 26.6, 46.2, 48.5, and 86.2). *In vitro* digestion (right) using specific time points was assessed using SDS PAGE. **(B)** Western blotting of Fn and dFn using rabbit anti-Fn antibodies. Note the antibody detection only for higher molecular weight Fn-fragments. **(C)** Western blotting of bacterial-bond Fn and dFn. Rabbit anti-Fn antibodies were used for detection.

Although trypsin and thrombin enzymes led to the digestion of full-length Fn according to the **Figure 11B** and **Figure 12B**, analysis of Western blotting of bacterial-bond dFn only identified a fragment with a size corresponding to full-length Fn. A final digestion test was performed using caspase I and factor Xa enzymes, aiming for complete Fn digestion and antibody identification of Fn-fragments (**Figure 13**). Caspase I enzyme was expected to cleave Fn in two sites producing three fragments, but complete digestion of full-length Fn and a clear digestion pattern were not achieved (**Figure 13A**). In the case of factor Xa enzyme, Fn cleavage was expected in one site resulting in two Fn-fragments. The presence of the expected two fragments were identified after 8 h of digestion, along with other fragments and undigested Fn. Factor Xa digestion of high-molecular-weight fragments was not achieved even after 24 h digestion (**Figure 13B**).

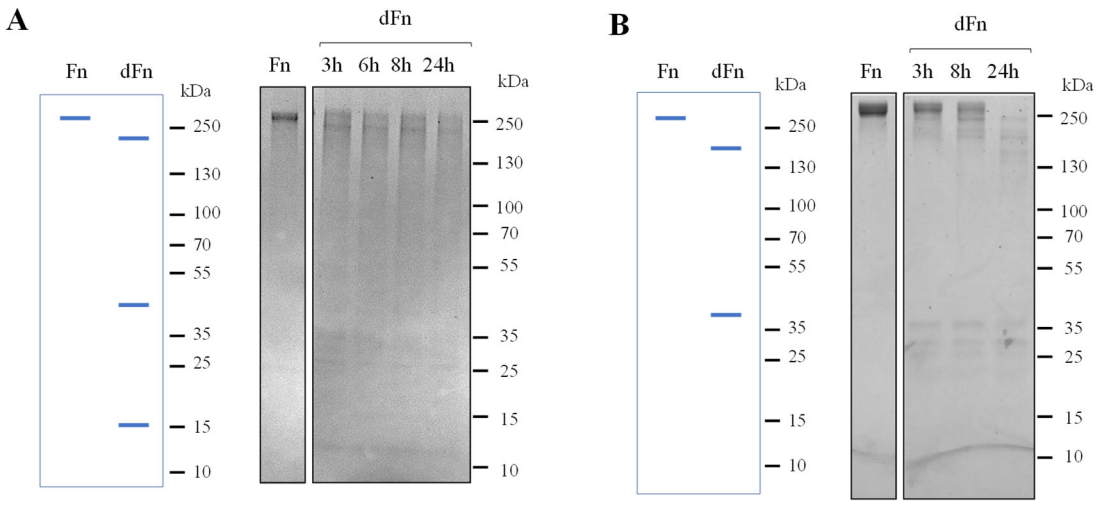


**Figure 13. Limited proteolysis approach using caspase I and factor Xa enzymes.** Purified plasma Fn was digested using caspase I or factor Xa enzymes for selected time points. **(A)** Fn digestion (dFn) using caspase I enzyme. *In silico* digestion (left) predicted three Fn-fragments after full digestion (kDa: 15.1, 44.4, and 203.2). *In vitro* digestion (right) using specific time points was assessed using SDS PAGE. **(B)** Fn digestion (dFn) using factor Xa enzyme. *In silico* digestion (left) predicted two Fn-fragments after full digestion (kDa: 41 and 220). *In vitro* digestion (right) using specific time points was assessed using SDS PAGE.

The approach of Fn proteolysis and bacterial incubation used in this chapter suffered from two significant drawbacks. First, complete digestion of full-length Fn was not achieved with any of the enzymes used by this approach; therefore, the only Fn-fragment identified binding bacteria was the one corresponding to a full-length Fn size. Second, not all the Fn-fragments produced after digestion were recognised by the rabbit anti-Fn antibodies, implying that the

identification of Fn-fragments with BadA affinity was restricted to the antibody recognition of Fn-fragments. Based on the previous limitations, this approach was no longer pursued for the functional analysis of BadA binding site in Fn.

### 3.2.2 Analysis of BadA binding sites in Fn using Fn fragments approach

To localise the Fn regions important for BadA binding, commercially available proteolytic Fn-fragments were obtained and used in bacterial binding assays. The fragments used for this assay included the heparin I (hep I) & gelatin-binding fragment (70 kDa fragment), the hep I-binding fragment (30 kDa fragment), the gelatin-binding fragment (45 kDa fragment), the cell-binding fragment (120 kDa fragment), and the heparin II (hep II)-binding fragment (40 kDa fragment). The name of each fragment corresponded to their affinities to other ECM components and cell adhesion molecules mentioned in the product description (**Figure 14**). The sequence coverage of each fragment was analysed using DDA-MS acquired spectra and PEAKS (version X) program (supplementary information, **Section 6.1**). This assay revealed the extension of each fragment related to the full-length Fn sequence: the hep I & gelatin-binding fragment included FnI 1-9, FnII 1-2; the hep I-binding fragment included FnI 1-5; the gelatin-binding fragment included FnI 6-9, FnII 1-2; the cell-binding fragment included FnIII 2-10, and the hep II-binding fragment included FnIII 13-15. The sequence coverage analysis revealed that only a few regions of the Fn molecule were not covered by the proteolytic fragments (FnIII 11-12,16, FnI 10-12, see **Figure 14**).

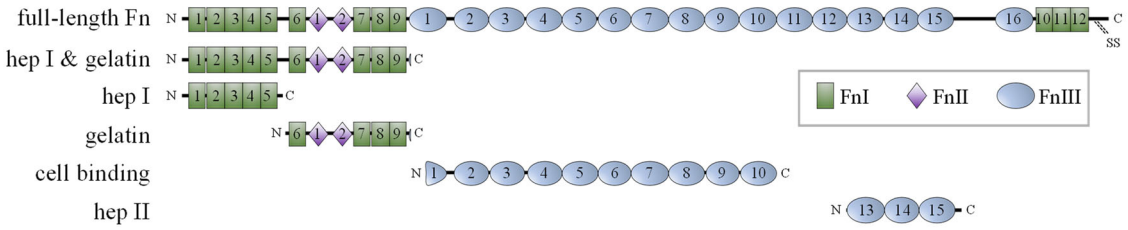


**Figure 14. Schematic representation of monomeric human full-length Fn and Fn-fragments.** Fn is composed of 12 type I domains (FnI), 2 type II domains (FnII), and 16 type III domains (FnIII). The distribution of five proteolytic fragments is depicted in the schematic representation. The names for the fragments correspond to their affinity to specific extracellular matrix components, as reported in the product description. A detailed analysis of the fragments' sequence coverage is given in supplementary information, **Section 6.1**. This figure was adapted from [104].

The purity of the Fn fragments was also evaluated by SDS PAGE, revealing the presence of additional bands in the hep II-binding fragment (**Figure 15A**). This result is congruent with the MS analysis observed for this fragment (**Section 6.1**). Western blotting of the fragments using rabbit anti-Fn antibodies showed that the hep I-binding Fn was not immunoreactive to the antibodies (**Figure 15B**). This fact limited the application of a suspension-based approach in binding assays between bacteria and proteolytic Fn fragments.

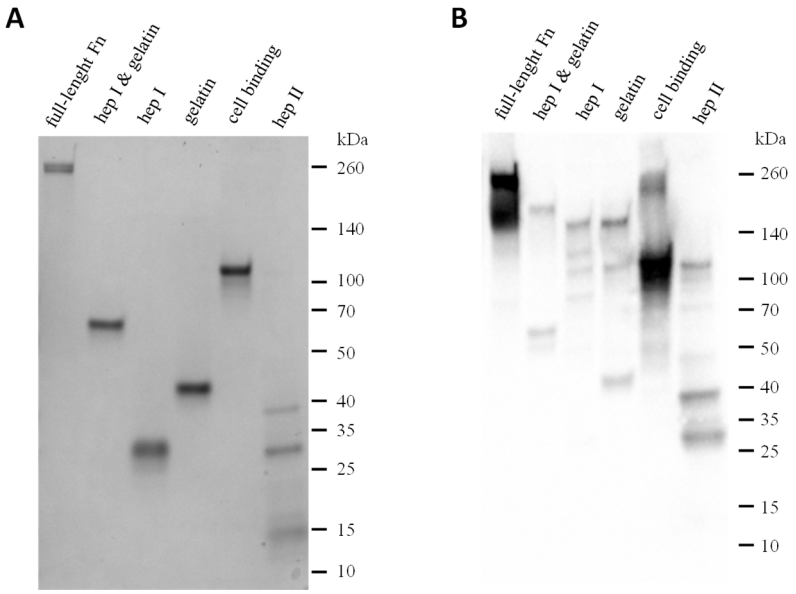


**Figure 15. Evaluation of purity and immunoreaction of proteolytic Fn fragments. (A)** SDS PAGE analysis of full-length Fn and proteolytic Fn fragments. The fragments used in this assay were the heparin I (hep I) & gelatin-binding fragment (70 kDa), the hep I-binding fragment (30 kDa), the gelatin-binding fragment (45 kDa), the cell-binding fragment (120 kDa), and the heparin II (hep II)-binding fragment (40 kDa). Note the presence of additional fragments (about 30 and 15 kDa) in the hep II-binding fragment. **(B)** Western blotting of full-length Fn and proteolytic Fn fragments using rabbit anti-Fn polyclonal antibodies. Note that the antibodies did not detect the expected 30 kDa fragment corresponding to the hep I-binding fragment.

The characterisation of BadA binding to full-length Fn or proteolytic Fn fragments was assessed using an ELISA approach. The bacterial (WT or BadA$^-$) adherence to immobilised Fn on microtiter wells was assessed using anti-*B. henselae* antibodies (**Figure 16**). The data showed interaction of *B. henselae* WT to full-length Fn and a strongly reduced interaction of *B. henselae* BadA$^-$, demonstrating the importance of BadA for Fn binding as evaluated in **Section 3.1**. Furthermore, the ELISA revealed that BadA-dependent interactions occurred with Fn fragments harbouring the hep I- or hep II-binding domains without significant differences compared to the full-length Fn. The cell-binding domain of Fn showed a lesser BadA-dependent interaction with *B. henselae*, whereas the gelatin-binding region did not show any interaction. The adherence of *B. henselae* WT to the latter two fragments (cell-binding and gelatin) was strongly reduced compared to full-length Fn.

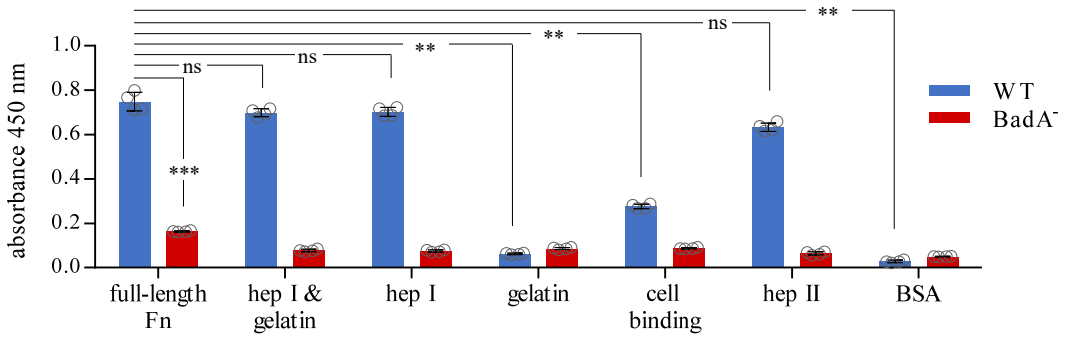


**Figure 16. Characterisation of the BadA binding site in Fn.** Microtiter wells were coated with full-length Fn, Fn fragments or BSA (negative control) and incubated with *B. henselae* WT or BadA$^-$ (OD = 0.3). Fn-bond bacteria were detected using rabbit anti-*B. henselae* and HRP conjugated anti-rabbit IgG antibodies. The mean and SD of quadruplicates are depicted. Statistical significance was determined using one-way ANOVA with Dunnett's multiple comparisons test (for the WT samples against the full-length Fn) and two-tailed unpaired Student's t-test (between WT or BadA$^-$ and full-length Fn), [ns: not significant; ** P-value < 0.0006, *** P-value = 0.0001]. The figure was adapted from [104].

### 3.2.3 Evaluation of competition between BadA and heparin for Fn binding

Taking into account the described interaction between Fn and heparin in the extracellular environment [61, 65], the functional role of the Fn domains hep I and hep II for BadA binding were further evaluated. As proof of principle, competition experiments between bacteria and heparin for Fn binding were carried out using ELISA and suspension-based assays.

As an initial approach, *B. henselae* and heparin were set in competition assays for binding to immobilised full-length Fn and Fn fragments. Fn-bond bacteria were detected using anti-*B. henselae* antibodies in an ELISA format. As a result, the presence of heparin reduced in a dose-dependent manner bacterial binding to immobilised full-length Fn and the corresponding Fn fragments (i.e. hep I/gelatin, hep I, and hep II fragments) (**Figure 17A**). Additionally, a suspension-based approach was used, incubating bacteria, heparin and full-length Fn together. Bacterial bond Fn was identified using mouse anti-Fn antibodies, demonstrating reduced Fn interaction when heparin was included (**Figure 17B**). The interaction between *B. henselae* WT and heparin was evaluated in bacterial binding assays to immobilised heparin in an ELISA format. This assay demonstrated that *B. henselae* WT failed to bind immobilised heparin, in contrast to the control full-length Fn (**Figure 17C**). The possibility that reduced bacterial binding to Fn observed in **Figure 17A and B** might be caused by an interfering interaction between *B. henselae* WT and heparin was excluded as bacteria failed to bind to immobilized heparin (**Figure 17C**).

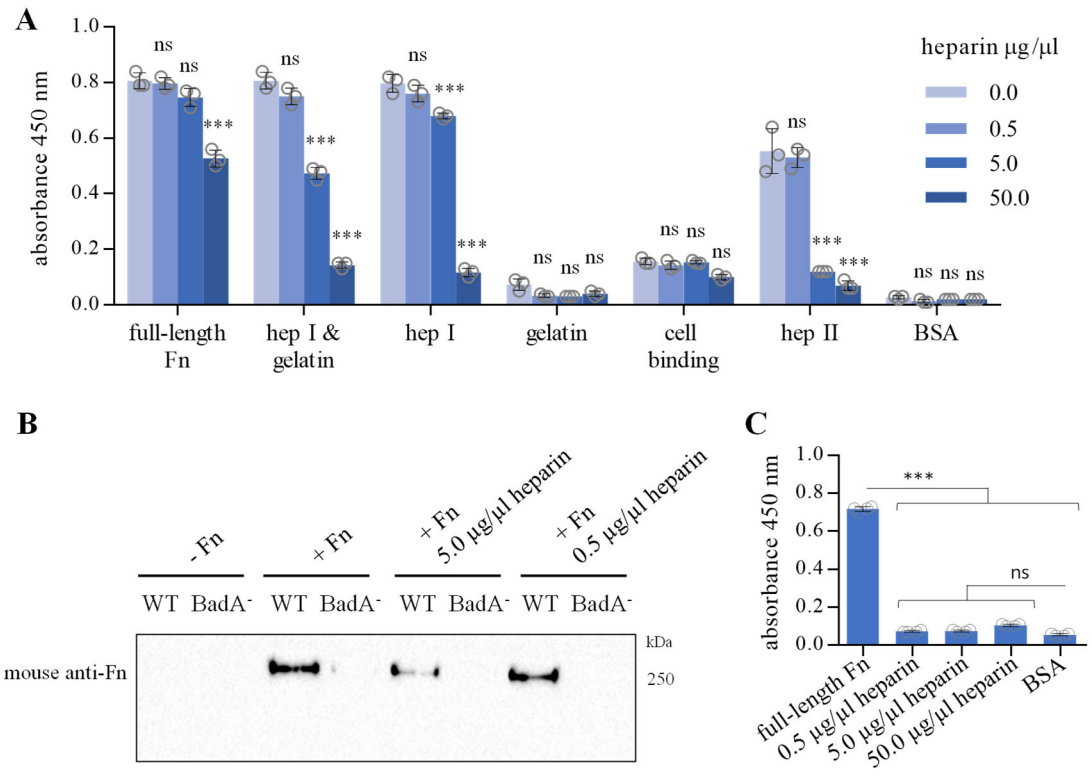


**Figure 17. Competition between BadA and heparin for Fn binding.** *B. henselae* WT and Fn binding was evaluated in competition assays with increased concentrations of heparin. **(A)** *B. henselae* WT (OD = 0.3) and increasing concentrations of heparin were added to Fn-coated microtiter wells, bacteria bond Fn was detected with rabbit anti-*B. henselae* and HRP-conjugated anti-rabbit IgG antibodies using an ELISA-based approach. The mean and SD of triplicates are depicted. Statistical significance was determined using two-way ANOVA with Dunnett's multiple comparisons test [ns: no significant; *** P-value < 0.0001]. **(B)** WT bacteria, Fn, and heparin were incubated in suspension. Bacterial pellets were washed, and bacterial-bond Fn was detected using Western blotting. The protein load (10 µg /lane) was quantified using BCA assay. Fn was detected using mouse anti-Fn and HRP-conjugated anti-mouse IgG antibodies. For a complete image of the membrane, please refer to supplementary information (**Section 6.4**). **(C)** *B. henselae* WT binding to various concentrations of immobilised heparin (or controls: Fn and BSA) was detected with rabbit anti-*B. henselae* and HRP-conjugated anti-rabbit IgG antibodies using an ELISA-based approach. The mean and SD of quadruplicates are depicted. Statistical significance was determined using one-way ANOVA with Šídák's multiple comparisons test [ns: no significant; *** P-value < 0.0001]. This figure was adapted from [104].

Hence, this section confirmed that BadA binding to Fn predominantly occurs within the hep I- and hep II-binding domains of Fn and competition with heparin inhibited BadA-mediated interaction with Fn in a dose-dependent manner.

### 3.2.4 Evaluation of binding inhibition using Fn-directed monoclonal antibodies

The assays from **Sections 3.2.2** and **3.2.3** revealed that hep I- and hep II-binding domains in Fn are important BadA interacting sites. Fn-directed monoclonal antibodies raised against these two domains were used to assess the binding inhibition of *B. henselae* by blocking these specific areas.

The immunogenic target of the monoclonal antibodies was mapped in the Fn sequence based on the product description information provided for each antibody, corresponding to the amino acids 32-307 for antibody TA803784 and a peptide mapping near the C-terminus [FnIII 12–14 [118]] for antibody SC18827 (**Figure 18A**). The specificity of the Fn-directed monoclonal antibodies was tested in Western blotting using Fn proteolytic fragments (for details about Fn fragments, refer to **Section 3.2.2**). This assay confirmed the specificity of the antibodies and evidenced that TA803784 might target the last part of hep I-binding region as it failed to detect this fragment (**Figure 18B**). Additionally, the antibody BD610078 reactive against the cell-binding domain was included as a negative control for the following experiment, as this Fn region was not of interest for BadA-mediated binding (**Section 3.2.2**).

Bacterial binding inhibition using Fn-directed monoclonal antibodies was tested in an ELISA-based approach. Fn-coated wells were incubated with the Fn-directed monoclonal antibodies, *B. henselae* binding was detected using rabbit anti-*B. henselae* antibodies. The assay demonstrated a slight inhibitory effect in *B. henselae* WT binding when using all antibodies but more prominently when blocking the hep II-binding domain with the antibody SC18827 (**Figure 18C**).

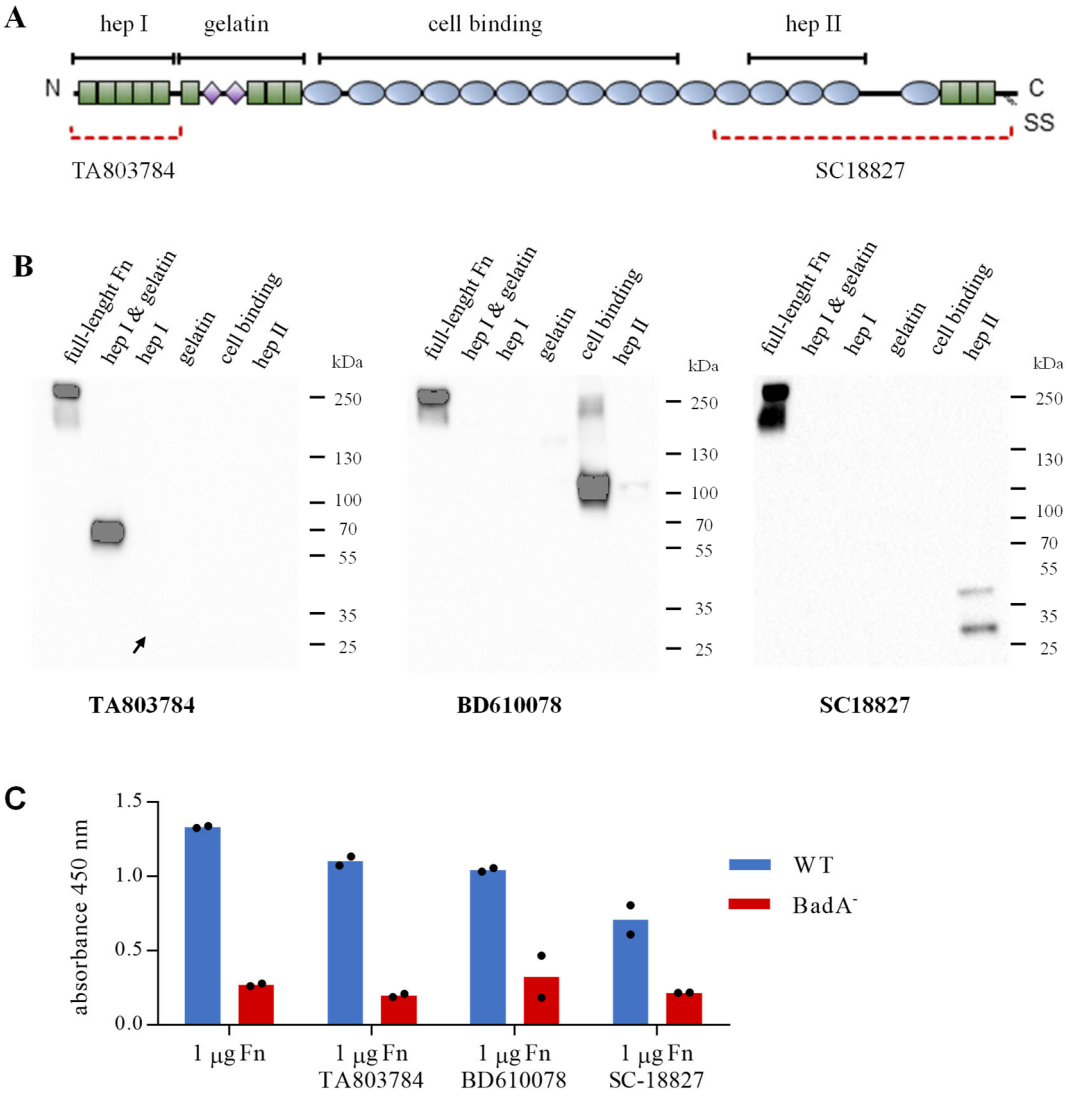


**Figure 18. Binding inhibition of BadA to Fn using Fn-directed monoclonal antibodies.** **(A)** Schematic representation of monomeric human full-length Fn, the coverage of the Fn proteolytic fragments is depicted on top of Fn. The immunogenic sequence reported for antibody production is shown in dotted lines and was obtained from the product specification and references [118]. For antibody BD610078 the immunogenic sequence is unknown. **(B)** Antibody specificity was assessed by Western blotting of proteolytic Fn fragments using mouse anti-Fn monoclonal antibodies (TA803784, BD610078 and SC18827) and anti-mouse antibodies. Note that TA803784 did not detect the hepI-binding fragment (arrow). BD610078 antibody directed against the cell-binding domain was included as a negative control, as this Fn-region reported lesser importance for BadA-mediated binding (**Section 3.2.2**). **(C)** Bacterial binding inhibition assay using Fn-directed monoclonal antibodies. Fn-coated wells were incubated with Fn monoclonal antibodies (TA803784, BD610078 and SC18827), wells were washed and incubated with *B. henselae* WT and BadA$^-$ (as a control). Bacterial binding was detected using rabbit anti-*B. henselae* and HRP-conjugated anti-rabbit IgG antibodies. The mean of duplicate samples is depicted.

Additional assays using increasing concentrations of inhibitor (Fn-directed monoclonal antibody) and other antibodies targeting the hep I-binding region should be performed to conclusively determine the importance of each of the heparin-binding domains for BadA binding.

### 3.3 Analysis of the interaction sites between BadA and Fn using crosslinking mass spectrometry (XL-MS)

In the previous section, BadA interactions with Fn were identified within Fn's hep I- and hep II-binding domains (**Section 3.2**). In order to analyse BadA-Fn interactions on a molecular level, whole *B. henselae* were incubated with Fn; interactions were analysed using liquid chromatography-MS (LC-MS).

As BadA binds both plasma and cellular Fn (**Sections 3.1.1** and **3.1.2**), Fn from different sources was used for these assays: recombinant (Rn) Fn, cellular Fn, and plasma Fn (adsorbed by *B. henselae* from hCBA plates). Depending on the Fn type, two groups of samples were analysed. Simple sample referred to Rn Fn as this represents a pure preparation. Complex samples referred to cellular and plasma Fn as they contain: a mixture of different isoforms (cellular Fn, **Figure 9A**) or other human proteins present in the blood (plasma Fn obtained from hCBA plates). Extensive washing followed the incubation with Fn; subsequently, covalent crosslinking of the N-terminal lysine residues was performed using DSS. The crosslinked samples were digested with trypsin and analysed using DDA-MS. The program pLink 2 was used for the data processing (**Figure 19**).

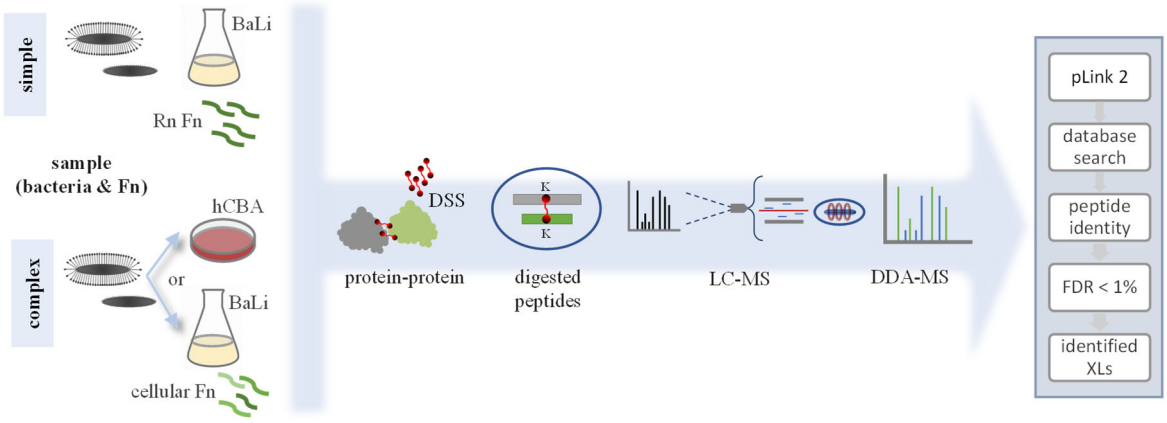


**Figure 19. Graphical scheme for crosslinking mass spectrometry analysis approach.** Whole-cell *B. henselae* (WT or BadA$^-$) were incubated together with recombinant (Rn) Fn [simple sample], and plasma Fn (hCBA) or cellular Fn [complex samples]. *B. henselae* BadA$^-$ was used as a negative control for the identification of false crosslinked peptide pairs. Interacting N-terminal lysine (k) residues were covalently crosslinked using disuccinimidyl suberate (DSS). Proteins were digested with trypsin, and the peptides were analysed by liquid chromatography-MS (LC-MS) and further data-dependent acquisition MS-based analysis (DDA-MS). pLink 2 software was used for the identification of crosslinks (XLs). The peptide identity was reported with a false discovery rate (FDR) of less than 1%. This figure was adapted from [104].

### 3.3.1 Evaluation of Fn isoforms for the crosslinking analysis

For the crosslinking analysis using the pLink program, every set of samples required a database including the proteins of interest. The database contained BadA (GenBank: MK993576.1) and human Fn (UniProt: P02751) amino acid sequences. The decision about the Fn isoform sequence to be used for the analysis was performed as follows.

For Rn Fn samples, the sequence of Fn isoform 1 was selected as this was used for the recombinant expression of *FN1* in HEK 293 cells (provider specifications). For plasma Fn (hCBA) samples, isoform 1 sequence was used as this was reported as canonical Fn sequence in UniProt, and a clear Fn fragment was observed after Western blotting of bacterial bond Fn from hCBA plates (**Figure 5A**). For cellular Fn samples, a mixture of Fn isoforms was expected based on the observations from **Figure 9A**. An alignment (MUSCLE) using the Fn isoforms available in UniProt (16 sequences) revealed sequence variation located in the EIIIB and EIIIA alternatively spliced regions and at the C-terminus (**Figure 20**, protein alignment). To identify the most prominent isoform in *B. henselae* WT samples incubated with cellular Fn, crosslinked samples were evaluated using DDA-MS and PEAKS program,

including the *Homo sapiens* proteome. The analysis showed isoform 14 as the most prominent in *B. henselae* WT samples, with a protein sequence coverage of 60%. Isoform 14 was closely followed by isoforms -9, -10, and -8 (**Figure 20**, sequence coverage in WT samples). Interestingly, the isoforms with the highest coverage percentage did not contain the EIIIB or EIIIA regions which have been described as more prominently present in cellular Fn [66].

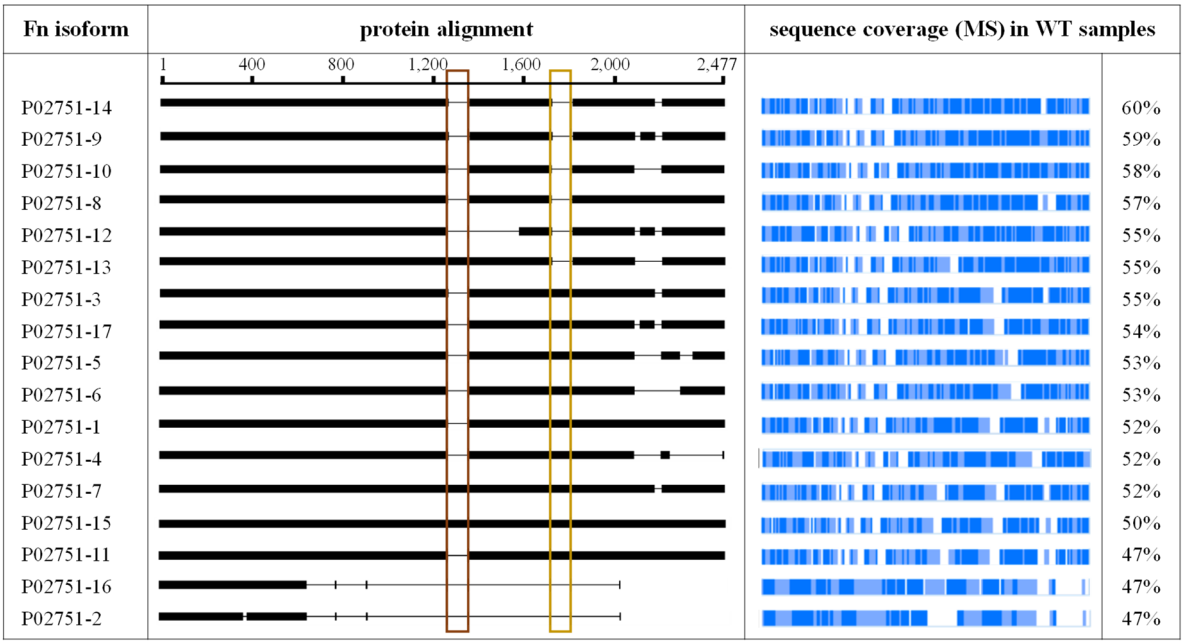


**Figure 20. Protein sequence alignment of reported Fn isoforms and peptide sequence coverage for cellular Fn samples.** Protein alignment of Fn isoforms reported in UniProt using MUSCLE alignment. The location for EIIIB and EIIIA sequences are depicted by brown and yellow rectangles, respectively. On the right-hand side, the sequence coverage for each isoform in crosslinked *B. henselae* WT samples is depicted. For this, WT samples were incubated with cellular Fn; interactions were crosslinked and prepared for mass spectrometry analysis (MS) using the data-dependent acquisition (DDA) method. The percentage of protein sequence covered by the peptides identified in MS was determined using PEAKS program. The coverage is visualised by coloured bars where: light blue blocks represent part of the sequence covered by low-confidence peptides; dark blue blocks represent parts covered by high-confidence peptides. The percentage of coverage of each Fn isoform identified in cellular Fn samples is depicted. The sequence coverage analysis was performed in collaboration with Dr Lotta Happonen (Lund University, Sweden). This figure was adapted from [104].

Crosslinked cellular Fn samples were analysed in pLink using the isoform with the highest peptide sequence coverage (isoform 14) in the database. As the sequence coverage for the other isoforms was closely related and to evaluate variability in the crosslinked peptides identification, the analysis was repeated in two independent tests using isoform 15 (includes

EIIIB and EIIIA regions) and isoform 1 (canonical sequence). The results from the three separate analyses showed the same list of crosslinked peptides as when using isoform 14. On this basis, the Fn isoform 1 sequence was selected for the database analysis of all the samples included in this research.

### 3.3.2 Evaluation of sample pre-treatments to enrich inter-crosslinks identification

The crosslinking analysis from all samples revealed a total of 462 crosslinks (XLs) corresponding to both intra-protein XLs (BadA-BadA or Fn-Fn) and inter-protein XLs (BadA-Fn). Inter-protein XLs accounted for 6.3% (n = 29) of the total XLs identified and were identified in both, simple samples (n = 17) and complex samples (n = 12) (**Figure 21A**). Moreover, as whole intact bacteria were used for crosslinking, a combination of approaches was applied to reduce the background noise from intracellular bacterial proteins and facilitate the XLs identification. First, two concentrations of DSS crosslinker were tested (500 and 2,000 μM); and second, after crosslinking, half of each sample was directly processed for MS (i.e. whole-cell *B. henselae* with adsorbed Fn), while the other half was first treated by limited proteolysis to release surface-proteins before MS processing (i.e. surface-attached *B. henselae* proteins with adsorbed Fn). The inter-protein XLs identified were found in all treatment types but predominantly when using the lower crosslinker concentration and in the surface-attached proteins, demonstrating improvement for inter-XLs using these treatments. The XLs found in the samples using the BadA$^-$ strain (negative) accounted for false-positive identifications due to the complex background proteome and were not included in the analysis. None of the exact inter-protein XLs found in *B. henselae* WT (positive) samples were identified in *B. henselae* BadA$^-$ (negative) samples (**Figure 21B**).

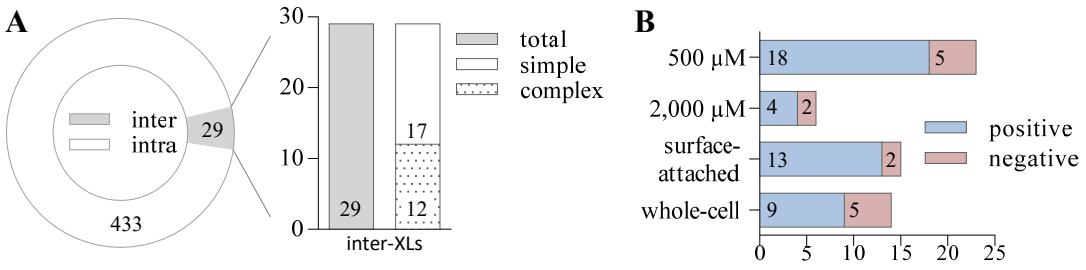


**Figure 21. Evaluation of sample pre-treatments to improve inter-crosslinks (XLs) identification**. **(A)** Total number of BadA and Fn-related XLs identified, including intra-XLs (BadA-BadA/Fn-Fn) and inter-XLs (BadA-Fn). The inter-XLs (n = 29) identified in complex samples (hCBA and cellular Fn; n = 12) and simple samples (Rn Fn; n = 17) are depicted in bars. **(B)** Analysis of sample treatment for inter-XLs identification. The effect of different DSS concentrations (500 µM or 2,000 µM) and sample pre-treatment (surface proteins or whole-cell proteins) was evaluated. Interactions found for positive samples (*B. henselae* WT, blue bars) and negative control samples (*B. henselae* BadA$^-$, pink bars) are given. This figure was adapted from [104].

### 3.3.3 Synopsis of BadA-Fn interacting sites

As unique interactions were identified in the sample pre-treatment described in the previous section, all inter-protein XLs identified in positive samples were included for further evaluation (n = 22). A total of 16 BadA-Fn interaction interfaces were identified in cellular, plasma (hCBA), and Rn samples. Some interactions were observed in more than one-time occurrence within the same sample type. The location of the crosslinked peptides was traced in Fn and BadA sequences. A summary of the XLs identified is described in **Table 24**.

**Table 24.** Inter-protein crosslinked peptides identified for BadA and Fn. Interacting peptides identified in Rn, plasma, and cellular samples using pLink 2. Interactions with a reported false discovery rate (FDR) less than 1 are shown. This table was adapted from [104].

| Fn source | | XLs code | occurrence | Fn | | BadA | |
|---|---|---|---|---|---|---|---|
| | | | | peptide | location | peptide | location |
| simple | Rn | d | 1 | IGDTWSKKDNR | FnI 5 [hep I] | TVNGEGKEEEK | stalk [18, 22, 26] |
| | | e | 1 | IGDQWDKQHDMGHMMR | FnI 7 [gelatin] | VKTVNGEGK | stalk [14,16,18,20,22,24,26,28] |
| | | i | 1 | WLPSSSPVTGYRVTTTPKNGPGPTK | FnIII 11 | LEKGVSKATQENSK | stalk [15,19,23] |
| | | j | 1 | TIKPDVR | FnIII 14 [hep II] | VNNNVTNKFNELTQSITNVTQQVK | stalk [19,23] |
| | | k | 3 | YEKPGSPPR | FnIII 15 [hep II] | VEDKLTEAVGK | stalk [13,17,21,25] |
| | | l | 1 | DQQRHKVR | FnIII 16 | VKTVTGEGK | stalk [2] |
| | | m | 1 | DQQRHKVR | FnIII 16 | GQLDKGLK | stalk [4-5,8-9] |
| | | n | 1 | GATYNVIVEALKDQQR | FnIII 16 | VEDKLTEAVGK | stalk [13,17,21,25] |
| | | o | 4 | WCHDNGVNYKIGEK | FnI 11 | DGKKNNVTFDVAR | TRP ring/unpredicted |
| complex | cellular | a | 1 | PEAEETCFDKYTGNTYR | FnI 2 [hep I] | GASKATQENSK | stalk [2,6,10] |
| | | c | 1 | IGDTWSKKDNR | FnI 5 [hep I] | LEKGASK | stalk [27] |
| | | f | 1 | IGDQWDKQHDMGHMMR | FnI 7 [gelatin] | LTHVENGDVSEKSK | stalk [29] |
| | | g | 1 | IGFKLGVR | FnIII 6 [cell binding] | QMKIVLDDAK | unpredicted (close to anchor) |
| | plasma hCBA | b | 1 | IGDTWSKK | FnI 5 [hep I] | ATQENSKITYLLDGDVSK | stalk [2,6,10] |
| | | h | 1 | TEIDKPSQMQVTDVQDNSISVK | FnIII 10 and 11 | LTEAVGKVTQQVK | stalk [13,17,21,25] |
| | | j | 1 | TIKPDVR | FnIII 14 [hep II] | VNNNVTNKFNELTQSITNVTQQVK | stalk [19,23] |
| | | p | 1 | IGEKWDR | FnI 11 | TVNGEGKEEEK | stalk [18,22,26] |

The distribution of the identified crosslinked peptides in the protein sequences reveals a complex network of interaction at the interface between BadA and Fn (**Figure 22**). BadA interactions were identified in Fn regions covered by the proteolytic Fn fragments, for which information about bacterial binding could be gathered from the ELISA assay (**Section 3.2.2**). Other XLs were identified in regions that were not covered by the Fn fragments. Fn interactions in BadA were mainly distributed along the BadA neck/stalk region and predominantly identified in the repetitive domains (domains= 2/6/10/27, 13/17/21/25, 18/22, 19/23). It is worth noting that the BadA interactions with cellular Fn were observed only within the hep I-binding domain, while the interactions with plasma and Rn Fn were detected in hep I- and hep II-binding domains, but mostly within the regions not included in the ELISA assay.

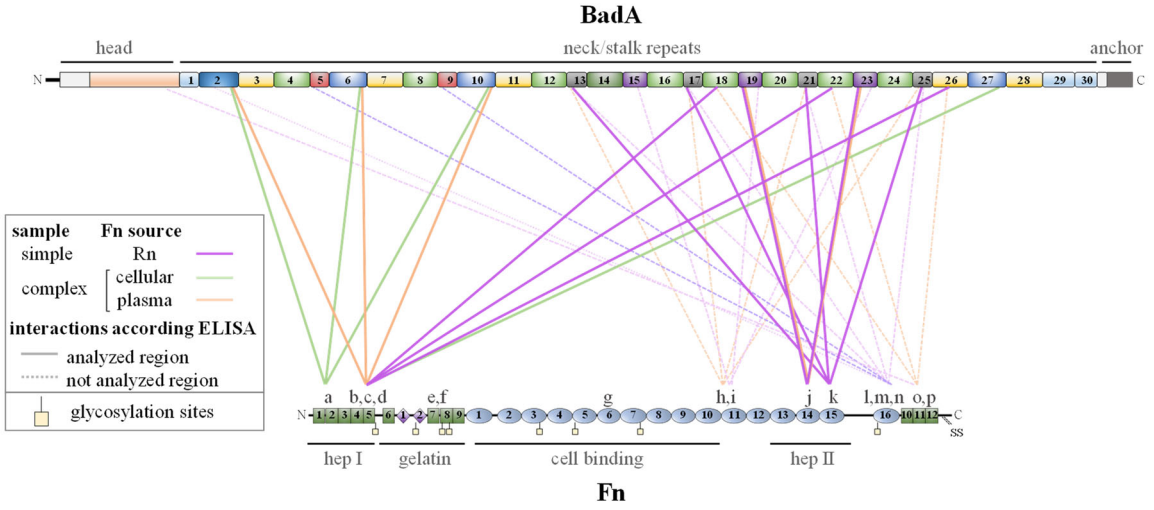


**Figure 22. Schematic map of identified crosslinked BadA-Fn interactions.** For BadA, the BadA regions (head, neck/stalk repeats, and anchor) and similar domains are depicted in matching colours. For Fn, the extension of the proteolytic fragments identified by their interaction with other ECM components, as well as the glycosylation sites reported in the literature [119] are shown. The BadA-Fn crosslinked peptides are indicated as "a"- "p" (for sequence details, please refer to **Table 24**). The interactions occurring within areas analysed by ELISA (see **Section 3.2.2** for details) are shown in continuous lines, while interactions occurring in Fn regions for which no proteolytic fragments were available are given in dotted lines. Three XLs within gelatin and cell-binding Fn regions ("e","f","g") were not supported by ELISA. This figure was adapted from [104].

One XL was detected between the BadA head region and the C-terminus of Fn (XL "o"). The crosslinked sequence corresponded to a BadA region with an available three-dimensional structure. By rendering the BadA head domain (PDB: 3D9X) [45] and the FnI 11 (PDB: 2EC3) structures next to each other, it was corroborated that the crosslinked

lysine residues are surface exposed. This highlighted the feasibility of the identified interaction interface (**Figure 23**).

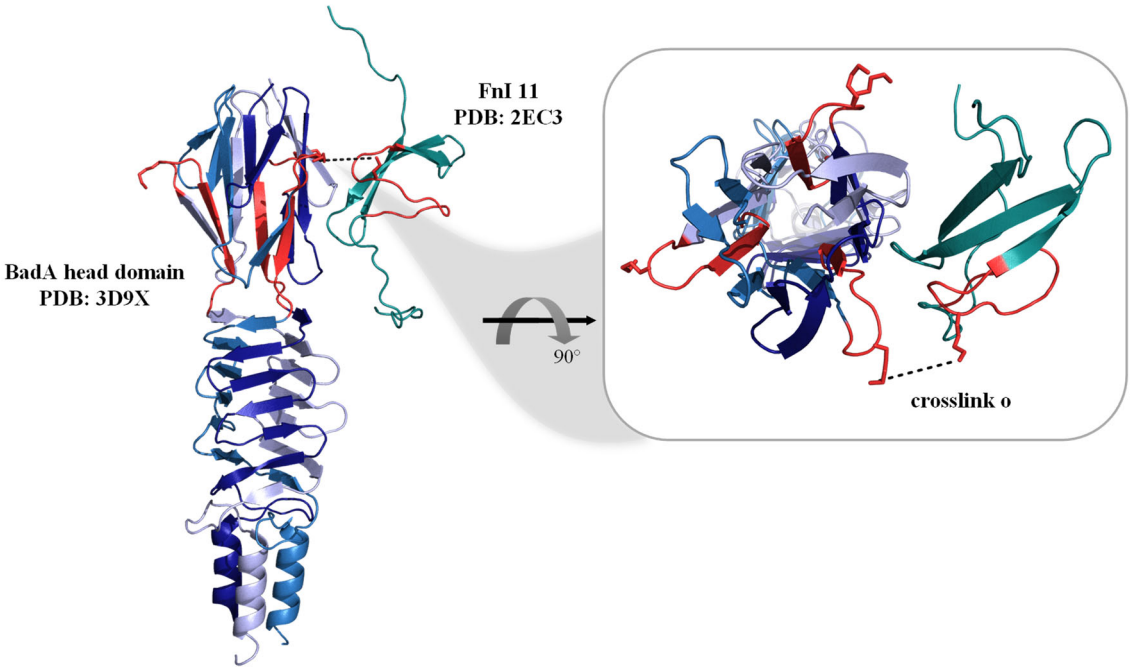


**Figure 23. Analysis of crosslink "o" identified between the BadA head and C-terminus of Fn.** BadA head domain crystal structure (PDB: 3D9X) [120] rendered next to the FnI 11 NMR structure (PDB 2EC3). The three BadA monomers are shown in shades of blue, and the FnI 11 domain in dark cyan. The peptides identified as crosslinked are indicated in red (crosslink "o" in **Table 24**), and the identified crosslink between one of the BadA monomers and the Fn fragment is indicated as a black dotted line drawn between the lysine (K) residues. The insert shows a top view (turn 90°C) of the interacting peptides using one of the monomers as an example. Figure generated using PyMOL. This figure was adapted from [104].

Taken together, several possible interaction interfaces between BadA and Fn were identified, some of which (XLs = a, b, c, d, j, k) were supported by the complementary ELISA-based assays using proteolytic Fn fragments (**Section 3.2.2**).

### 3.4 Evaluation of CRISPR-Cas-mediated *FN1* knockout in human ECs

*FN1* knockout ECs were generated to evaluate the role of Fn in bacterial adherence to ECs. *FN1* gene was targeted using single or dual guide RNA (gRNA) directed lentiviral CRISPR-Cas9. Two types of ECs were tested for *FN1* knockout to select a host cell model for bacterial adherence under loss-of-function conditions.

#### 3.4.1 Evaluation of Fn knockout strategies using single or dual gRNA

The transcription starting site (TSS), the 5′ untranslated region (UTR), and introns 1 and 3 were targeted, the selection of gRNA was based on their specificity to *FN1* and off-target prediction. Furthermore, treatments using dual gRNA (ECs 1 - 5) or single gRNA (ECs 6, 7) were tested for Fn knockout efficiency. An empty vector (without gRNA) was included in the treatments to maintain the WT phenotype (ECs vector). The distribution of gRNA in *FN1* and gRNA combination is depicted in **Figure 24**.

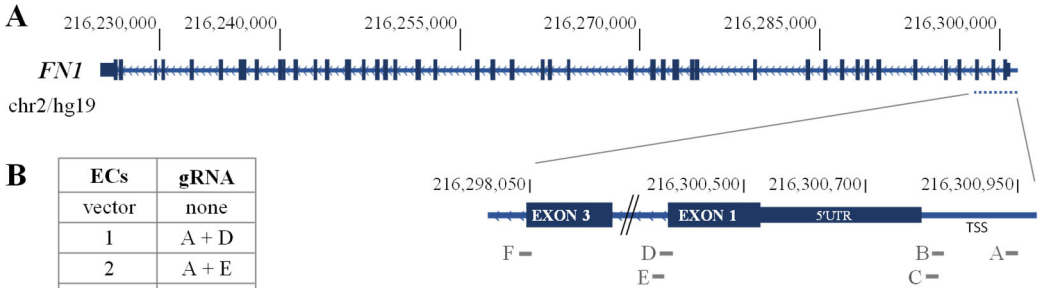


**B**

| ECs | gRNA |
|---|---|
| vector | none |
| 1 | A + D |
| 2 | A + E |
| 3 | B + D |
| 4 | B + E |
| 5 | C + D |
| 6 | D |
| 7 | F |

**Figure 24. Schematic draft of the *FN1* gene and targeted areas by guide RNAs (gRNA). (A)** The *FN1* sequence gene was rendered from the UCSC Genome Human Assembly Feb. 2009 (GRCh37/hg19). In the figure, an enlargement of the region targeted by the gRNAs is shown including the 5′ untranslated region (UTR), transcription starting site (TSS), introns 1 and 3 (left to the respective exons) as a reference. The selected gRNAs and the target regions are shown (A – F). **(B)** Treatments applied for the generation of *FN1* knockout ECs. The ECs vector sample was used as a control, it contains the empty vector (no gRNA) and produces the WT phenotype. The combinations used for dual gRNA treatment are shown for ECs 1 to 5, single gRNA treatment was applied for ECs 6 to 7. This figure was adapted from [104].

For an initial knockout test, *in house* isolated HUVECs (passage 3) were evaluated using the gRNA combinations described in **Figure 24B**. The knockout treatments were evaluated via mRNA levels (RT-qPCR) and protein presence (Western blot). The mRNA levels and protein Fn analysis revealed that dual gRNA strategies ECs 1, 3, and 5 produce a successful *FNI* knockout, in contrast to single gRNA strategies (ECs 8, 9). The dual gRNA ECs 2 and 4 failed to generate *FN1* knockout cells, possibly related to the target efficiency of the shared gRNA E. The approaches targeting the transcription start site (TSS, gRNA A) or 5′ UTR (gRNA B, C) and the intron 1 region (gRNA D) led to more efficient *FN1* knockout (**Figure 25**).

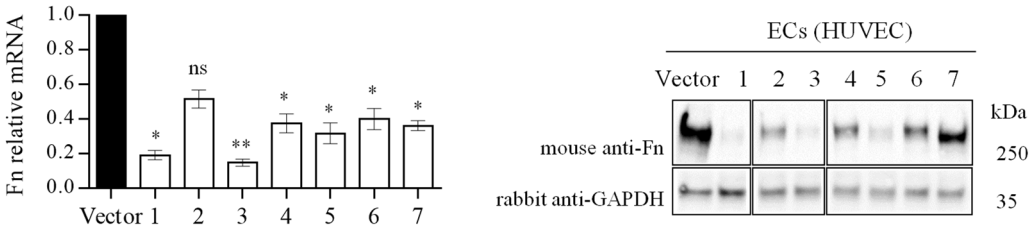


**Figure 25. Evaluation of *FN1* knockout using single or dual gRNA strategies.** Relative quantification of normalised *FN1* mRNA levels is depicted (left). RNA was extracted from different HUVECs treatments, and mRNA relative quantification was evaluated using *beta-actin* as a housekeeping gene for calibration. The mean and SD of triplicates are depicted. Statistical significance was determined using one-way ANOVA with Dunnett's multiple comparison test (ns: not significant; * P-value $< 0.0096$; ** P-value $= 0.0007$). Fn protein in HUVECs was evaluated using Western blotting (right). Protein extracts were separated using SDS PAGE, and Fn protein was identified using mouse anti-Fn antibodies. Identification of GAPDH protein was included as a control and was detected using rabbit anti-GAPDH antibodies. Please refer to supplementary information for a complete image of the membranes (**Section 6.4**). This figure was adapted from [104].

Each knockout treatment generated a polyclonal population of HUVECs observable by the presence of groups of cells with Fn staining in immunofluorescence. Furthermore, phenotypic changes were identified within the same treatment, with the presence of fibroblast-like cells (elongated thin cells) after cell passages. For these reasons, a second experiment was performed, including early passage HUVECs (Promocell, passage 1) and HMEC-1, as a cell line intended for monoclonal isolation. For this assay, only the successful dual gRNA strategies (ECs 1, 3 and 5) were included (**Figure 26**). ECs 1 and 3 were selected for further evaluation.

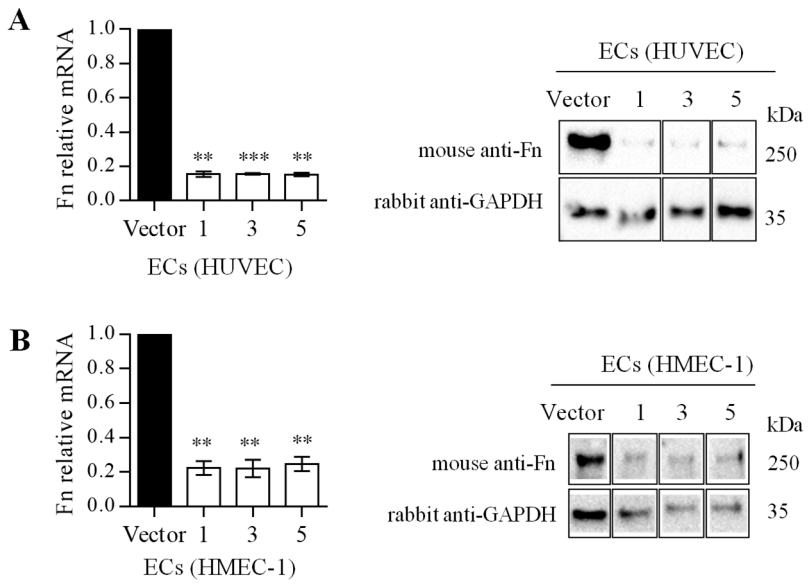


**Figure 26. Evaluation of *FN1* knockout using dual gRNA strategies in HUVEC and HMEC-1.** Early passage HUVEC **(A)** and HMEC-1 **(B)** were tested for *FN1* knockout using dual gRNA approaches. Relative quantification of normalised *FN1* mRNA levels is depicted (left). RNA was extracted from different ECs treatments, and mRNA relative quantification was evaluated using *beta-actin* as a housekeeping gene for calibration. The mean and SD of triplicates are depicted. Statistical significance was determined using one-way ANOVA with Dunnett's multiple comparison test (For HUVEC: ** P-value < 0.0003, *** P-value < 0.0001; for HMEC-1: ** P-value < 0.0017). The presence of Fn protein in ECs was identified using Western blotting (right). Protein extracts were separated using SDS PAGE, and Fn protein was detected using mouse anti-Fn antibodies; identification of GAPDH protein was included as a control using rabbit anti-GAPDH antibodies. Please refer to supplementary information for a complete image of the membranes (**Section 6.4**).

### 3.4.2 Evaluation of two ECs for the study of Fn role in bacterial adherence

Fn deposition in the pericellular environment of HUVEC and HMEC-1 was assessed using immunofluorescence microscopy to evaluate the suitability of each cell type in Fn-mediated bacterial adherence studies. The microscopy evaluation revealed that pericellular Fn was less abundant in HMEC-1 compared to HUVEC. The difference between both cell types became more evident after prolonged incubation (**Figure 27**). Based on the previous, HUVECs were selected for the following assays, and the possibility of producing a monoclonal *FN1* knockout population was not further pursued.

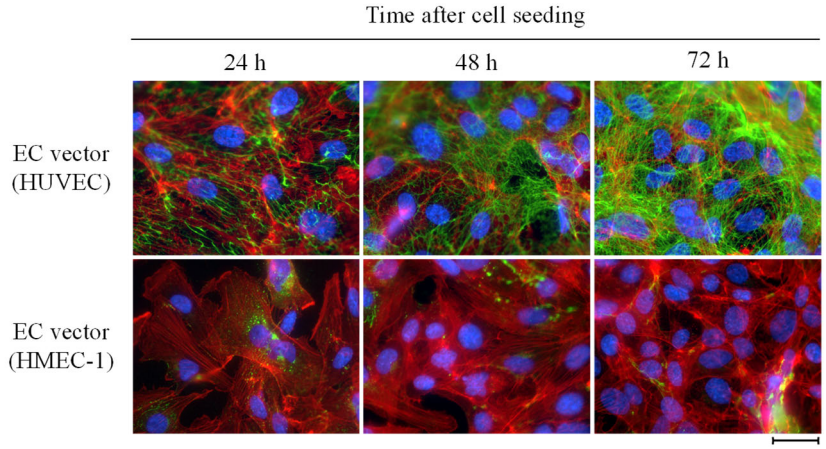


**Figure 27. Immunofluorescence microscopy of HMEC-1 and HUVEC**. Endothelial cells (ECs) containing the empty vector plasmid (vector) were seeded onto coverslips using $1.5x10^5$ HUVECs or $3x10^5$ HMEC-1 and incubated for 24 h, 48 h, and 72 h. Cells were fixed and stained for immunofluorescence microscopy evaluation using rabbit anti-Fn and Alexa 488 conjugated anti-rabbit IgG, TRITC conjugated phalloidin, and DAPI (Fn: green, beta-actin: red, nuclei: blue). Scale bar: 30 µm.

Based on the polyclonal nature of the HUVECs treatments, *FN1* knockout HUVEC were incubated for 24, 48 and 72 h to identify treatments with the best knockout efficiency. Immunofluorescence microscopy revealed the presence of pericellular Fn on some regions of the coverslip related to cells presenting the WT phenotype. The treatments ECs 1 and ECs 3 showed a reduced presence of Fn even after 72 h incubation (**Figure 28**).

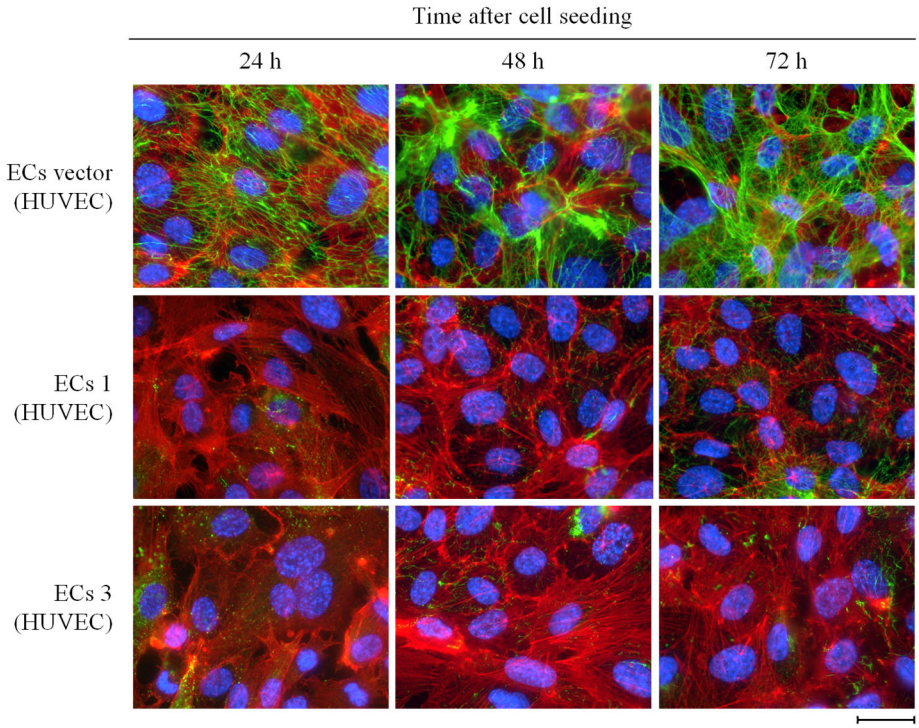


**Figure 28. Immunofluorescence microscopy of HUVEC knockout treatments**. HUVECs containing the empty vector plasmid (ECs vector) or the dual gRNA approach (ECs 1 or ECs 3) were seeded onto coverslips using $1.5x10^5$ HUVECs and incubated undisturbed for 24 h, 48 h, and 72 h to evaluate the presence of pericellular Fn. Cells were fixed and stained for immunofluorescence microscopy using rabbit anti-Fn and Alexa 488 conjugated anti-rabbit IgG, TRITC conjugated phalloidin, and DAPI (Fn: green, beta-actin: red, nuclei: blue). Scale bar: 30 µm.

Additionally, as Fn acts as a scaffold for the deposition of other ECM proteins [66], the pericellular deposition of collagen V and laminin was evaluated using immunofluorescence microscopy. Collagen V and laminin appeared to be unaffected in *FN1* knockout HUVEC treatments (ECs 1 and 3) compared to HUVECs expressing *FN1* (ECs vector) (**Figure 29**).

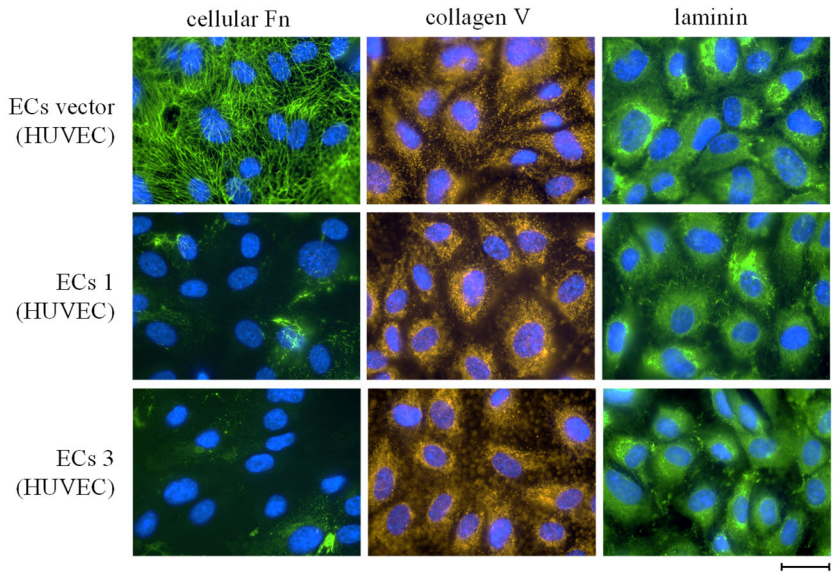


**Figure 29. Immunofluorescence microscopy of extracellular matrix proteins from HUVEC knockout treatments.** HUVECs containing empty vector plasmid (ECs vector) or with dual gRNA combination (ECs 1 or ECs 3) were seeded onto coverslips using $1.5x10^5$ HUVECs and incubated for 24 h. Cells were fixed and stained for immunofluorescence microscopy evaluation using rabbit anti-Fn and Alexa 488 conjugated anti-rabbit IgG, Alexa 488 conjugated rabbit anti-laminin, Alexa 647 conjugated rabbit anti-collagen V, and DAPI. (Fn or laminin: green, collagen V: orange, nuclei: blue). Scale bar: 30 µm. This figure was adapted from [104].

Taking together, the herein generated *FN1* knockout HUVECs (ECs 1 and 3) were selected to represent a tool for functional analysis of Fn-dependent bacterial binding to ECs.

## 3.5 Analysis of the Bad-Fn dependent interaction for *B. henselae* adherence to ECs.

The role of pericellular Fn on host cells for *B. henselae* adhesion was evaluated using the *FN1* knockout HUVECs generated in **Section 3.4**. ECs vector (control HUVEC expressing *FN1*) and ECs $Fn^-$ (*FN1* knockout HUVECs, ECs 1) were used for *B. henselae* adherence assays.

### 3.5.1 Evaluation of *B. henselae* adherence to ECs using adherence assays

To evaluate the role of BadA and Fn in bacterial adherence, *B. henselae* strains (WT or BadA$^-$) were tested for adherence to ECs vector or ECs Fn$^-$. After infection (60 min), bacterial binding was assessed using immunofluorescence microscopy and qPCR (**Figure 30**). Bacterial adherence was qualitatively evaluated using immunofluorescence microscopy, demonstrating a reduced bacterial binding when BadA or/and Fn were not present (**Figure 30A**). Moreover, absolute quantification of adherent bacteria was done using qPCR for the calculation of adherent bacteria per EC using bacterial (*glyA*) and human (*hmbs*) gene equivalents (**Figure 30B**). Here, a significant reduction in host cell adhesion of *B. henselae* WT was observed for ECs Fn$^-$ compared to the control (ECs vector). In line with this observation, no significant difference was observed between *B. henselae* BadA$^-$ adhesion to ECs Fn$^-$ or ECs vector. Together, these results evidence the important role of pericellular Fn presence for *B. henselae* adherence to ECs.

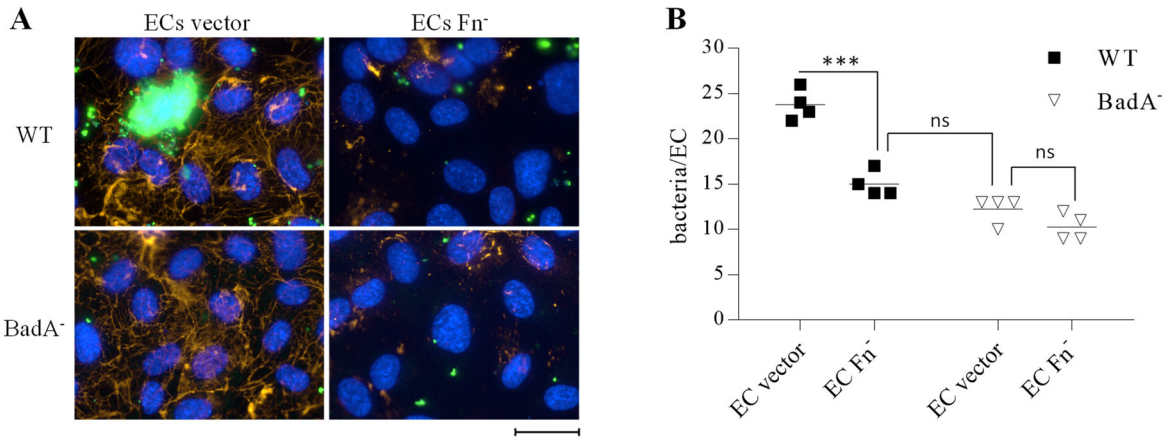


**Figure 30. Evaluation of *B. henselae* adherence to ECs using infection assays.** **(A)** Immunofluorescence microscopy of ECs vector (HUVEC WT phenotype, control) and ECs Fn$^-$ (HUVEC *FN1* knockout, ECs 1) infected with *B. henselae* WT or BadA$^-$ (MOI: 200). Infection time: 60 min. Cells were fixed and stained for immunofluorescence microscopy evaluation using rabbit anti-*B. henselae*, mouse anti-Fn and Alexa 488 conjugated anti-rabbit IgG, Cy5 conjugated anti-mouse IgG, and DAPI. (Fn: orange, bacteria: green, nuclei: blue. Scale bar: 30 µm). **(B)** Absolute quantification of bacterial binding to HUVEC via qPCR (bacteria: *glyA* gene equivalents; ECs: *hmbs* gene equivalents). The mean and SD of quadruplicates are depicted. Statistical significance was determined using two-way ANOVA with Šídák's multiple comparisons test (ns: not significant; *** P-value < 0.0001). The figure was adapted from [104].

### 3.5.2 Role of abundantly deposited pericellular Fn on *B. henselae* adherence

Fn presence in the extracellular environment is more prominent after a prolonged seeding time (see **Section 3.4.2**). To evaluate if the abundance of pericellular Fn impacts bacterial adherence, infection assays were performed using cells seeded for 24h and 48h. Infection was performed for 60 min, and bacterial adherence was evaluated using immunofluorescence microscopy and qPCR quantification (**Figure 31**). Microscopy evaluation of ECs vector or ECs Fn$^-$ infected with *B. henselae* WT showed a slight increment in bacterial adherence to ECs vector seeded for 48 h, noticed by the formation of clumps of bacteria (**Figure 31A**). In line with this observation, absolute quantification of bacteria per EC using gene equivalents quantitatively demonstrated a slight increment in *B. henselae* WT adherence to ECs vector seeded for 48h. However, the WT or BadA$^-$ binding to ECs Fn$^-$ seeded for 48h remained primarily unchanged (**Figure 31B**).

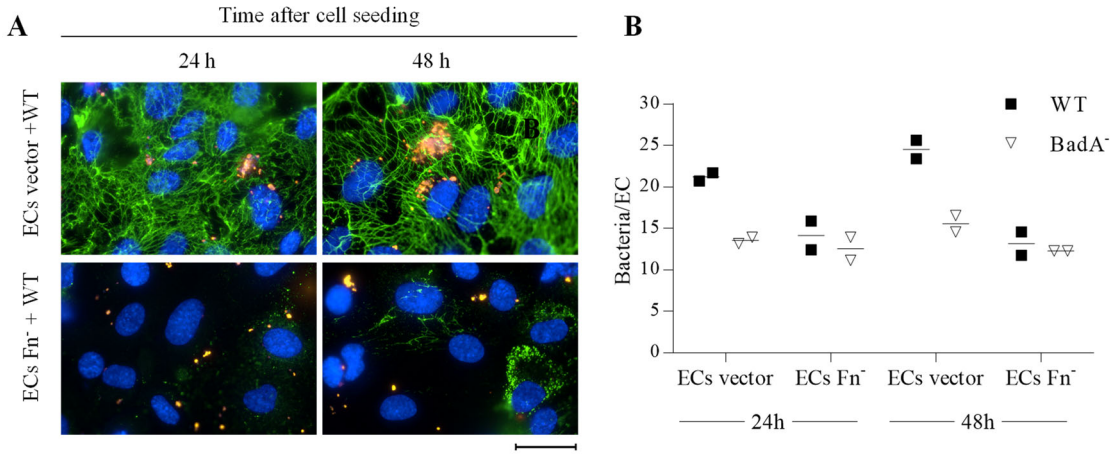


**Figure 31. Evaluation of *B. henselae* adherence to ECs in correlation to Fn abundance.** **(A)** Immunofluorescence microscopy of ECs vector (HUVEC WT phenotype, control) and ECs Fn$^-$ (HUVEC *FN1* knockout, ECs 1) infected with *B. henselae* WT (MOI: 200). Infection time: 60 min. Cells were fixed and stained for immunofluorescence microscopy; evaluation was done using rabbit anti-*B. henselae*, mouse anti-Fn, Alexa 488 conjugated anti-mouse IgG, Cy5 conjugated anti-rabbit IgG, and DAPI. (Fn: green, bacteria: orange, nuclei: blue. Scale bar: 30 µm). **(B)** Absolute quantification of bacterial (*B. henselae* WT or BadA$^-$) binding to ECs via qPCR (bacteria: *glyA* gene equivalents; ECs: *hmbs* gene equivalents). The mean of duplicates is depicted.

### 3.5.3 Analysis of BadA binding to collagen

The results from the previous sections revealed that BadA-Fn interaction is of significant importance for *B. henselae* adhesion to ECs. Nevertheless, the absence of both proteins (*B. henselae* BadA$^-$ infecting ECs Fn$^-$) did not completely reduce bacterial binding (binding reduction of approx. 60%), suggesting that additional binding mechanisms might be involved in host cell adhesion (e.g. other ECM components). In this regard, *B. henselae* binding to collagen was quantitatively evaluated in binding assays using purified collagen I and cellular Fn as a reference (**Figure 32**). Results demonstrated a statistically significant difference in binding between *B. henselae* WT or BadA$^-$ at 2 µg collagen I. *B. henselae* WT was observed to bind collagen I but to a lesser extent than cellular Fn according to this data.

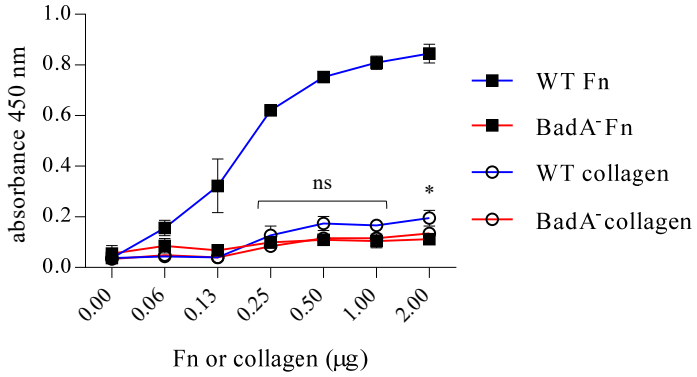


**Figure 32. Binding of *B. henselae* WT and BadA$^-$ to increasing amounts of immobilised collagen I or cellular Fn.** Binding of *B. henselae* WT and BadA$^-$ (OD600 = 0.3) to increasing amounts of immobilised collagen I (empty circles) or cellular Fn (filled squares), used as a reference. Adherent bacteria were detected using rabbit anti-*B. henselae* antibodies. The mean and SD of triplicates are depicted. Statistical significance was determined for collagen I using two-way ANOVA with Šídák's for multiple comparisons test (ns: not significant; * P-value = 0.009).

## 3.6 Analysis of the role of Fn in host cell adherence in other bacteria

The influence of Fn on bacterial adherence was evaluated in a broader spectrum, including other bacterial genera: *Acinetobacter baumannii*, *Borrelia burgdorferi*, and *Staphylococcus aureus*. Bacteria and Fn interaction was first evaluated in binding assays using increasing amounts of purified Fn in an ELISA setup. Furthermore, to assess the effect of Fn removal on bacterial adherence, the interaction was analysed in infection experiments using the *FN1* knockout HUVECs generated in **Section 3.4**, ECs vector (control HUVEC expressing *FN1*) and ECs Fn$^-$ (*FN1* knockout HUVECs, ECs 3). *B. henselae* WT was included in these assays as a reference.

### 3.6.1 Analysis of the interaction between various bacterial genera and Fn

The Fn-bacterial binding evaluation in this section was performed using bacterial-coated wells exposed to increasing amounts of Fn. A modification to the whole-cell ELISA assay first reported in **Section 3.1.1** was performed due to the *B. burgdorferi* binding to BSA used for blocking, as observed in a preliminary setup assay described in supplementary information (**Section 6.2**). In the new setup, bacteria-bond Fn was identified using mouse anti-Fn antibodies (**Figure 33**). This assay demonstrated a dose-dependent Fn binding for all bacteria assessed. A statistically significant difference was identified for *B. henselae* and *S. aureus* when using Fn amounts as low as 0.2 µg. In the case of *A. baumannii* and *B. burgdorferi*, higher amounts of Fn (>1.5 µg) were required to identify a significant difference. This result showed the difference of particular bacterial genera in binding to Fn.

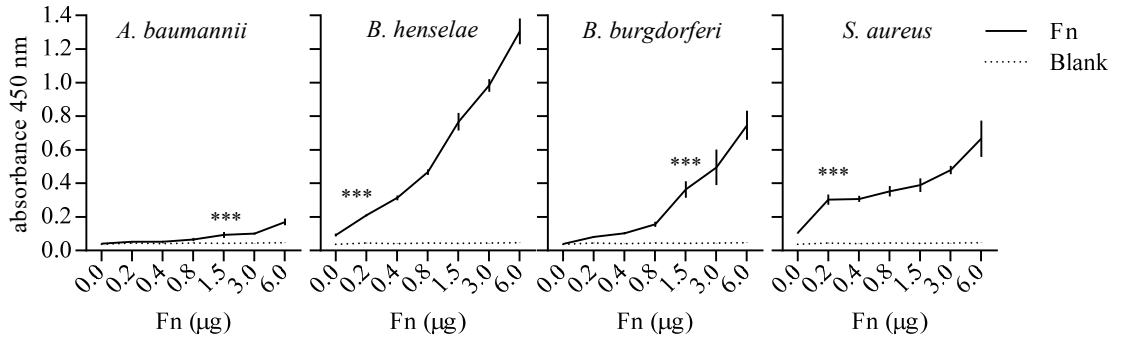


**Figure 33. Fn-binding to immobilised bacteria using whole-cell ELISA**. Microliter wells were coated with *A. baumannii*, *B. henselae*, *B. burgdorferi*, and *S. aureus* and exposed to increased amounts of Fn (from 0.2 to 6.0 μg). For blank, bacteria were omitted. Bond Fn was detected using mouse anti-Fn antibodies. Bacterial adherence to the wells was confirmed using specific rabbit anti-bacteria antibodies. The mean and SD of triplicates are depicted. Statistical significance was determined for each bacteria genera using a two-way ANOVA with Šídák's multiple comparisons test between bacteria-coated or blank wells (*** P-value < 0.001, conditions with μg lower than the starts were not significant).

### 3.6.2 Analysis of the Fn-dependent ECs adherence for various bacterial genera.

The role of pericellular Fn in bacterial adherence to ECs was assessed. Here, WT bacteria were analysed for their adherence capacity to ECs vector (control HUVEC expressing *FN1*) or ECs $Fn^-$ (*FN1* knockout HUVECs, ECs 3). The experimental part was carried out in collaboration with Ms. Fabienne Frenzel (medical student). The absolute quantification of bacteria-bound ECs was evaluated as described in **Section 3.5.1**, using the normalised results from two independent experiments (**Figure 34**). The number of adherent bacteria detected in $Fn^-$ HUVEC was reduced for all bacterial genera tested compared to ECs vector (*A. baumannii*: -25%; *B. henselae*: -58%, *B. burgdorferi*: -34%, *S. aureus*: -79%). Only *A. baumannii* did not demonstrate a statistically significant reduction in bacterial adherence but presented a higher data dispersion.

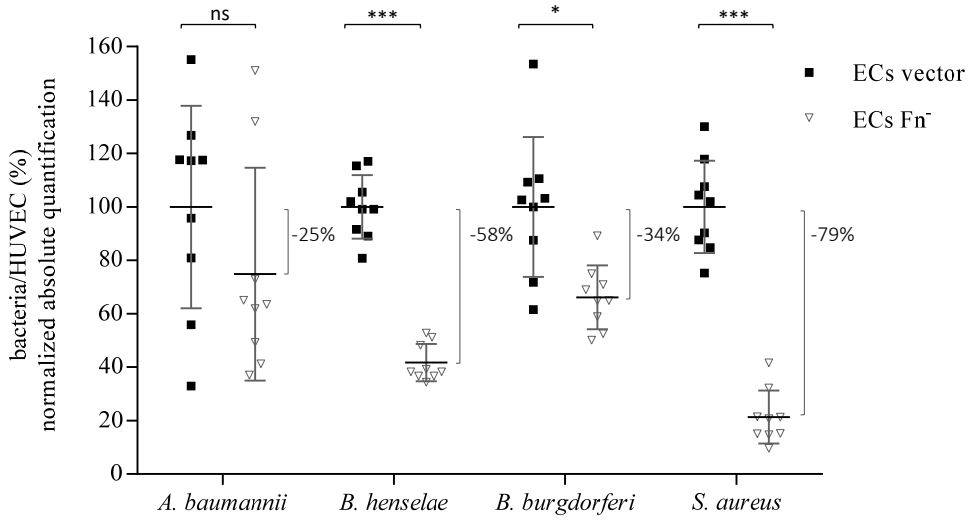


**Figure 34. Evaluation of bacterial adherence to ECs using infection assays.** ECs vector (control HUVEC expressing *FN1*) or ECs Fn$^-$ (*FN1* knockout HUVECs, ECs 3) were infected with *A. baumannii*, *B. henselae*, *B. burgdorferi*, or *S. aureus* (*B. henselae* and *S. aureus*: MOI 200; *A. baumannii* and *B. burgdorferi*: MOI 500). Infection time: 60 min. Absolute quantification of bacterial binding to ECs was performed via qPCR using gene equivalents [bacteria: *glyA* for *B. henselae* (120 bp), *rpoB* for *A. baumannii* (110 bp), *rpoB* for *S. aureus* (123 bp), and 16S ribosomal RNA gene for *B. burgdorferi* (107 bp); ECs: *hmbs* (207 bp)]. The data presented was normalised from two independent experiments using the mean of the ECs control binding as 100%. The mean and SD of nine replicates are depicted. Statistical significance was determined using two-way ANOVA with Šídák's multiple comparisons test. A P-value $< 0.05$ was considered significant as results from two independent experiments were included (ns: not significant; * P-value = 0.013; *** P-value < 0.0001).

# 4 DISCUSSION

## 4.1 BadA presence is crucial for *B. henselae* adherence to Fn

Studying the complex interactions of adhesins and host cell receptors can greatly advance our understanding of the molecular mechanisms involved in bacterial adhesion. Bacteria use different means to adhere to host cells, and bacterial binding to Fn protein conceivably is an interesting strategy for colonization due to the ubiquitous distribution of Fn in the pericellular environment. This is corroborated by the large variety of bacterial FnBPs in many pathogenic species [1, 2]. For *B. henselae*, BadA represents the principal adhesin and plays a crucial role in bacterial adhesion to ECs and ECM proteins, including Fn [20]. This exclusive dependence on one adhesin makes the description of the molecular mechanisms involved in *B. henselae* adherence to Fn and ECs an interesting model in the study of bacterial adhesion to host cells.

### 4.1.1 BadA-mediated binding to Fn

BadA has been described as the major pathogenicity factor and adhesin of *B. henselae* [20]. The description of three *B. henselae* adhesins, i.e. Omp 43, Omp 89, and Pap 31 (hemin binding protein A-HbpA), with affinities to Fn, have been reported in literature [27, 28]. Although the three OMPs were also identified in the two *B. henselae* strains (WT and BadA$^-$) used by this study (**Figure 10**), the presence of BadA was confirmed to be the primary determinant for *B. henselae* binding to Fn (**Figure 5**). It is possible that the background *B. henselae* BadA$^-$ binding to Fn observed in Western blotting and immunoelectron microscopy (**Figure 6** and **Figure 8**) might account for the role that the additional OMPs play in Fn binding.

It has been postulated that selective expression of adhesins might play a role in the adaptation of *Bartonella* to other environments (e.g. arthropod vector, mammalian host). This has been observed for hemin-binding proteins, including Pap 31, where transcriptional regulation occurs during variable hemin concentrations and ECs infection [121–123]. In the case of BadA, *badA* expression remains a common feature in all reported human virulent

*B. henselae* strains, where variations in the length of the neck/stalk region of BadA have been reported but maintaining Fn binding [41, 44].

### 4.1.2 BadA binds cellular and plasma Fn

Two types of Fn are present in the human body, a globular or soluble found in blood, saliva, and other fluids (plasma Fn); and a fibril-forming or insoluble secreted by fibroblasts and ECs (cellular Fn). This research demonstrated that *B. henselae* binds Fn purified from both plasma and cellular sources (**Figure 7B** and **Figure 9B**). According to the peptide-peptide interaction obtained in the XL-MS analysis, BadA interactions to cellular Fn are localized within hep I-binding domain (FnI 1 and FnI 5), while those in the plasma and Rn Fn are distributed in multiple sites, i.e. at the end of the hep I-binding domain, hep II-binding domain, and the C-terminus (**Figure 22**).

In accordance with the different natures of plasma and cellular Fn [67, 69], it can be speculated that BadA particularly binds regions in cellular Fn (fibrillar structure) that might not be exposed in the molecular structure of plasma Fn (e.g. hep I-binding domain) and vice-versa [67] (**Figure 3**). Furthermore, mutations in FnIII 13 and FnIII 14 (part of hep II-binding domain) have proven to destabilize Fn fibrilar conformation leading to kidney disease associated with glomerulopathy due to non-fibrillar Fn aggregates [66, 124]. It has been suggested that under normal conditions, the Fn-Fn interactions occurring with the hep II-binding domains are crucial in stabilizing the compact conformation of cellular Fn [66]; therefore, bacterial interactions might not be feasible in such tight conformation. It is important to indicate that the identified XLs might have favoured the interactions occurring in the most conserved region between Fn isoforms (N-terminus including the hep I-binding domain p52-p272; **Figure 20**). Therefore, other BadA-cellular Fn interactions not identified by the XL-MS analysis due to its lower abundance might be plausible.

The results obtained here indicate BadA site-specific interactions with each of the Fn types. *B. henselae* binding to plasma Fn could, therefore, represent a bacterial strategy to escape the immune response by being masked with plasma Fn, but still retaining the bacterium's ability to attach to host cells via the pericellular Fn “bridge”. Additionally, such mechanisms

may also help to further enhance bacterial adhesion to tissues through the interaction of coated Fn with other host proteins [27] (**Figure 35**).

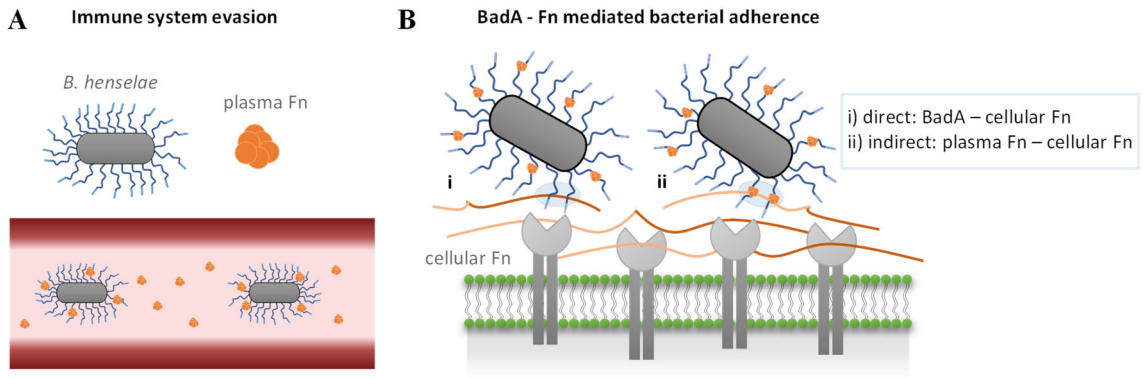


**Figure 35. Graphical summary of *B. henselae* interaction with plasma and cellular Fn.** **(A)** Bacterial coating with plasma Fn might represent a bacterial mechanism to escape the host immune system. Bacteria circulating in blood vessels get in contact with plasma Fn in globular conformation (orange). The neck/stalkregion of BadA (dark blue) from *B. henselae* interacts with Fn molecule (end of the hep I-binding domain, hep II-binding domain, and the C-terminus). **(B)** At the extracellular environment, bacteria get in contact with cellular Fn in fibrillar conformation (shades of orange). Cellular Fn is connected to ECs via integrins (grey). Due to the abundance of BadA fibers and the repetitive stalk/neck domains, bacterial adherence to cellular Fn might be promoted by two ways: i) direct, via interaction of BadA with the N-terminal of cellular Fn; ii) indirect via interaction of plasma Fn (coating BadA) with cellular Fn or other ECM component via a Fn - Fn "bridging" mechanism. BadA head (light blue) does not play a significant role in Fn-mediated adherence [46].

TAA-mediated binding to Fn has also been described for *Yersinia* adhesin A (YadA) from *Y. pseudotuberculosis*, UpaG from uropathogenic *E. coli*, and ubiquitous surface protein A (UspA)-1 and -2 from *Moraxella catarrhalis* [125–127]. The possibility of similar interactions between Fn and other TAAs of pathogenic bacteria needs to be analysed in greater experimental detail as deciphering similarities in binding motifs, particularly in the TAA's passenger domains, might not be easily predictable due to the reported variable structures within TAAs [30].

### 4.1.3 BadA and Fn interaction mediates *B. henselae* adherence to ECs

BadA-mediated adherence to ECs and ECM proteins was earlier described [20]; nevertheless, the importance of Fn-mediated BadA interaction to support *B. henselae* binding was not functionally evaluated. To assess the role of Fn in *B. henselae* adherence,

*FN1* knockout ECs (EC 1) were used in infection assays for loss of function analyses. *B. henselae* adherence to ECs was reduced under Fn and BadA deficient conditions as evidence of the crucial role that the BadA and Fn interaction play in bacterial adherence (**Figure 30**). A slight increment in bacterial adherence was also observed when abundantly deposited Fn was present on the pericellular environment of cells after prolonged seeding time (**Figure 31**), indicating that Fn presence contributes to bacterial adherence.

Although BadA-Fn interaction proved to be the major determinant for *B. henselae* adherence to ECs under Fn-deficient conditions, bacterial binding was not completely reduced. The intervention of other host targets for BadA, such as collagen I, III, IV, and laminin [128], could account for bacterial binding under Fn-deficient conditions. In this research, BadA-mediated binding to collagen I was observed under high collagen concentrations, but this interaction happened in lesser extend compared to the BadA-mediated binding observed to cellular Fn (**Figure 32**). These results suggest that the interaction of BadA with other ECM protein components and the intervention of additional binding mechanisms (e.g. other adhesins) could promote bacterial binding to ECs under Fn or BadA deficient conditions.

Furthermore, in the big picture of *B. henselae* pathogenesis, additional binding mechanisms might be applied by *B. henselae* under different circumstances modulating the expression of bacterial adhesins and virulence factors accordingly (e.g. binding to epithelial or migratory cells) [4, 121]. In the context of *B. henselae* pathogenicity during EC infection, after Fn-mediated adherence to ECs via BadA interaction, the intervention of BadA and other secretion systems as the virB/D T4SS play a role in further steps triggering proliferation of ECs and interference with host cells mechanisms [18, 19]. The understanding of *B. henselae* adherence to host cells and the interplay between different virulent factors during pathogenicity has not been fully deciphered, and it has been hampered by the lack of *in vivo* animal models.

### 4.2 Heparin-binding domains in Fn as important BadA binding regions

Heparin interaction with Fn facilitates the assembly process to bring together Fn molecules and promote fibrillogenesis [65]. Fn contains two major heparin-binding domains that

interact with heparan sulphate proteoglycans. The strongest heparin-binding site is located at the C-terminus of Fn (hep II-binding domain), and a weaker binding domain is situated at the N-terminus (hep I-binding domain) of Fn [61]. These two Fn regions have already been observed as important interacting sites for adhesins from many pathogenic Gram-positive and negative bacteria [64, 129].

### 4.2.1 Dissecting the BadA binding sites in Fn

Due to the complexity in size and structure of BadA and Fn, the interaction was analysed using proteolytic Fn fragments to localize regions with strong BadA-binding capacity. To analyse the interaction, proteolysis of Fn and bacterial binding assays were first tested without success due to incomplete digestion of full-length Fn and limited detection of proteolytic Fn fragments using Fn-antibodies (**Section 3.2.1**). A second approach was pursued using purified Fn fragments covering the full length of Fn and bacterial binding assays in an ELISA setup. Within the regions covered by the Fn fragments, it was observed that the heparin-binding domains were the strongest BadA binding sites with no difference when compared to the full-length Fn (**Figure 16**), revealing the major role that the heparin-binding domains of Fn play in the TAA-mediated adhesion of *B. henselae*.

The hep I-binding region in Fn (FnI 2–FnI 5) has been termed as a "canonical binding site" for many FnBPs in Gram-positive such as FnBPA and FnBPB from *S. aureus* [72], and possibly other Gram-negative bacteria such as Lpf1 from enterohemorrhagic *E. coli* and RevA from *B. burgdorferi* [87, 130]. Further "non-canonical binding sites" (e.g. hep II-binding domain in Fn) have also been cited as important for other autotransporter adhesins, e.g. ShdA from *Salmonella enterica* and for the surface-exposed protein BB0347 from *B. burgdorferi* [82, 131] (**Figure 4**). According to literature, BadA is the only adhesin that binds both heparin-binding domains in Fn; and as previously discussed, targeting different Fn domains in cellular and plasma Fn could be perceived as a strategy seeking bacterial adherence and persistence of infection (**Section 4.1.2**).

### 4.2.2 BadA-mediated binding to Fn is outcompeted by heparin

As proof of principle of BadA interaction with the heparin-binding domains in Fn (Hep I and Hep II), heparin was included as a competitor in bacterial binding assays (**Figure 17**). Here it was demonstrated that under increasing amounts of heparin, bacterial binding to Fn was reduced in a dose-dependent manner. The possibility of interfering interactions between bacteria and heparin as a cause of bacterial reduction was ruled out after the observation that bacteria failed to bind heparin-coated wells.

The use of heparin as a competitor for binding between adhesin and Fn has been described previously by other authors. Concentrations as low as 16 μM heparin were enough to reduce ShdA adhesin (*S. enterica* serotype Typhimurium) binding to Fn, as ShdA and heparin bind to the same domain in Fn (FnIII 13) [131]. In other research using Pap 31 (*B. henselae*), a concentration of 1.6 μM heparin reduced adhesin binding to Hep II-binding domains in Fn [28]. Nevertheless, in both cases, purified recombinant proteins were used with heparin to compete for Fn binding, in contrast to the whole-cell binding assay performed by this research.

BadA is abundantly present on the surface of *B. henselae* (**Figure 1A**) and binds both heparin-binding domains of Fn. Higher doses of heparin might be required to inhibit BadA-mediated *B. henselae* binding to Fn, as observed in the assays carried out in this research, where an inhibitory effect was detected starting from 280 μM heparin (5 μg/μl). The possibility of undesired inhibition due to excessive heparin was ruled out based on unaffected binding in domains without heparin affinity (e.g. cell-binding domain) (see **Figure 17 A**). Additionally, the heparin inhibitory binding effect is observed more dramatically when used to compete for hep II-binding domain, in congruency with this domain being the stronger heparin binder in Fn [65].

## 4.3 XL-MS and functional binding assays in the identification of host-pathogen interactions

Interspecies protein interactions are essential for bacterial infection. Membrane-associated proteins play pivotal roles in bacterial pathogenesis mediating many aspects of host-pathogen interactions (e.g. adhesion, secretion and invasion). Interaction studies of membrane-associated proteins often require significant dedicated efforts, as the partially hydrophobic surfaces of membrane proteins and the lack of stability confer challenges for conventional structural characterization (e.g. protein crystallography) [132, 133]. Advanced technologies offer the potential to shed light on large-scale protein-protein interactions and their structural interfaces. By using chemical crosslinking followed by XL-MS, novel interspecies protein-protein interactions have been described providing a deeper understanding of their role in bacterial pathogenicity [108, 133, 134]. The application of large-scale analysis, such as XL-MS, alongside binding assays (e.g. ELISA, in-suspension binding) aids in the discrimination of relevant interactions to support bacterial-host interactions.

### 4.3.1 Advantages and drawbacks of using XL-MS to study TAA-Fn interactions

Chemical XL-MS approaches have broadened the knowledge of protein interaction studies. The usage of finite crosslinker length and the covalent linkage of two amino acid side chains enable the estimation of the proximity of interactions occurring during a particular time of infection. This approach also offers great potential to identify transient or long-lived interactions chemically stabilized from a mixture of purified proteins or from *in vivo* studies. For the identification of BadA-Fn interactions, whole-cell bacteria were incubated with Fn, and the protein-protein interactions were chemically crosslinked for further analysis using LC-MS (**Figure 19**). Based on the repetitive nature of BadA, it has been suggested by previous research that BadA-mediated adhesion to Fn and ECs might be assisted by the long and modularly arranged neck/stalk region [47]. This hypothesis is now confirmed by the XL-MS data generated in this research, where many areas in the BadA neck/stalk repeats are shown to assist in Fn-binding (**Figure 22**).

Despite significant advances in MS instrumentation and more robust software for the analysis of protein-protein interactions, difficulties related to the enrichment of interactions of interest and the reliability of the identified crosslinked peptides are challenges to overcome methodologically [135, 136]. In this research, the use of negative samples (*B. henselae* BadA$^-$) was incorporated to discriminate spurious protein-protein interactions that could be identified due to the large amount of data generated [136]. Furthermore, the identification of inter-protein XLs in the background of intra-protein XLs is the most general and complex problem to solve [135]. The trimeric structure of BadA and the heterodimer structure of Fn represented a challenge in the identification of inter-protein XLs, which are expected to be present in lower abundance. Consequently, a significant majority of the crosslinked peptides identified in this research represented intra-protein XLs (94%). Finally, due to the complexity of the samples and to reduce the background noise coming from intracellular bacterial proteins, different conditions were assessed; the usage of lower concentrations of crosslinker and the enrichment of surface-attached proteins favoured the identification of BadA-Fn interactions (**Figure 21**).

### 4.3.2 Identification of relevant interactions to support bacterial binding to Fn

Validation of the crosslinked peptides and their importance in the biological question is another challenge considering the large amount of data generated from MS analysis [135]. Regarding Bad-Fn interaction, it was identified by this research that the heparin-binding domains of Fn are important BadA binding sites (**Section 4.2**). In the XL-MS analysis, the BadA interactions happening with the heparin-binding domains in Fn were distributed along the BadA neck/stalk region and were predominantly identified in the repetitive domains (i.e. domains 2/6/10/27, 13/17/21/25, 18/22, 19/23) and domain 26. Notably, the herein-identified interaction with the domain 27 in the stalk region confirms the earlier demonstrated Fn-binding in a mutant *B. henselae* producing a truncated BadA with a short neck/stalk fragment (domains from 27 to 30) [47]. Recent research suggested that a peptide in the DALL motif of domain 27 could be responsible for Fn binding [137]; this peptide includes the sequence identified in the XL-MS analysis interacting with FnI 5 domain. By rendering the predicted domain 27 structure next to the FnI 5 structures, the feasibility

of the crosslinked interaction was theoretically confirmed (see **Figure 36**). Additionally, the importance of domains 19 and 25 for *B. henselae* adherence to Fn was confirmed by recent research using *B. henselae* mutants producing truncated BadA proteins [137].

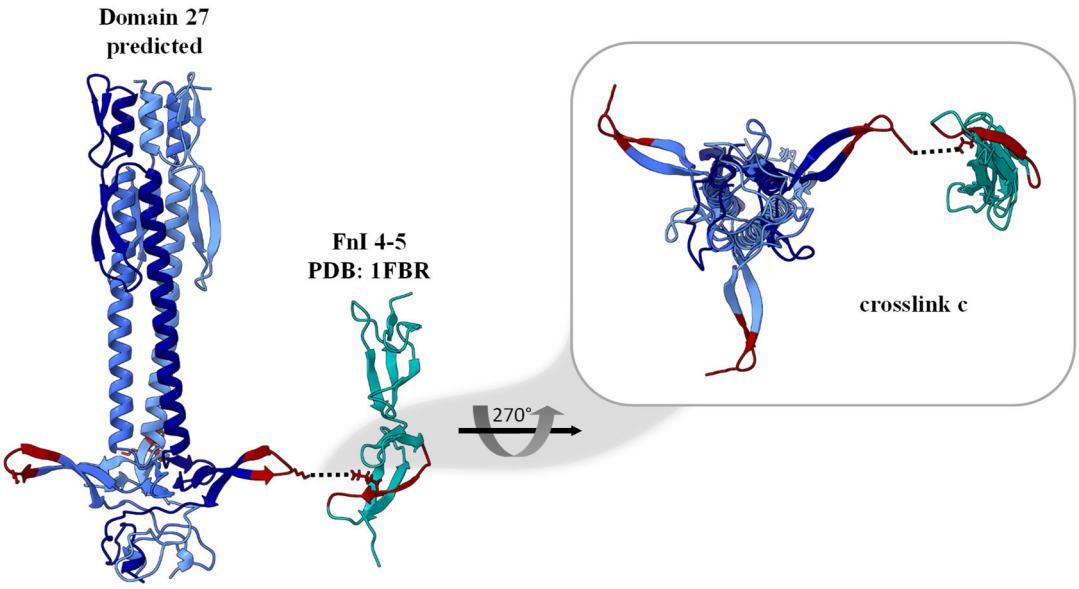


**Figure 36. Analysis of crosslink "c" identified between the BadA domain 27 and FnI 5.** The predicted structure of domain 27 from the neck/stalk region of BadA was rendered next to the FnI 4-5 NMR structure (PDB: 1FBR). The three BadA monomers are shown in shades of blue, and the FnI 4-5 domains in cyan. The peptides identified as crosslinked are indicated in red (crosslink "c" in **Table 24**), and the identified crosslink between one of the BadA monomers and the Fn fragment is indicated as a black dotted line drawn between the lysine (K) residues. The insert shows a top view of the interacting peptides using one of the monomers as an example. The structure for domain 27 was predicted using AlphaFold2 [50]. For details, please refer to (**Section 6.3**). The figure was generated using PyMOL.

The binding assays also demonstrated that the interactions between BadA and the gelatin- or cell-binding domains in Fn were not crucial for BadA binding (**Section 3.2.2**). In accordance, only three XLs (i.e. XLs "e", "f", "g") were detected in these regions (**Figure 22** and **Table 24**), and two of them (XLs "f", "g") were BadA domains previously described with non-functional Fn-binding (domain 29 and unpredicted region close to anchor) [47]. Additionally, it was previously postulated that the BadA head might act as a first initiator for bacterial binding via collagen interaction, as no Fn-binding was observed for a *B. henselae* mutant producing the BadA head fused to a drastically truncated neck/stalk element [46]. In this research, only one interaction between the BadA head and Fn was identified in the XL-MS analysis and the feasibility of this interaction was theoretically

confirmed using the only available structure for BadA protein and the Fn counterpart (**Figure 23**).

These results suggest that although some interactions identified by XL-MS might be possible to occur, as per the theoretically confirmed available structures. The individual interaction might not be strong enough to support bacterial binding by itself, as observed for interactions with gelatin- and cell-binding domains. Therefore, these interactions might act as accessory binding for the already strong neck/stalk interactions with Fn. As described for other adhesins, bacterial binding to host cell surfaces could be accomplished by the avidity of multiple weak binding sites [138], leading to tighter and more effective binding, especially under shear stress. This seems highly "economical" because repetitive elements facilitate recombination events which can modulate the specificity of the adhesin for its biological purpose [30]. This type of recombination event has been observed for *badA* from various virulent *B. henselae* strains, where variations in the length of the repetitive neck/stalk sequences have been reported, but Fn binding remained unaffected [41, 44].

### 4.3.3 Further exploration of so far unidentified BadA-Fn interactions

The role in bacterial adherence of other BadA peptides interacting with Fn-regions that were not covered by proteolytic Fn fragments should be further analysed using functional binding studies. Additionally, as inter-protein interactions were scarce in the analysis, the occurrence of other interactions not detected by the XL-MS analysis can not be ruled out. In line with the previous, a recent research used a mutant *B. henselae* producing a truncated BadA containing domain 16 and proved to recover Fn binding [137], this domain was not identified in the XL-MS analysis. Furthermore, protein glycosylation has been described to play a significant role in host-pathogen interaction, and a vast majority of membrane proteins are glycosylated [139]. The glycosylation status of Fn was reported to facilitate the TAA-mediated bacterial adhesion of *A. baumannii* [140]. The XL-MS data generated identified interactions in non-glycosylated Fn regions (see **Figure 22**), suggesting that other interactions apart from glycan-protein occur between Fn and BadA. Nevertheless, the role of Fn-glycosylation for BadA binding remained unclear in the XL-MS approach used by this research and might need further exploration using glycan-protein XL-MS methods [141].

## 4.4 Role of Fn for host cell adherence of pathogenic bacteria

The endothelium consists of a single layer of ECs lining the interior surface of blood and lymphatic vessels and is one of the largest organ-like surfaces in the human body. Because of the exposed location of ECs, their interaction with circulating pathogens is a likely event [142]. Infected ECs might represent a cellular niche from which infectious pathogens can further disseminate and reach different organs in the human host. Based on the broad description of bacterial adhesins with reported affinities to ECM components, targeting the ECM protein layer on the ECs for adhesion might be a plausible strategy to support colonisation and avoid clearance [64, 143]. Efforts to clarify the relevance of the interactions between adhesins and ECM proteins have been focused on loss-of-function assays deleting the particular bacterial adhesin. However, the role of the host target (e.g. Fn) in supporting bacterial adhesion has not been conclusively described, although it is indispensable for pathogenesis.

### 4.4.1 Endothelial cells as a model for Fn-mediated adherence

This research evaluated HUVEC and HMEC-1 as potential cell models for Fn-mediated bacterial adherence to ECs. HUVEC are primary cells originated from a large vessel of the placenta. These cells are frequently used as a model for bacterial adhesion research due to their wide availability and relatively easy isolation [142]. On the other hand, HMEC-1 are microvascular ECs isolated from human foreskins and immortalized after transfection with pSVT vector (Simian virus 40 A gene product). This cell line is characterized by retaining many morphologic, phenotypic, and functional characteristics of microvascular ECs [144]. The advantage of working with immortalized cells over primary cells relays on the capacity to maintain phenotypic and functional characteristics after prolonger passage in culture, in contrast to the limited lifespan observed primary cells [144].

In this research, it was observed that pericellular Fn on HUVEC was more prominent than in HMEC-1. This difference became even more evident after extended incubation periods demonstrating a more profuse Fn layer on HUVECs (**Figure 27**). Based on this, the isolation of *FN1* knockout monoclonal ECs from HMEC-1 was no longer pursued, and HUVEC were

selected for further analysis. The usage of *FN1* knockout HUVEC potentially containing a polyclonal population (*FN1* expressing and *FN1* knockout) did not demonstrate a noticeable impact on pericellular Fn presence, not even after extended incubation periods (up to 72 h after seeding) (**Figure 28**). With these observations, the viability of the herein-generated *FN1* knockout HUVEC (ECs 1 and ECs 3) was confirmed.

Some ECM proteins (e.g. collagens, fibrillin) use the Fn matrix as a scaffold for the deposition of independently structured fibres [145, 146]. In contrast, the initiation of the basement membrane assembly does not involve Fn but relies on laminin-integrin interactions [147]. As Fn seems to play a role in the stability of the ECM and due to the description of many bacterial adhesins with reported affinities to other ECM proteins (e.g. collagen and laminin) [1], the presence of other ECM proteins was verified in the pericellular environment of *FN1* expressing and *FN1* knockout HUVEC. Collagen V and laminin appeared to be unaffected in *FN1* knockout HUVECs (ECs 1 and ECs 3) and did not demonstrate a visible difference compared to the control cells (ECs vector), being Fn the only modification (**Figure 29**). With this clarified, the herein-generated *FN1*-knockout HUVEC were considered a valuable tool for evaluating Fn-mediated bacterial adherence to ECs.

### 4.4.2 Fn as an underestimated host target in bacterial binding to host cells

The abundance of Fn in the ECM environment of ECs (**unpublished data**) conceptually makes it an interesting target for bacterial adherence *per se* and possibly a common mediator for bacterial adhesion. In order to evaluate the role of Fn in bacterial adhesion, loss of function experiments using the *FN1* knockout HUVECs (EC 3) were performed, including a set of Gram-negative and Gram-positive bacteria (**Figure 34**). In this assay, bacterial adhesion to *FN1* knockout HUVEC was reduced by 79%, 58%, 34% and 25% for *S. aureus, B. henselae, B. burgdorferi* and *A. baumannii,* respectively. As discussed before (**Section 4.1.3**), BadA-Fn interactions are essential for *B. henselae* adherence to ECs and the important role of Fn in *B. henselae* adherence was again confirmed here when *FN1* knockout ECs with a different knockout strategy was used (ECs 3). In the case of *S. aureus*, FnBPA and FnBPB adhesins have been described as crucial for Fn-binding and *S. aureus* internalisation into ECs [92]. For both bacteria, the disruption of Fn-mediated interaction

certainly impacts their adhesion to host cells and could prevent further steps of bacterial infection.

In the case of *B. burgdorferi* and *A. baumannii*, Fn-mediated adhesion might also represent an essential bacterial adherence strategy supported by additional host cell receptors. The adhesion of *B. burgdorferi* to ECs is known to be mediated by the interaction of various adhesins and host receptors [148]. Many *Borrelia* proteins with binding affinities to Fn and adherence to host cells have been reported (e.g. BBK32, CspA, CspZ, BB0347, RevA and RevB). [82, 84, 87, 149, 150]. Nevertheless, interactions of other *Borrelia* adhesins (e.g. BmpA-D, DbpA-B, BBA33, ErpX) and host targets (e.g. collagen, laminin, decorin) might also account for bacterial binding in the absence of Fn [151]. For *A. baumannii*, bacterial adherence to ECs was reported to be mediated via the Ata protein [152]. Ata demonstrated binding affinities to laminin and various collagens and, to a lower extent, to Fn [32]. This was confirmed in our infection assays where Fn removal (*FN1* knockout HUVEC) seems to have a less pronounced effect on bacterial binding, in congruence with the relatively low binding capacity to purified Fn (**Figure 33**).

The scenario of bacterial adhesion to the host shows a complex interplay of multiple variables. The presence of selective adhesion mechanisms dependent on the time of infection, host cell tropism, ECM composition, and the redundancy of interaction between adhesins and cellular receptors are all aspects to consider. For instance, infections with *B. henselae* and *S. aureus* have been associated with infective endocarditis with direct involvement of ECs [153]. In the case of *B. burgdorferi* and *A. baumannii*, bacterial interaction with ECs might represent a way to reach deeper tissue, evade the host´s immune response, and attain persistence, as proposed for *B. burgdorferi* invasion of ECs [154, 155]. Likewise, more selective adhesion mechanisms can be employed by bacteria under different physiological conditions, changing its adherence mechanism as observed for *A. baumannii* binding to human lung epithelial cells (A549 cells), where interaction between Fn and three OMPs (TonB-dependent copper, OmpA, and 34 kDa Omp) was crucial for epithelial adherence [76]. Finally, interaction with Fn could play a role in stabilizing bacterial adherence to ECs, as described for BBK32 from *B. burgdorferi* using a catch bond mechanism to bind Fn [149].

### 4.4.3 Future perspectives

The results demonstrated that in the context of pathogen adherence, the interaction of Fn on ECs with Gram-positive or Gram-negative bacteria plays an important role in bacterial adherence. Fn-mediated interaction might be a crucial clue for infections caused by bacteria with endothelial tropism (*B. henselae* and *S. aureus*) and for bacteria whose interaction with ECs represents an initial step for pathogen dissemination and persistence (*B. burgdorferi* and *A. baumannii*). Describing the molecular mechanisms involved in bacteria-ECM interactions might bring significant information regarding the complex bacterium-host interplay and provide strategies for interfering with this interaction to prevent bacterial infections.

Bacterial binding interference is a novel anti-virulence approach [156, 157]. The development of molecules blocking specific bacterial adhesin domains that interact with the host protein has been explored for pathogenic bacteria such as uropathogenic *E. coli* and *Aeromonas veronii* [158, 159]. Moreover, the application of functionalized beads coated with bacterial adhesins to prevent infections with Gram-positive bacteria has been explored with promising perspectives [160–162]. Further approaches could aim at developing molecules mimicking specific domains of ECM protein reported as canonical for bacterial binding (e.g. the heparin-binding domains of Fn). Under this approach, binding inhibition could be achieved by competition with the host target protein using a broad-spectrum inhibitor to block many adhesins of pathogenic bacteria (e.g. Pap 31 and BadA from *B. henselae*, RevA, BBK32, and BB0347 from *B. burgdorferi*, FnBPA and FnBPB from *S. aureus*).

Finally, many aspects need to be overcome before the successful application of such approaches. The redundancy of interaction between one adhesin and many cellular receptors is a fact for many bacteria (e.g. BadA affinity to several ECM proteins). In addition, the possibility that by interfering with pathogen attachment (e.g. via competitors mimicking heparin-binding domains of Fn), host mechanisms might be affected (e.g. matrix assembly, Fn fibrillation), leading to undesirable consequences for the host and representing challenges for the use of “anti-ligands” as anti-infective compounds in the near future.

# 5 CONCLUSIONS AND OUTLOOK

This research proved that BadA is the principal mediator for *B. henselae* binding to Fn. This was verified after the observation that BadA presence was the primary determinant for Fn binding, although additional OMPs with reported affinity to Fn were detected in *B. henselae*. The molecular interactions between BadA and Fn were identified in detail using functional binding assays and XL-MS methods. It was determined that BadA and Fn interactions occurred between the repetitive domains of the BadA neck/stalk region and the heparin-binding domains of Fn. Furthermore, it was identified that BadA interacts with plasma and cellular Fn. BadA interaction with globular Fn circulating in the blood and fibrillar Fn present in the pericellular environment of ECs seems to contribute to bacterial adherence to the host cell and to represent an important mechanism supporting bacterial infection. The extent of this hypothesis should be further explored, using, for example, polymer-coated surfaces to promote the different conformations of Fn, atomic force microscopy or surface plasmon resonance to evaluate the interaction, and functional analysis to verify the role of each interaction in the biological function.

Concerning bacterial adherence to the host, this research identified that BadA and Fn interaction is the principal mediator for *B. henselae* adherence to ECs. This was done by using an *FN1*-deficient EC model in infection experiments. Fn was also identified as a host target protein for adherence of other human pathogenic bacteria such as *S. aureus*, *B. burgdorferi*, and *A. baumannii*, but in a different extent of importance (higher for *S. aureus* than *A. baumannii*), possibly in congruence with their endothelial tropism. Fn-mediated interaction may be essential in stabilizing bacterial binding under vascular shear stress at the surface of ECs. Therefore, infection assays using dynamic flow conditions might lead to a more drastic reduction in bacterial adherence under Fn-deficient conditions. Finally, based on the broad description of bacterial adhesins with Fn affinity, further exploration in the field of “anti-ligands” interfering with Fn-binding might represent a promising anti-infective approach. Applying XL-MS assays might assist in deciphering specific bacterial interactions with the host cells, even under a more complex setup.

# 6 SUPPLEMENTARY INFORMATION

## 6.1 Fn-fragments sequence coverage analysis

Sequence coverage of each fragment was assessed using DDA-MS acquired spectra and PEAKS (version X) program. The analysis in PEAKS was performed in collaboration with Dr Lotta Happonen (Lund University, Sweden) as part of the Marie Sklodowska-Curie program from the European Union. The sequence coverage was determined using the information described in the product description regarding enzymatic digestion for each fragment and reported affinities. The analysis revealed the extension of each fragment related to the full-length Fn sequence.

**Figure 37. Analysis of sequence coverage of proteolytic Fn-fragments**. DDA-MS analysis of proteolytic Fn fragments. The sequence coverage of each fragment is depicted below the sequence as blue bars (grey bars represent *de novo* identification). The post-translational modification sites are indicated in yellow for carbamidomethylation of cysteine [C], red for deamidation of asparagine [N] or glutamine[Q)], and blue for oxidation of methionine [M]. The sequenced coverage is indicated in each case with a red outline and was based on both the DDA-MS analysis and the manufacturer product information. Note that the hep II-binding fragment is not completely pure and contains other parts of the Fn molecule, including hits for the hep I-binding domain and the C-terminal part of the Fn sequence, possibly related the purification procedure for this fragment (chymotryptic digestion of human plasma Fn and purified with heparin-sepharose column chromatography according to manufacturer´s specification). The figures were adapted from [104].

hep I & gelatin-binding fragment

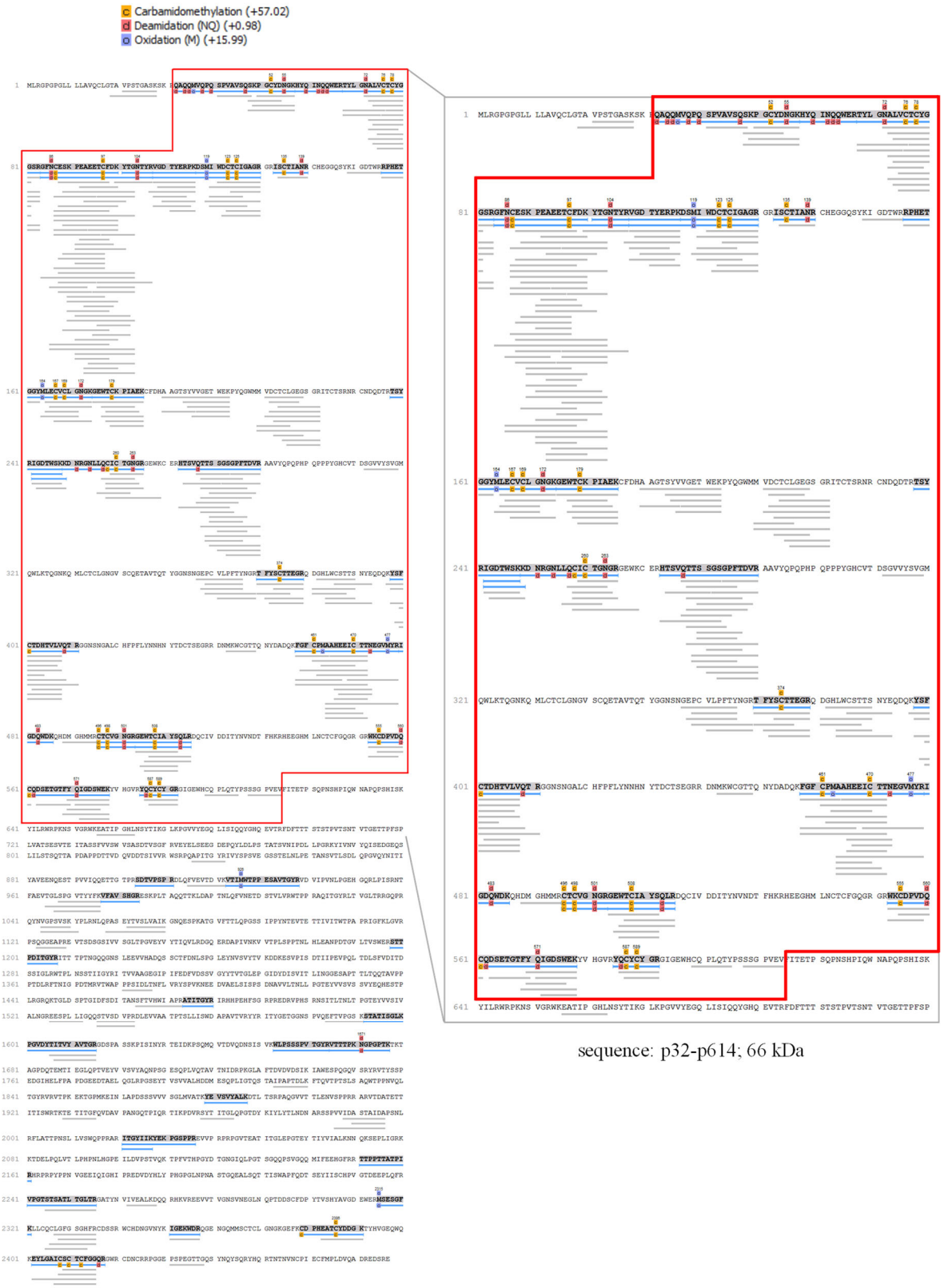


sequence: p32-p614; 66 kDa


hep I-binding fragment
Carbamidomethylation (+57.02)
Deamidation (NQ) (+0.98)
Oxidation (M) (+15.99)
sequence: p32-p290; 29 kDa

gelatin-binding fragment

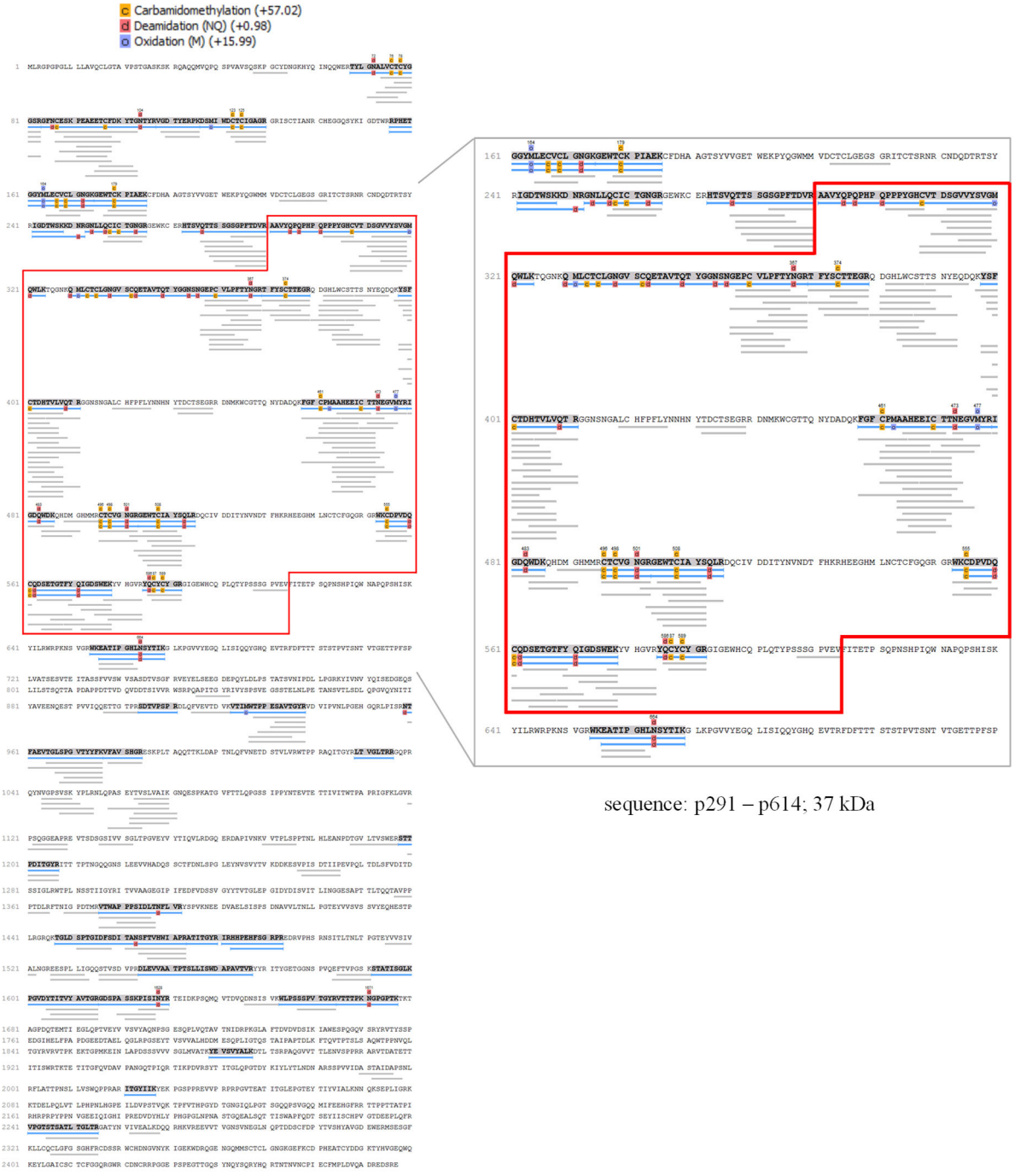


sequence: p291 – p614; 37 kDa


cell-binding fragment
C Carbamidomethylation (+57.02)
d Deamidation (NQ) (+0.98)
o Oxidation (M) (+15.99)
sequence: p654 – p1540; 96 kDa

hep II-binding fragment


sequence: p654 – p1540; 32 kDa

### 6.2 Preliminary setup test for whole-cell ELISA using *B. burgdorferi*

The bacterial binding to Fn was first intended using Fn-coated wells and exposed to bacteria for binding evaluation. Preliminary tests were carried out in order to set up working conditions for each bacterial species. A test using different cell numbers of *B. burgdorferi* revealed bacterial binding in all wells, including the ones that only contained the blocking solution and were not Fn-coated (i.e. 0 μg Fn) (**Figure 38**). Based on these results, bacteria and Fn interaction was further evaluated with a modified whole-cell ELISA using bacterial-coated wells exposed to increasing amounts of Fn.

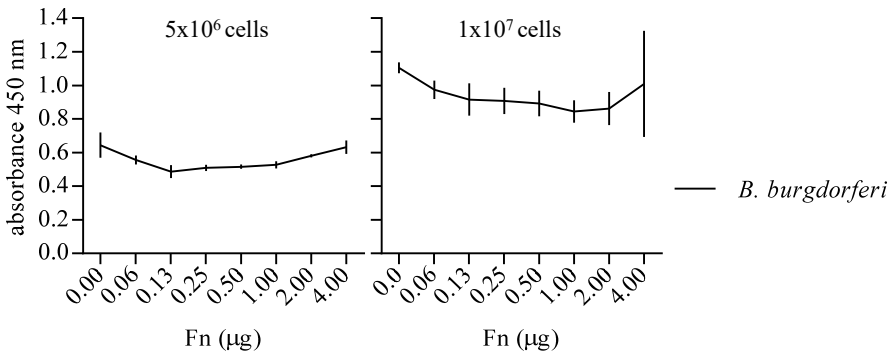


**Figure 38. Binding of *B. burgdorferi* to increasing amounts of immobilised plasma Fn.** Binding of *B. burgdorferi* (cell number = $5x10^6$ and $1x10^7$ cells) to increasing amounts of Fn-coated wells (0.06 to 4.00 μg). Adherent bacteria were detected using rabbit anti-*B. burgdorferi* antibodies.

### 6.3 Prediction of domain 27 using AlphaFold2

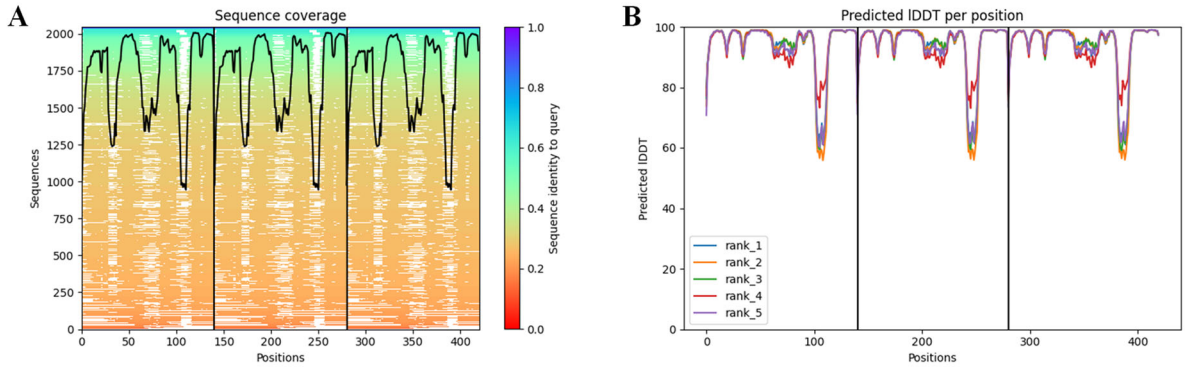


**Figure 39. Prediction quality and AlphaFold2 confidence measures for domain 27. (A)** Sequence coverage. Analysis was done by multiple sequence alignment (MSA) of evolutionary-related proteins. The sequence identity to query is colour coded. The amino acid location is given in consecutive order for the three chains of the homotrimer. **(B)** Predicted LDDT per position (pLDDT). Generates by a per-residue estimation of the prediction confidence on a scale from 0 – 100; a higher pLDDT is better. The region corresponding to the peptide identified in XL c is located within p105 - 111, p245 - 251, p385 - 391. The rank for the five structures generated is presented in colour coded. The graphics were obtained from ColabFold AlphaFold2.

## 6.4 Complete images of Western blot membranes

**Figure 5A**

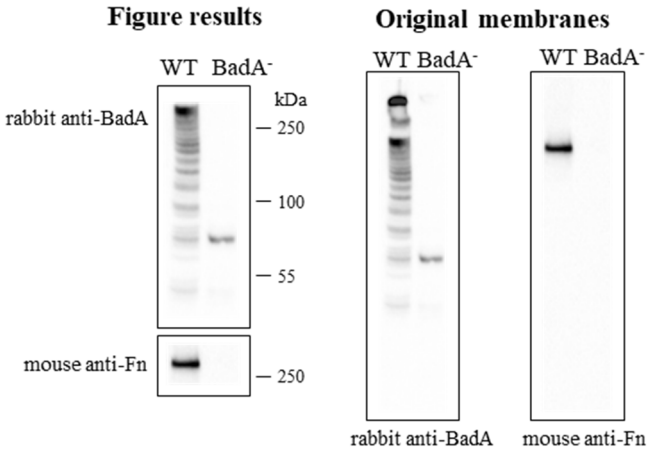


**Figure 6**

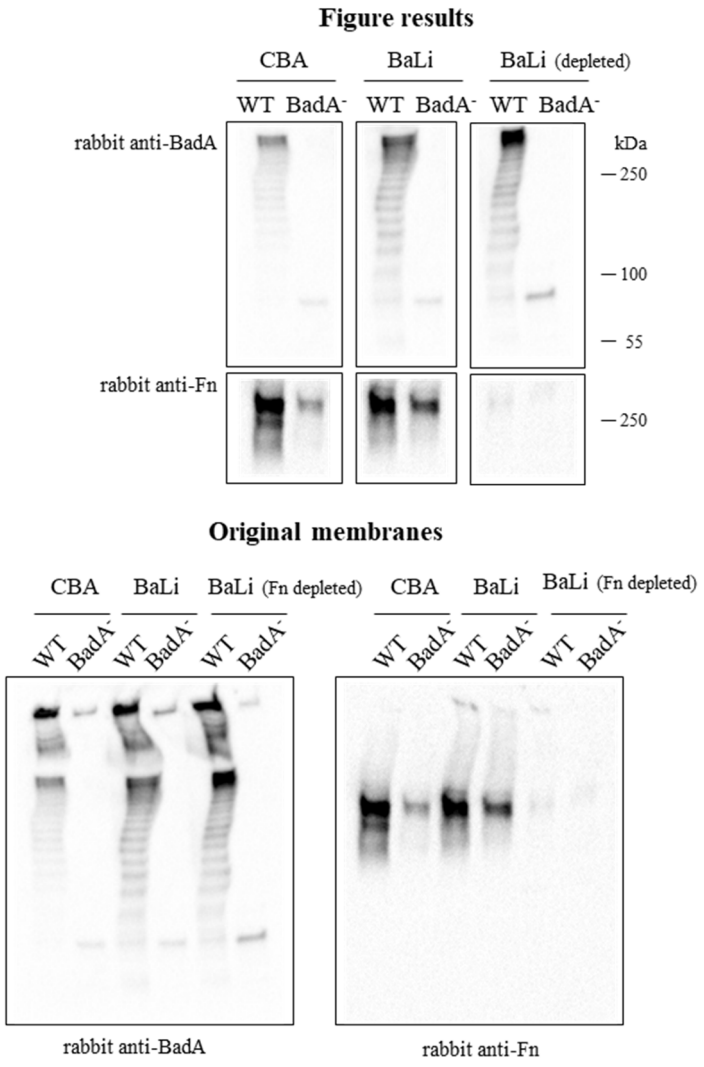

**Figure 17 B**

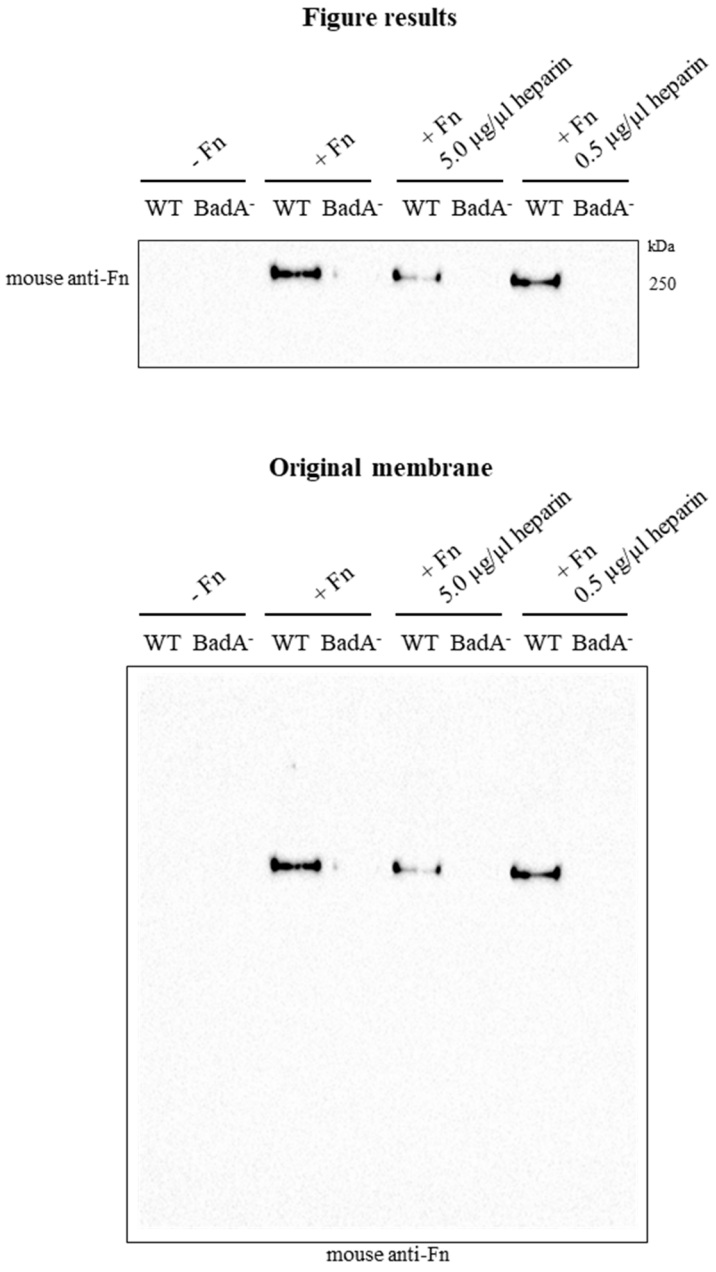
Figure results
- Fn
+ Fn
+ Fn 5.0 µg/µl heparin
+ Fn 0.5 µg/µl heparin
WT BadA- WT BadA- WT BadA- WT BadA-
mouse anti-Fn
kDa
250
Original membrane
- Fn
+ Fn
+ Fn 5.0 µg/µl heparin
+ Fn 0.5 µg/µl heparin
WT BadA- WT BadA- WT BadA- WT BadA-
mouse anti-Fn

**Figure 25**

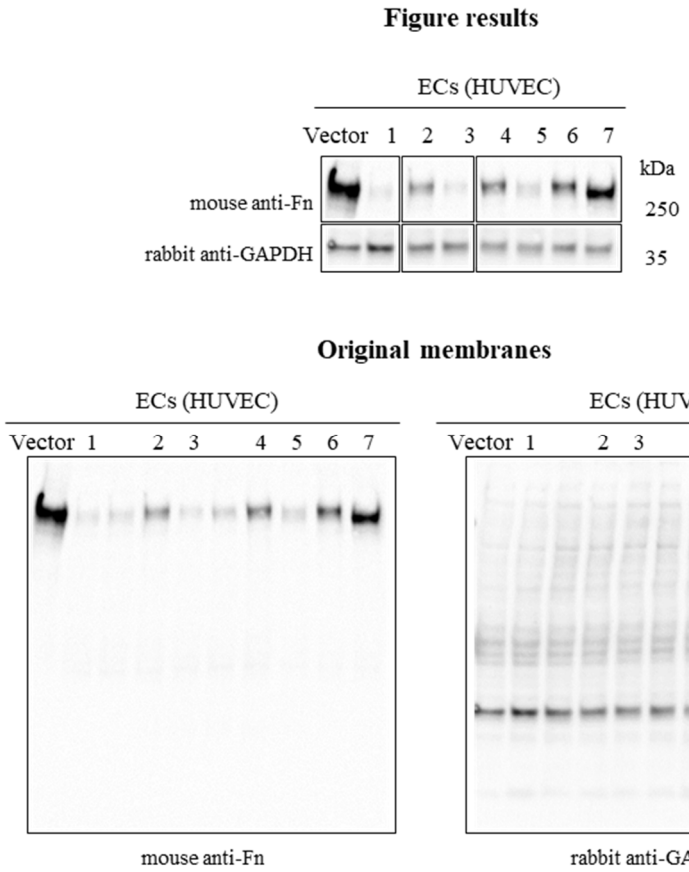


**Figure 26A**

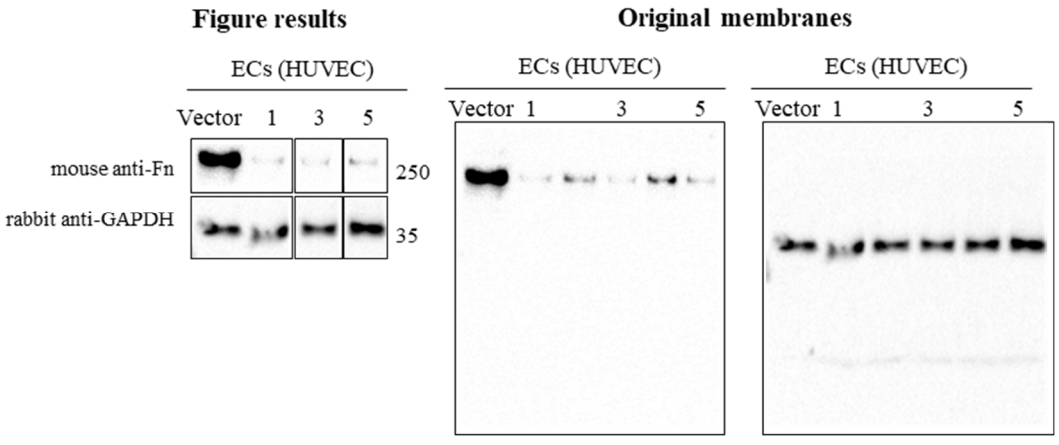

**Figure 26B**

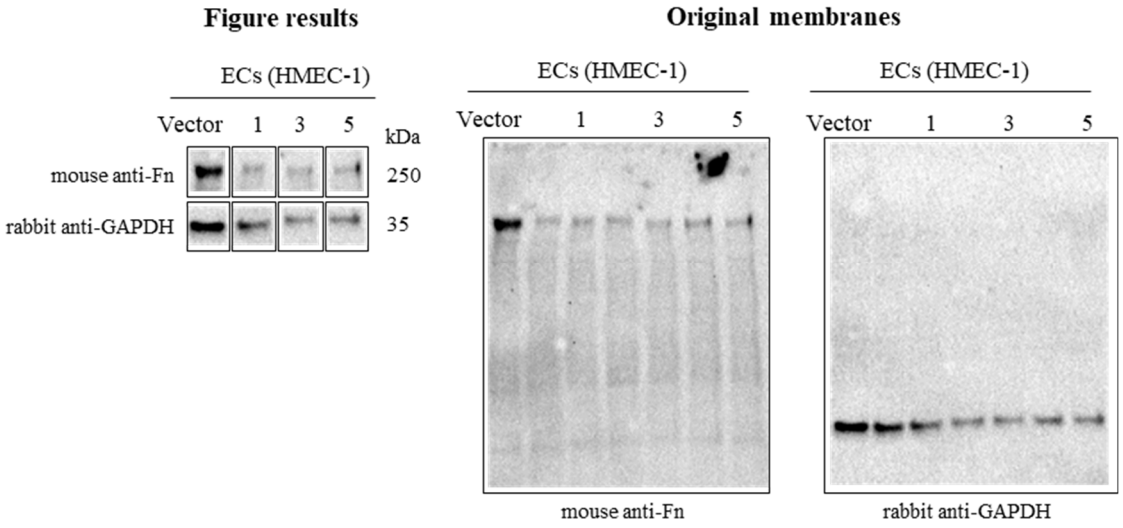
Figure results
ECs (HMEC-1)
Vector 1 3 5
kDa
mouse anti-Fn
250
rabbit anti-GAPDH
35
Original membranes
ECs (HMEC-1)
Vector 1 3 5
mouse anti-Fn
ECs (HMEC-1)
Vector 1 3 5
rabbit anti-GAPDH

# 7 ABSTRACT

The capacity of pathogenic bacteria to adhere to host cells and to avoid subsequent clearance by the host´s immune response is the initial and most decisive step leading to infections. Human pathogenic bacteria circulating in the bloodstream need to find ways to interact with endothelial cells (ECs) lining the blood vessels to infect and colonise the host. The extracellular matrix (ECM) of ECs might represent an attractive initial target for bacterial interaction, as many bacterial adhesins have reported affinities to ECM proteins, particularly fibronectin (Fn). Trimeric autotransporter adhesins (TAA) have been described as important pathogenicity factors of Gram-negative bacteria. The TAA from human pathogenic *Bartonella henselae*, *Bartonella* adhesin A (BadA), is one of the longest and best characterised adhesin and represents a prototypic TAA due to its domain architecture. *B. henselae,* the causative agent of cat scratch disease, endocarditis, and bacillary angiomatosis, adheres to ECs and ECM proteins via BadA interaction.

In this research, it was determined that the interaction between BadA and Fn is essential for *B. henselae* host cell adhesion. BadA interactions were identified within the heparin-binding domains of Fn, and the exact binding sites were revealed by mass spectrometry analysis of chemically crosslinked whole-cell bacteria and Fn. It turned out that specific BadA interactions with defined Fn regions represent the molecular basis for bacterial adhesion to ECs. These data were confirmed by using BadA-deficient bacteria and CRISPR-Cas *FN1* knockout ECs. It was also identified that BadA binds to Fn from both cellular and plasma origin, suggesting that *B. henselae* binding to Fn might possibly take part in other infection processes apart from bacterial adherence, e.g. evasion from the host cell immune system.

Interactions between TAAs and Fn represent a key step for adherence of *B. henselae* to ECs. Still, Fn-mediated binding is of more significant importance for pathogenic bacteria than broadly recognised. Fn removal from the ECM environment of ECs, also reduced adherence of *Staphylococcus aureus*, *Borrelia burgdorferi*, and *Acinetobacter baumannii* to host cells Interactions between adhesins and Fn might therefore represent a crucial step for the adhesion of human-pathogenic Gram-negative and Gram-positive bacteria targeting the ECs as a niche of infection or as means for persistence.

This research demonstrated that combining large-scale analysis approaches to describe protein-protein interactions with supportive functional readouts (binding assays) allows for the discrimination of crucial interactions involved in bacterial adhesion to the host. The herein-described experimental approaches and tools might guide future research for other pathogenic bacteria and represent an initial point for the future generation of anti-virulence strategies to inhibit bacterial binding to host cells.

# 8 ZUSAMMENFASSUNG

## Einleitung

Humanpathogene Bakterien, die im Blutkreislauf zirkulieren, müssen einen Weg finden, um mit den, die Blutgefäße auskleidenden Endothelzellen (EC), zu interagieren, um den Wirt nachfolgend infizieren zu können. Die extrazelluläre Matrix (ECM) der EC könnte dabei ein attraktives erstes Ziel für die bakterielle Interaktion darstellen. Fibronektin (Fn), ein Bestandteil der ECM, kommt in verschiedenen Formen vor: als plasmatisches Fn in Körperflüssigkeiten und als zelluläres Fn auf den Oberflächen von Zellen als Verbindung zu der perizellulären Umgebung und anderen ECM-Komponenten. Fn wurde als Interaktionspartner für viele bakterielle Adhäsine beschrieben, die Wirtszelladhäsion und nachfolgend bakterielle Virulenz vermitteln.

Trimere Autotransporter-Adhäsine (TAA) wurden als wichtige Pathogenitätsfaktoren von gramnegativen Bakterien beschrieben. TAA werden auf der Bakterienoberfläche exprimiert und sind durch eine Membran-Ankerdomäne am C-Terminus, eine sich wiederholende Hals-/Stielstruktur und einer Kopfdomäne am N-Terminus gekennzeichnet. Das *Bartonella*-Adhäsin A (BadA) ist eines der längsten, charakterisierten TAA und stellt aufgrund seiner Domänenarchitektur ein prototypisches TAA dar. BadA ist ein wesentlicher Pathogenitätsfaktor von *B. henselae*, dem Erreger der Katzenkratzkrankheit und vaskuloproliferativen Erkrankungen bei immunsupprimierten Patienten. Das Vorhandensein von BadA ist entscheidend für die Bindung von *B. henselae* an EC und ECM-Proteine, einschließlich Fn.

Die Untersuchung der Mechanismen der bakteriellen Wirtszelladhäsion kann einen Anhaltspunkt für die Verhinderung von Infektionen geben. Moderne Proteom-Technologien zur Analyse von Protein-Protein-Wechselwirkungen stellen ein großes Potenzial für die Beschreibung von Wirt-Pathogen-Wechselwirkungen dar. Die Identifizierung molekularer Mechanismen, die an der bakteriellen Adhäsion beteiligt sind, könnten eine Grundlage für

die Entwicklung neuer anti-Virulenz-basierter Therapiealternativen für antibiotikaresistente Bakterien bilden.

### Zielsetzung

Ziel dieser Arbeit war es, die Interaktion von BadA und Fn und die Bedeutung von Fn für die bakterielle Adhärenz zu untersuchen. Dabei wurden insbesondere folgende Punkte berücksichtigt: (1) Die Bedeutung von BadA als Hauptdeterminante für die Bindung von *B. henselae* an Fn sollte mit Hilfe der Quantifizierung der Proteinhäufigkeit sowie Bindungsassays aufgeklärt werden. (2) Die Interaktion von BadA mit zellulärem Fn bzw. plasmatischem Fn sollte mit Hilfe von Bindungsassays und massenspektrometrischen (MS)-Analysen bewertet werden. (3) Die molekulare Interaktion von BadA mit Fn sowie Fn-Regionen, die für die Bindung von BadA wichtig sind, sollten mit Hilfe von MS und Bindungsassays aufgeklärt werden. (4) *FN1* defiziente EC sollten mit Hilfe von CRISPR-Cas für den Einsatz in Infektionsversuchen generiert werden. (5) Die Rolle von Fn bei der bakteriellen Adhäsion im Allgemeinen sollte durch die Verwendung einer Reihe pathogener Bakterien (z. B. *Acinetobacter baumannii*, *B. henselae*, *Borrelia burgdorferi* und *Staphylococcus aureus*) in Infektionsexperimenten mit *FN1* defizienten EC untersucht werden.

### BadA als wichtigste Determinante für die Bindung von *B. henselae* an Fn

Drei *B. henselae*-Außenmembranproteine (OMP), Omp 43, Omp 89 und Pap 31, mit Affinität zu Fn, wurden zuvor in der Literatur beschrieben. Das Vorkommen dieser OMP wurden bei den beiden, in dieser Studie verwendeten, *B. henselae*-Stämmen (WT und BadA$^-$) mittels MS nachgewiesen. Die für *B. henselae* BadA$^-$ beobachtete Hintergrund-Fn-Bindung könnte durch diese OMPs erklärt werden.

Darüber hinaus wurde mit Hilfe von Bindungstests das Vorhandensein von BadA als primäre und wichtigste Determinante für die Bindung von *B. henselae* an Fn bestätigt. Mit Hilfe von

Bindungsassays wurde nachgewiesen, dass *B. henselae* sowohl an aus Plasma als auch aus zellulären Quellen gereinigtes Fn bindet. Gemäß der durch XL-MS-Analyse nachgewiesenen Peptid-Peptid-Interaktion ist die Interaktion von BadA mit zellulärem Fn innerhalb der Hep I-Bindungsdomäne lokalisiert, während sich die Interaktion mit plasmatischem Fn auf mehrere Stellen verteilt (Hep I-Bindungsdomäne, Hep II-Bindungsdomäne, C-Terminus). Die Ergebnisse deuten auf eine Domänen-spezifische Interaktion von BadA mit Plasma-Fn bzw. zellulärem Fn hin. Aufgrund der unterschiedlichen Beschaffenheit von plasmatischem und zellulärem Fn kann spekuliert werden, dass BadA an Regionen im zellulären Fn bindet, die aufgrund der Molekularstruktur von plasmatischem Fn nicht exponiert sind und daher kein Bindungsmotiv darstellen. Die Maskierung von *B. henselae* mit plasmatischem Fn könnte eine bakterielle Strategie darstellen, um der Immunantwort des Wirts zu entgehen, aber dennoch die Fähigkeit zu behalten, über perizelluläres Fn an Wirtszellen binden zu können.

**Heparin-bindende Domänen in Fn als wichtige BadA-Bindungsstellen**

Die heparinbindenden Regionen von Fn wurden als Interaktionsstellen für Adhäsine vieler pathogener Bakterien beschrieben. Gereinigte Fn-Fragmente, die die volle Länge von Fn abdecken, wurden in Bindungsversuche zur Lokalisation von Regionen mit BadA-Bindungskapazität, eingesetzt. Die Heparin-bindenden Domänen konnten als stärkste Bindungsstellen für BadA identifiziert werden, und zwar in ähnlichem Ausmaß im Vergleich zum kompletten. Diese Beobachtung belegt, dass die Heparin-bindenden Domänen von Fn die Hauptrolle bei der TAA-vermittelten Adhäsion von *B. henselae* spielen. Um die Interaktion von BadA mit den Heparin-bindenden Domänen von Fn zu beweisen, wurde Heparin als Kompetitor in bakterielle Bindungstests einbezogen. Es konnte gezeigt werden, dass die Bindung der Bakterien an Fn dosisabhängig mit zunehmender Menge an Heparin reduziert wurde.

### Identifizierung der molekularen Wechselwirkungen zwischen BadA und Fn

In der XL-MS-Analyse wurden die BadA-Interaktionen, die innerhalb der Heparin-bindenden Domänen in Fn identifiziert wurden, den sich wiederholenden Domänen der BadA-Hals/Stiel-Region zugeordnet. Kürzlich durchgeführte Forschungsarbeiten bestätigten die hier identifizierten Interaktionen unter Verwendung von *B. henselae* Mutanten, die jeweils ein verkürztes, mit den relevanten Domänen ausgestattetes, BadA exprimieren. Zusätzliche XL-MS-Wechselwirkungen wurden in anderen Regionen als den Heparin-bindenden Domänen identifiziert und anhand der verfügbaren Proteinstrukturen *in silico* bestätigt. Diese Wechselwirkungen wurden in früheren Untersuchungen als nicht Fn-bindende BadA-Regionen beschrieben und könnten eine Ergänzung zu den bereits starken Hals-Stiel-Wechselwirkungen mit Fn insbesondere unter Scherbelastung, wie sie natürlicherweise in Blutgefäßen vorkommt, darstellen und diese verstärken.

### Die Bedeutung von Fn für die Anhaftung von pathogenen Bakterien

Die Eignung von HUVEC und HMEC-1 wurde für die Durchführung eines CRISPR-Cas-vermittelten *FN1*-Knockout getestet, um ein geeignetes EC-Modell zu etablieren. HUVEC mit der effizientesten Knockout-Behandlung wurden für Infektionsversuche ausgewählt. Funktionsverlust-Infektionsexperimente mit den *FN1*-Knockout-HUVEC wurden mit gramnegativen und grampositiven Bakterien (*A. baumannii*, *B. henselae*, *B. burgdorferi* und *S. aureus*) durchgeführt. Die an EC gebundenen Bakterien wurden durch absolute Quantifizierung der bakteriellen und menschlichen Genkopien bewertet. Bei Verwendung von *FN1*-Knockout-Zellen war die Zahl der an HUVEC haftenden Bakterien bei allen Bakteriengattungen deutlich reduziert (*A. baumannii*: um 25 %; *B. henselae*: um 58%, *B. burgdorferi*: um 34%, *S. aureus*: um 79%).

Die Wechselwirkungen zwischen BadA und Fn sind für die Adhärenz von *B. henselae* an EC unerlässlich. Die maßgebliche Rolle von Fn für die Adhärenz von *B. henselae* wurde durch Einsatz von *FN1*-Knockout-EC belegt. Im Fall von *S. aureus* wurden die Adhäsine FnBPA und FnBPB bereits als entscheidend für die Fn-Bindung an und Internalisierung in

EC beschrieben. Bei *B. henselae* und *S. aureus* hat die Inhibition der Fn-vermittelten Interaktion signifikante Auswirkungen auf ihre Adhäsion an Wirtszellen. Im Falle von *B. burgdorferi* und *A. baumannii* könnte die Fn-vermittelte Adhäsion ebenfalls eine wesentliche bakterielle Adhäsionsstrategie darstellen. Es ist bekannt, dass die Adhäsion von *B. burgdorferi* an EC durch die Interaktion verschiedener Adhäsine und Wirtsrezeptoren vermittelt wird. Bei *A. baumannii* wurde berichtet, dass die bakterielle Adhäsion an ECs durch das Ata-Protein (ein Vertreter der Klasse der TAA) vermittelt wird, das eine geringere Bindungskapazität an Fn als an andere ECM-Proteine (z. B. Laminin, Kollagene) aufweist.

Das Szenario der bakteriellen Adhäsion an den Wirt ist durch ein komplexes Zusammenspiel mehrerer Variablen charakterisiert. Das Vorhandensein selektiver Adhäsionsmechanismen in Abhängigkeit vom Wirtszelltropismus, der ECM-Zusammensetzung und der Redundanz der Interaktion zwischen Adhäsinen und zellulären Rezeptoren beeinflussen allesamt – wahrscheinlich im gegenseitigen Wechselspiel - die bakterielle Adhärenz. Die in dieser Arbeit erzielten Ergebnisse zeigen eindeutig, dass der Interaktion von grampositiven oder gramnegativen Bakterien mit endothelialem Fn eine wesentliche Rolle für die bakterielle Adhäsion an den Wirt zukommt. Die Fn-vermittelte Interaktion könnte ein entscheidender Ausgangspunkt für Infektionen mit Bakterien mit Endotheltropismus (z. B. *B. henselae* oder *S. aureus*) sein, sowie für pathogene Bakterien, deren Interaktion mit EC einen ersten Schritt für eine Erregerpersistenz darstellt (z. B. *B. burgdorferi* und *A. baumannii*). Die Beschreibung molekularer Mechanismen, die an den Interaktionen zwischen Bakterien und EC beteiligt sind, liefern wichtige Informationen über das komplexe Zusammenspiel zwischen Bakterium und Wirt und stellen die Grundlage für neue Strategien zur Beeinflussung dieser Interaktionen dar, um zukünftig bakterielle Infektionen durch Modulation der Adhärenz (sog. „anti-Liganden“) therapeutisch zu verhindern.

# 9 REFERENCES


1. Singh B, Fleury C, Jalalvand F, Riesbeck K. (2012) Human pathogens utilize host extracellular matrix proteins laminin and collagen for adhesion and invasion of the host. FEMS Microbiol Rev 36:1122–1180.
2. Henderson B, Nair S, Pallas J, Williams MA. (2011) Fibronectin: a multidomain host adhesin targeted by bacterial fibronectin-binding proteins. FEMS Microbiol Rev 35:147–200.
3. Okaro U, Addisu A, Casanas B, Anderson B. (2017) *Bartonella* species, an emerging cause of blood-culture-negative endocarditis. Clin Microbiol Rev 30:709–746.
4. Harms A, Dehio C. (2012) Intruders below the Radar: Molecular pathogenesis of *Bartonella* spp. Clin Microbiol Rev 25:42–78.
5. Koehler JE, Glaser CA, Tappero JW. (1994) *Rochalimaea henselae* infection. A new zoonosis with the domestic cat as reservoir. JAMA 271:531–535.
6. Chomel BB, Kasten RW, Floyd-Hawkins K, Chi B, Yamamoto K, Roberts-Wilson J, Gurfield AN, Abbott RC, Pedersen NC, Koehler JE. (1996) Experimental transmission of *Bartonella henselae* by the cat flea. J Clin Microbiol 34:1952–1956.
7. Chomel BB, Boulouis H-J, Breitschwerdt EB, Kasten RW, Vayssier-Taussat M, Birtles RJ, Koehler JE, Dehio C. (2009) Ecological fitness and strategies of adaptation of *Bartonella* species to their hosts and vectors. Vet Res 40:29.
8. Chomel BB. (2000) Cat-scratch disease. OIE Rev Sci Tech 19:136–150.
9. Resto-Ruiz S, Burgess A, Anderson BE. (2003) The role of the host immune response in pathogenesis of *Bartonella henselae*. DNA Cell Biol 22:431–440.
10. Mohle-Boetani JC, Koehler JE, Berger TG, LeBoit PE, Kemper CA, Reingold AL, Plikaytis BD, Wenger JD, Tappero JW. (1996) Bacillary angiomatosis and bacillary peliosis in patients infected with human immunodeficiency virus: clinical characteristics in a case-control study. Clin Infect Dis 22:794–800.
11. Jost M, Latz A, Ballhorn W, Kempf VAJJ. (2018) Development of a specific and sensitive enzyme-linked immunosorbent assay as an *in vitro* diagnostic tool for detection of *Bartonella henselae* antibodies in human serum. J Clin Microbiol 56:e01329-18.
12. Vermeulen MJ, Herremans M, Verbakel H, Bergmans AMC, Roord JJ, van Dijken

PJ, Peeters MF. (2007) Serological testing for *Bartonella henselae* infections in The Netherlands: clinical evaluation of immunofluorescence assay and ELISA. Clin Microbiol Infect 13:627–634.

13. Jensen WA, Fall MZ, Rooney J, Kordick DL, Breitschwerdt EB. (2000) Rapid identification and differentiation of *Bartonella* species using a single-step PCR assay. J Clin Microbiol 38:1717–1722.
14. Hobson C, Le Brun C, Beauruelle C, Maakaroun-Vermesse Z, Mereghetti L, Goudeau A, Lanotte P. (2017) Detection of *Bartonella* in cat scratch disease using a single-step PCR assay kit. J Med Microbiol 66:1596–1601.
15. Houpikian P, Raoult D. (2005) Blood culture-negative endocarditis in a reference center. Medicine (Baltimore) 84:162–173.
16. Vaca DJ, Dobler G, Fischer SF, Keller C, Konrad M, von Loewenich FD, Orenga S, Sapre SU, van Belkum A, Kempf VAJ. (2022) Contemporary diagnostics for medically relevant fastidious microorganisms belonging to the genera *Anaplasma*, *Bartonella*, *Coxiella*, *Orientia*, and *Rickettsia*. FEMS Microbiol Rev 1–19.
17. Kordick DL, Brown TT, Shin K, Breitschwerdt EB. (1999) Clinical and pathologic evaluation of chronic *Bartonella henselae* or *Bartonella clarridgeiae* infection in cats. J Clin Microbiol 37:1536–1547.
18. Kempf VAJ, Schaller M, Behrendt S, Volkmann B, Aepfelbacher M, Cakman I, Autenrieth IB. (2000) Interaction of *Bartonella henselae* with endothelial cells results in rapid bacterial rRNA synthesis and replication. Cell Microbiol 2:431–441.
19. Kempf VAJ, Hitziger N, Riess T, Autenrieth IB. (2002) Do plant and human pathogens have a common pathogenicity strategy? Trends Microbiol 10:269–275.
20. Riess T, Andersson SGE, Lupas A, Schaller M, Schäfer A, Kyme P, Martin J, Wälzlein J-HH, Ehehalt U, Lindroos H, Schirle M, Nordheim A, Autenrieth IB, Kempf VAJ. (2004) *Bartonella* adhesin A mediates a proangiogenic host cell response. J Exp Med 200:1267–1278.
21. Dehio C, Meyer M, Berger J, Schwarz H, Lanz C. (1997) Interaction of *Bartonella henselae* with endothelial cells results in bacterial aggregation on the cell surface and the subsequent engulfment and internalisation of the bacterial aggregate by a unique structure, the invasome. J Cell Sci 110:2141–2154.
22. Kempf VAJ, Lebiedziejewski M, Alitalo K, Wälzlein J-H, Ehehalt U, Fiebig J, Huber S, Schütt B, Sander CA, Müller S, Grassl G, Yazdi AS, Brehm B, Autenrieth IB.

(2005) Activation of hypoxia-inducible factor-1 in bacillary angiomatosis: evidence for a role of hypoxia-inducible factor-1 in bacterial infections. Circulation 111:1054–1062.

23. Schmid MC, Schulein R, Dehio M, Denecker G, Carena I, Dehio C. (2004) The VirB type IV secretion system of *Bartonella henselae* mediates invasion, proinflammatory activation and antiapoptotic protection of endothelial cells. Mol Microbiol 52:81–92.
24. Kempf VAJ, Volkmann B, Schaller M, Sander CA, Alitalo K, Riess T, Autenrieth IB. (2001) Evidence of a leading role for VEGF in *Bartonella henselae*-induced endothelial cell proliferations. Cell Microbiol 3:623–632.
25. Okaro U, Green R, Mohapatra S, Anderson B. (2019) The trimeric autotransporter adhesin BadA is required for *in vitro* biofilm formation by *Bartonella henselae*. npj Biofilms Microbiomes 5:10.
26. Burgess AWO, Anderson BE. (1998) Outer membrane proteins of *Bartonella henselae* and their interaction with human endothelial cells. Microb Pathog 25:157–164.
27. Dabo SM, Confer AW, Saliki JT, Anderson BE. (2006) Binding of *Bartonella henselae* to extracellular molecules: Identification of potential adhesins. Microb Pathog 41:10–20.
28. Dabo SM, Confer AW, Anderson BE, Gupta S. (2006) *Bartonella henselae* Pap31, an extracellular matrix adhesin, binds the fibronectin repeat III13 module. Infect Immun 74:2513–2521.
29. Zimmermann R, Kempf VAJ, Schiltz E, Oberle K, Sander A. (2003) Hemin binding, functional expression, and complementation analysis of Pap 31 from *Bartonella henselae*. J Bacteriol 185:1739–1744.
30. Linke D, Riess T, Autenrieth IB, Lupas A, Kempf VAJ. (2006) Trimeric autotransporter adhesins: variable structure, common function. Trends Microbiol 14:264–270.
31. Mühlenkamp M, Oberhettinger P, Leo JC, Linke D, Schütz MS. (2015) *Yersinia* adhesin A (YadA) – Beauty & beast. Int J Med Microbiol 305:252–258.
32. Bentancor L V, Camacho-Peiro A, Bozkurt-Guzel C, Pier GB, Maira-Litrán T. (2012) Identification of Ata, a multifunctional trimeric autotransporter of *Acinetobacter baumannii*. J Bacteriol 194:3950–3960.
33. Serruto D, Spadafina T, Scarselli M, Bambini S, Comanducci M, Höhle S, Kilian M,

Veiga E, Cossart P, Oggioni MR, Savino S, Ferlenghi I, Taddei AR, Rappuoli R, Pizza M, Masignani V, Aricò B. (2009) HadA is an atypical new multifunctional trimeric coiled-coil adhesin of *Haemophilus influenzae* biogroup aegyptius, which promotes entry into host cells. Cell Microbiol 11:1044–1063.

34. Meng G, Surana NK, St Geme JW, Waksman G. (2006) Structure of the outer membrane translocator domain of the *Haemophilus influenzae* Hia trimeric autotransporter. EMBO J 25:2297–2304.
35. Malito E, Biancucci M, Faleri A, Ferlenghi I, Scarselli M, Maruggi G, Lo Surdo P, Veggi D, Liguori A, Santini L, Bertoldi I, Petracca R, Marchi S, Romagnoli G, Cartocci E, Vercellino I, Savino S, Spraggon G, Norais N, Pizza M, Rappuoli R, Masignani V, Bottomley MJ. (2014) Structure of the meningococcal vaccine antigen NadA and epitope mapping of a bactericidal antibody. Proc Natl Acad Sci 111:17128–17133.
36. Hoiczyk E. (2000) Structure and sequence analysis of *Yersinia* YadA and *Moraxella* UspAs reveal a novel class of adhesins. EMBO J 19:5989–5999.
37. Zhang P, Chomel BB, Schau MK, Goo JS, Droz S, Kelminson KL, George SS, Lerche NW, Koehler JE. (2004) A family of variably expressed outer-membrane proteins (Vomp) mediates adhesion and autoaggregation in *Bartonella quintana*. Proc Natl Acad Sci 101:13630–13635.
38. Leo JC, Grin I, Linke D. (2012) Type V secretion: mechanism(S) of autotransport through the bacterial outer membrane. Philos Trans R Soc B Biol Sci 367:1088–1101.
39. Albenne C, Ieva R. (2017) Job contenders: roles of the β-barrel assembly machinery and the translocation and assembly module in autotransporter secretion. Mol Microbiol 106:505–517.
40. Bassler J, Hernandez Alvarez B, Hartmann MD, Lupas AN. (2015) A domain dictionary of trimeric autotransporter adhesins. Int J Med Microbiol 305:265–275.
41. Thibau A, Hipp K, Vaca DJ, Chowdhury S, Malmström J, Saragliadis A, Ballhorn W, Linke D, Kempf VAJ. (2022) Long-Read sequencing reveals genetic adaptation of *Bartonella* adhesin A among different *Bartonella henselae* isolates. Front Microbiol 13:1–17.
42. Tu N, Lima A, Bandeali Z, Anderson B. (2016) Characterization of the general stress response in *Bartonella henselae*. Microb Pathog 92:1–10.
43. Batterman HJ, Peek JA, Loutit JS, Falkow S, Tompkins LS. (1995)

*Bartonella henselae* and *Bartonella quintana* adherence to and entry into cultured human epithelial cells. Infect Immun 63:4553–4556.

44. Riess T, Raddatz G, Linke D, Schäfer A, Kempf VAJ. (2007) Analysis of *Bartonella* adhesin A expression reveals differences between various *B. henselae* strains. Infect Immun 75:35–43.
45. Szczesny P, Linke D, Ursinus A, Bär K, Schwarz H, Riess TM, Kempf VAJ, Lupas AN, Martin J, Zeth K. (2008) Structure of the head of the *Bartonella* adhesin BadA. PLoS Pathog 4:e1000119.
46. Kaiser PO, Riess T, Wagner CL, Linke D, Lupas AN, Schwarz H, Raddatz G, Schäfer A, Kempf VAJ. (2008) The head of *Bartonella* adhesin A is crucial for host cell interaction of *Bartonella henselae*. Cell Microbiol 10:2223–2234.
47. Kaiser PO, Linke D, Schwarz H, Leo JC, Kempf VAJ. (2012) Analysis of the BadA stalk from *Bartonella henselae* reveals domain-specific and domain-overlapping functions in the host cell infection process. Cell Microbiol 14:198–209.
48. Schmidgen T, Kaiser PO, Ballhorn W, Franz B, Gottig S, Linke D, Kempf VAJ. (2014) Heterologous expression of *Bartonella* adhesin A in *Escherichia coli* by exchange of trimeric autotransporter adhesin domains results in enhanced adhesion properties and a pathogenic phenotype. J Bacteriol 196:2155–2165.
49. Kaiser PO, Riess T, O'Rourke F, Linke D, Kempf VAJ, O'Rourke F, Linke D, Kempf VAJ. (2011) *Bartonella* spp.: Throwing light on uncommon human infections. Int J Med Microbiol 301:7–15.
50. Mirdita M, Schütze K, Moriwaki Y, Heo L, Ovchinnikov S, Steinegger M. (2022) ColabFold: making protein folding accessible to all. Nat Methods 19:679–682.
51. Frantz C, Stewart KM, Weaver VM. (2010) The extracellular matrix at a glance. J Cell Sci 123:4195–4200.
52. Kadler KE, Baldock C, Bella J, Boot-Handford RP. (2007) Collagens at a glance. J Cell Sci 120:1955–1958.
53. Ricard-Blum S. (2011) The collagen family. Cold Spring Harb Perspect Biol 3:a004978.
54. Brodsky B, Persikov A V. (2005) Molecular structure of the collagen triple helix. Adv Protein Chem 70:301–339.
55. Sasaki T, Fässler R, Hohenester E. (2004) Laminin: the crux of basement membrane assembly. J Cell Biol 164:959–963.

56. Durbeej M. (2010) Laminins. Cell Tissue Res 339:259–268.
57. Aumailley M, Bruckner-Tuderman L, Carter WG, Deutzmann R, Edgar D, Ekblom P, Engel J, Engvall E, Hohenester E, Jones JCR, Kleinman HK, Marinkovich MP, Martin GR, Mayer U, Meneguzzi G, Miner JH, Miyazaki K, Patarroyo M, Paulsson M, Quaranta V, Sanes JR, Sasaki T, Sekiguchi K, Sorokin LM, Talts JF, Tryggvason K, Uitto J, Virtanen I, von der Mark K, Wewer UM, Yamada Y, Yurchenco PD. (2005) A simplified laminin nomenclature. Matrix Biol 24:326–332.
58. Hynes RO. (1990) Methods for identification of fibronectins, p. 7–23. *In* Fibronectins. Springer New York, New York, NY.
59. Cho J, Mosher DF. (2006) Role of fibronectin assembly in platelet thrombus formation. J Thromb Haemost 4:1461–1469.
60. Mao Y, Schwarzbauer JE. (2005) Fibronectin fibrillogenesis, a cell-mediated matrix assembly process. Matrix Biol 24:389–399.
61. Pankov R, Yamada K. (2002) Fibronectin at a glance. J Cell Sci 115:3861–3863.
62. Tressel T, McCarthy JB, Calaycay J, Lee TD, Legesse K, Shively JE, Pande H. (1991) Human plasma fibronectin. Demonstration of structural differences between the A- and B-chains in the III CS region. Biochem J 274:731–738.
63. Wilson CL, Schwarzbauer JE. (1992) The alternatively spliced V region contributes to the differential incorporation of plasma and cellular fibronectins into fibrin clots. J Cell Biol 119:923–933.
64. Vaca DJ, Thibau A, Schütz M, Kraiczy P, Happonen L, Malmström J, Kempf VAJ. (2020) Interaction with the host: the role of fibronectin and extracellular matrix proteins in the adhesion of Gram-negative bacteria. Med Microbiol Immunol 209:277–299.
65. Raitman I, Huang ML, Williams SA, Friedman B, Godula K, Schwarzbauer JE. (2018) Heparin-fibronectin interactions in the development of extracellular matrix insolubility. Matrix Biol 67:107–122.
66. Singh P, Carraher C, Schwarzbauer JE. (2010) Assembly of fibronectin extracellular matrix. Annu Rev Cell Dev Biol 26:397–419.
67. Johnson KJ, Sage H, Briscoe G, Erickson HP. (1999) The compact conformation of fibronectin is determined by intramolecular ionic interactions. J Biol Chem 274:15473–15479.
68. McDonald JA, Quade BJ, Broekelmann TJ, LaChance R, Forsman K, Hasegawa E,

Akiyama S. (1987) Fibronectin's cell-adhesive domain and an amino-terminal matrix assembly domain participate in its assembly into fibroblast pericellular matrix. J Biol Chem 262:2957–2967.

69. To WS, Midwood KS. (2011) Plasma and cellular fibronectin: distinct and independent functions during tissue repair. Fibrogenes Tissue Repair 4:1–17.
70. Chagnot C, Zorgani MA, Astruc T, Desvaux M. (2013) Proteinaceous determinants of surface colonization in bacteria: bacterial adhesion and biofilm formation from a protein secretion perspective. Front Microbiol 4:1–26.
71. Berne C, Ducret A, Hardy GG, Brun Y V. (2015) Adhesins involved in attachment to abiotic surfaces by Gram-negative bacteria. Microbiol Spectr 3:1–45.
72. Hymes JP, Klaenhammer TR. (2016) Stuck in the middle: fibronectin-binding proteins in Gram-positive bacteria. Front Microbiol 7:1504.
73. Lin Y-P, Chen Q, Ritchie JA, Dufour NP, Fischer JR, Coburn J, Leong JM. (2015) Glycosaminoglycan binding by *Borrelia burgdorferi* adhesin BBK32 specifically and uniquely promotes joint colonization. Cell Microbiol 17:860–875.
74. Heilmann C. (2011) Adhesion mechanisms of *Staphylococci*, p. 105–123. *In* Bacterial Adhesion. Linke D, Goldman A (eds.). Springer, Dordrecht, Dordrecht.
75. Bentancor L V, Routray A, Bozkurt-Guzel C, Camacho-Peiro A, Pier GB, Maira-Litrán T. (2012) Evaluation of the trimeric autotransporter Ata as a vaccine candidate against *Acinetobacter baumannii* infections. Infect Immun 80:3381–3388.
76. Smani Y, McConnell MJ, Pachón J. (2012) Role of fibronectin in the adhesion of *Acinetobacter baumannii* to host cells. PLoS One 7:e33073.
77. Smani Y, Dominguez-Herrera J, Pachon J. (2013) Association of the outer membrane protein Omp33 with fitness and virulence of *Acinetobacter baumannii*. J Infect Dis 208:1561–1570.
78. Kaiser PO, Riess T, Wagner CL, Linke D, Lupas AN, Schwarz H, Raddatz G, Schäfer A, Kempf VAJ. (2008) The head of *Bartonella* adhesin A is crucial for host cell interaction of *Bartonella henselae*. Cell Microbiol 10:2223–2234.
79. Probert WS, Johnson BJB. (1998) Identification of a 47 kDa fibronectin-binding protein expressed by *Borrelia burgdorferi* isolate B31. Mol Microbiol 30:1003–1015.
80. Kim JH, Singvall J, Schwarz-Linek U, Johnson BJB, Potts JR, Hook M. (2004) BBK32, a fibronectin binding MSCRAMM from *Borrelia burgdorferi*, contains a disordered region that undergoes a conformational change on ligand binding. J Biol

Chem 279:41706–41714.

81. Zhi H, Weening EH, Barbu EM, Hyde JA, Höök M, Skare JT. (2015) The BBA33 lipoprotein binds collagen and impacts *Borrelia burgdorferi* pathogenesis. Mol Microbiol 96:68–83.
82. Gaultney RA, Gonzalez T, Floden AM, Brissette CA. (2013) BB0347, from the lyme disease spirochete *Borrelia burgdorferi*, is surface exposed and interacts with the CS1 heparin-binding domain of human fibronectin. PLoS One 8:e75643.
83. Verma A, Brissette CA, Bowman A, Stevenson B. (2009) *Borrelia burgdorferi* BmpA is a laminin-binding protein. Infect Immun 77:4940–4946.
84. Hallström T, Haupt K, Kraiczy P, Hortschansky P, Wallich R, Skerka C, Zipfel PF. (2010) Complement regulator–acquiring surface protein 1 of *Borrelia burgdorferi* binds to human bone morphogenic protein 2, several extracellular matrix proteins, and plasminogen. J Infect Dis 202:490–498.
85. Brissette CA, Verma A, Bowman A, Cooley AE, Stevenson B. (2009) The *Borrelia burgdorferi* outer-surface protein ErpX binds mammalian laminin. Microbiology 155:863–872.
86. Brissette CA, Cooley AE, Burns LH, Riley SP, Verma A, Woodman ME, Bykowski T, Stevenson B. (2008) Lyme borreliosis spirochete Erp proteins, their known host ligands, and potential roles in mammalian infection. Int J Med Microbiol 298:257–267.
87. Brissette CA, Bykowski T, Cooley AE, Bowman A, Stevenson B. (2009) *Borrelia burgdorferi* RevA antigen binds host fibronectin. Infect Immun 77:2802–2812.
88. Brissette CA, Rossmann E, Bowman A, Cooley AE, Riley SP, Hunfeld K-P, Bechtel M, Kraiczy P, Stevenson B. (2010) The *Borrelial* fibronectin-binding protein RevA is an early antigen of human Lyme disease. Clin Vaccine Immunol 17:274–280.
89. Madani A, Garakani K, Mofrad MRK. (2017) Molecular mechanics of *Staphylococcus aureus* adhesin, CNA, and the inhibition of bacterial adhesion by stretching collagen. PLoS One 12:1–19.
90. Hansen U, Hussain M, Villone D, Herrmann M, Robenek H, Peters G, Sinha B, Bruckner P. (2006) The anchorless adhesin Eap (extracellular adherence protein) from *Staphylococcus aureus* selectively recognizes extracellular matrix aggregates

but binds promiscuously to monomeric matrix macromolecules. Matrix Biol 25:252–260.

91. Geraci J, Neubauer S, Pöllath C, Hansen U, Rizzo F, Krafft C, Westermann M, Hussain M, Peters G, Pletz MW, Löffler B, Makarewicz O, Tuchscherr L. (2017) The *Staphylococcus aureus* extracellular matrix protein (Emp) has a fibrous structure and binds to different extracellular matrices. Sci Rep 7:1–14.
92. Speziale P, Pietrocola G. (2020) The multivalent role of Fibronectin-Binding Proteins A and B (FnBPA and FnBPB) of *Staphylococcus aureus* in host infections. Front Microbiol 11:1–13.
93. Sottile J, Schwarzbauer J, Selegue J, Mosher DF. (1991) Five type I modules of fibronectin form a functional unit that binds to fibroblasts and *Staphylococcus aureus*. J Biol Chem 266:12840–12843.
94. Wells TJ, McNeilly TN, Totsika M, Mahajan A, Gally DL, Schembri MA. (2009) The *Escherichia coli* O157:H7 EhaB autotransporter protein binds to laminin and collagen I and induces a serum IgA response in O157:H7 challenged cattle. Environ Microbiol 11:1803–1814.
95. Hallström T, Singh B, Resman F, Blom AM, Mörgelin M, Riesbeck K. (2011) *Haemophilus influenzae* protein E binds to the extracellular matrix by concurrently interacting with laminin and vitronectin. J Infect Dis 204:1065–1074.
96. Sebghati TAS, Korhonen TK, Hornick DB, Clegg S. (1998) Characterization of the type 3 fimbrial adhesins of *Klebsiella* strains. Infect Immun 66:2887–2894.
97. Eberhard T, Virkola R, Korhonen T, Kronvall G, Ullberg M. (1998) Binding to human extracellular matrix by *Neisseria meningitidis*. Infect Immun 66:1791–1794.
98. Moschioni M, Emolo C, Biagini M, Maccari S, Pansegrau W, Donati C, Hilleringmann M, Ferlenghi I, Ruggiero P, Sinisi A, Pizza M, Norais N, Barocchi MA, Masignani V. (2010) The two variants of the *Streptococcus pneumoniae* pilus 1 RrgA adhesin retain the same function and elicit cross-protection *in vivo*. Infect Immun 78:5033–5042.
99. Alteri CJ, Xicohténcatl-Cortes J, Hess S, Caballero-Olín G, Girón JA, Friedman RL. (2007) *Mycobacterium tuberculosis* produces pili during human infection. Proc Natl Acad Sci U S A 104:5145–5150.
100. Drancourt M, Birtles R, Raoult D, Chaumentin G, Vandenesch F, Etienne J. (1996) New serotype of *Bartonella henselae* in endocarditis and cat-scratch disease. Lancet

347:441–443.

101. Babb K, McAlister JD, Miller JC, Stevenson B. (2004) Molecular characterization of *Borrelia burgdorferi* erp promoter/operator elements. J Bacteriol 186:2745–2756.
102. Novick R. (1967) Properties of a cryptic high-frequency transducing phage in *Staphylococcus aureus*. Virology 33:155–166.
103. Riess T, Dietrich F, Schmidt K V., Kaiser PO, Schwarz H, Schäfer A, Kempf VAJ. (2008) Analysis of a novel insect cell culture medium-based growth medium for *Bartonella* species. Appl Environ Microbiol 74:5224–5227.
104. Vaca DJ, Thibau A, Leisegang MS, Malmström J, Linke D, Eble JA, Ballhorn W, Schaller M, Happonen L, Kempf VAJ. (2022) Interaction of *Bartonella henselae* with fibronectin represents the molecular basis for adhesion to host cells. Microbiol Spectr 10:e0059822.
105. Sanjana NE, Shalem O, Zhang F. (2014) Improved vectors and genome-wide libraries for CRISPR screening. Nat Methods 11:783–784.
106. Livak KJ, Schmittgen TD. (2001) Analysis of relative gene expression data using Real-Time quantitative PCR and the 2−ΔΔCT method. Methods 25:402–408.
107. Weidensdorfer M, Chae JI, Makobe C, Stahl J, Averhoff B, Müller V, Schürmann C, Brandes RP, Wilharm G, Ballhorn W, Christ S, Linke D, Fischer D, Göttig S, Kempf VAJ. (2016) Analysis of endothelial adherence of *Bartonella henselae* and *Acinetobacter baumannii* using a dynamic human *ex vivo* infection model. Infect Immun 84:711–722.
108. Hauri S, Khakzad H, Happonen L, Teleman J, Malmström J, Malmström L. (2019) Rapid determination of quaternary protein structures in complex biological samples. Nat Commun 10:192.
109. Bauch A, Adamczyk I, Buczek P, Elmer F-J, Enimanev K, Glyzewski P, Kohler M, Pylak T, Quandt A, Ramakrishnan C, Beisel C, Malmstrom L, Aebersold R, Rinn B. (2011) openBIS: a flexible framework for managing and analyzing complex data in biology research. BMC Bioinformatics 12:468.
110. Teleman J, Dowsey AW, Gonzalez-Galarza FF, Perkins S, Pratt B, Röst HL, Malmström L, Malmström J, Jones AR, Deutsch EW, Levander F. (2014) Numerical compression schemes for proteomics mass spectrometry data. Mol Cell Proteomics 13:1537–1542.
111. Chambers MC, Maclean B, Burke R, Amodei D, Ruderman DL, Neumann S, Gatto L,

Fischer B, Pratt B, Egertson J, Hoff K, Kessner D, Tasman N, Shulman N, Frewen B, Baker TA, Brusniak M-Y, Paulse C, Creasy D, Flashner L, Kani K, Moulding C, Seymour SL, Nuwaysir LM, Lefebvre B, Kuhlmann F, Roark J, Rainer P, Detlev S, Hemenway T, Huhmer A, Langridge J, Connolly B, Chadick T, Holly K, Eckels J, Deutsch EW, Moritz RL, Katz JE, Agus DB, MacCoss M, Tabb DL, Mallick P. (2012) A cross-platform toolkit for mass spectrometry and proteomics. Nat Biotechnol 30:918–920.

112. Craig R, Beavis RC. (2003) A method for reducing the time required to match protein sequences with tandem mass spectra. Rapid Commun Mass Spectrom 17:2310–2316.
113. Geer LY, Markey SP, Kowalak JA, Wagner L, Xu M, Maynard DM, Yang X, Shi W, Bryant SH. (2004) Open mass spectrometry search algorithm. J Proteome Res 3:958–964.
114. Eng JK, Jahan TA, Hoopmann MR. (2013) Comet: An open-source MS/MS sequence database search tool. Proteomics 13:22–24.
115. Keller A, Nesvizhskii AI, Kolker E, Aebersold R. (2002) Empirical statistical model to estimate the accuracy of peptide identifications made by MS/MS and database search. Anal Chem 74:5383–5392.
116. Severin J, Lizio M, Harshbarger J, Kawaji H, Daub CO, Hayashizaki Y, Bertin N, Forrest ARR. (2014) Interactive visualization and analysis of large-scale sequencing datasets using ZENBU. Nat Biotechnol 32:217–219.
117. Chen Z-L, Meng J-M, Cao Y, Yin J-L, Fang R-Q, Fan S-B, Liu C, Zeng W-F, Ding Y-H, Tan D, Wu L, Zhou W-J, Chi H, Sun R-X, Dong M-Q, He S-M. (2019) A high-speed search engine pLink 2 with systematic evaluation for proteome-scale identification of cross-linked peptides. Nat Commun 10:3404.
118. Llopis-Hernández V, Cantini M, González-García C, Cheng ZA, Yang J, Tsimbouri PM, García AJ, Dalby MJ, Salmerón-Sánchez M. (2016) Material-driven fibronectin assembly for high-efficiency presentation of growth factors. Sci Adv 2:1–10.
119. Hsiao C-T, Cheng H-W, Huang C-M, Li H-R, Ou M-H, Huang J-R, Khoo K-H, Yu HW, Chen Y-Q, Wang Y-K, Chiou A, Kuo J-C. (2017) Fibronectin in cell adhesion and migration via N-glycosylation. Oncotarget 8:70653–70668.
120. Szczesny P, Lupas A. (2008) Domain annotation of trimeric autotransporter adhesins—daTAA. Bioinformatics 24:1251–1256.

121. Eicher SC, Dehio C. (2012) *Bartonella* entry mechanisms into mammalian host cells. Cell Microbiol 14:1166–1173.
122. Battisti JM, Sappington KN, Smitherman LS, Parrow NL, Minnick MF. (2006) Environmental signals generate a differential and coordinated expression of the heme receptor gene family of *Bartonella quintana*. Infect Immun 74:3251–3261.
123. Quebatte M, Dehio M, Tropel D, Basler A, Toller I, Raddatz G, Engel P, Huser S, Schein H, Lindroos HL, Andersson SGE, Dehio C. (2010) The BatR/BatS two-component regulatory system controls the adaptive response of *Bartonella henselae* during human endothelial cell infection. J Bacteriol 192:3352–3367.
124. Castelletti F, Donadelli R, Banterla F, Hildebrandt F, Zipfel PF, Bresin E, Otto E, Skerka C, Renieri A, Todeschini M, Caprioli J, Caruso RM, Artuso R, Remuzzi G, Noris M. (2008) Mutations in FN1 cause glomerulopathy with fibronectin deposits. Proc Natl Acad Sci U S A 105:2538–2543.
125. Valle J, Mabbett AN, Ulett GC, Toledo-Arana A, Wecker K, Totsika M, Schembri MA, Ghigo JM, Beloin C. (2008) UpaG, a new member of the trimeric autotransporter family of adhesins in uropathogenic *Escherichia coli*. J Bacteriol 190:4147–4161.
126. Tan TT, Nordström T, Forsgren A, Riesbeck K. (2005) The respiratory pathogen *Moraxella catarrhalis* adheres to epithelial cells by interacting with fibronectin through Ubiquitous Surface Proteins A1 and A2. J Infect Dis 192:1029–1038.
127. Heise T, Dersch P. (2006) Identification of a domain in *Yersinia* virulence factor YadA that is crucial for extracellular matrix-specific cell adhesion and uptake. Proc Natl Acad Sci 103:3375–3380.
128. Müller NF, Kaiser PO, Linke D, Schwarz H, Riess T, Schäfer A, Eble JA, Kempf VAJ. (2011) Trimeric autotransporter adhesin-dependent adherence of *Bartonella henselae*, *Bartonella quintana*, and *Yersinia enterocolitica* to matrix components and endothelial cells under static and dynamic flow conditions. Infect Immun 79:2544–2553.
129. Schwarz-Linek U, Werner JM, Pickford AR, Gurusiddappa S, Kim JH, Pilka ES, Briggs JAG, Gough TS, Höök M, Campbell ID, Potts JR. (2003) Pathogenic bacteria attach to human fibronectin through a tandem β-zipper. Nature 423:177–181.
130. Farfan MJ, Cantero L, Vidal R, Botkin DJ, Torres AG. (2011) Long polar fimbriae of enterohemorrhagic *Escherichia coli* O157:H7 bind to extracellular matrix proteins.

Infect Immun 79:3744–3750.

131. Kingsley RA, Keestra AM, De Zoete MR, Bäumler AJ. (2004) The ShdA adhesin binds to the cationic cradle of the fibronectin 13FnIII repeat module: evidence for molecular mimicry of heparin binding. Mol Microbiol 52:345–355.
132. Carpenter EP, Beis K, Cameron AD, Iwata S. (2008) Overcoming the challenges of membrane protein crystallography. Curr Opin Struct Biol 18:581–586.
133. Schweppe DK, Harding C, Chavez JD, Wu X, Ramage E, Singh PK, Manoil C, Bruce JE. (2015) Host-microbe protein interactions during bacterial infection. Chem Biol 22:1521–1530.
134. Happonen L, Hauri S, Svensson Birkedal G, Karlsson C, de Neergaard T, Khakzad H, Nordenfelt P, Wikström M, Wisniewska M, Björck L, Malmström L, Malmström J. (2019) A quantitative *Streptococcus pyogenes*–human protein–protein interaction map reveals localization of opsonizing antibodies. Nat Commun 10:2727.
135. Zybailov BL, Glazko G V, Jaiswal M, Raney KD. (2013) Large scale chemical cross-linking mass spectrometry perspectives. J Proteomics Bioinform 6:001.
136. Lenz S, Sinn LR, O'Reilly FJ, Fischer L, Wegner F, Rappsilber J. (2021) Reliable identification of protein-protein interactions by crosslinking mass spectrometry. Nat Commun 12:3564.
137. Thibau A, Vaca DJ, Bagowski M, Hipp K, Bender D, Ballhorn W, Linke D, Kempf VAJ. (2022) Adhesion of *Bartonella henselae* to fibronectin is mediated via repetitive motifs present in the stalk of *Bartonella* adhesin A. Microbiol Spectr 10:e0211722.
138. van Belkum A, Almeida C, Bardiaux B, Barrass S V., Butcher SJ, Çaykara T, Chowdhury S, Datar R, Eastwood I, Goldman A, Goyal M, Happonen L, Izadi-Pruneyre N, Jacobsen T, Johnson PH, Kempf VAJ, Kiessling A, Bueno JL, Malik A, Malmström J, Meuskens I, Milner PA, Nilges M, Pamme N, Peyman SA, Rodrigues LR, Rodriguez-Mateos P, Sande MG, Silva CJ, Stasiak AC, Stehle T, Thibau A, Vaca DJ, Linke D. (2021) Host-pathogen adhesion as the basis of innovative diagnostics for emerging pathogens. Diagnostics 11:1259.
139. Poole J, Day CJ, von Itzstein M, Paton JC, Jennings MP. (2018) Glycointeractions in bacterial pathogenesis. Nat Rev Microbiol 16:440–452.
140. Tram G, Poole J, Adams FG, Jennings MP, Eijkelkamp BA, Atack JM. (2021) The *Acinetobacter baumannii* autotransporter adhesin Ata recognizes host glycans as

high-affinity receptors. ACS Infect Dis 7:2352–2361.

141. Xie Y, Chen S, Li Q, Sheng Y, Alvarez MR, Reyes J, Xu G, Solakyildirim K, Lebrilla CB. (2021) Glycan–protein cross-linking mass spectrometry reveals sialic acid-mediated protein networks on cell surfaces. Chem Sci 12:8767–8777.
142. Valbuena G, Walker DH. (2006) The endothelium as a target for infections. Annu Rev Pathol Mech Dis 1:171–198.
143. Hammerschmidt S, Rohde M, Preissner KT. (2019) Extracellular matrix interactions with Gram-positive pathogens. Gram-Positive Pathog 108–124.
144. Ades EW, Candal FJ, Swerlick RA, George VG, Summers S, Bosse DC, Lawley TJ. (1992) HMEC-1: establishment of an immortalized human microvascular endothelial cell line. J Invest Dermatol 99:683–690.
145. Sottile J, Hocking DC. (2002) Fibronectin polymerization regulates the composition and stability of extracellular matrix fibrils and cell-matrix adhesions. Mol Biol Cell 13:3546–3559.
146. Kadler KE, Hill A, Canty-Laird EG. (2008) Collagen fibrillogenesis: fibronectin, integrins, and minor collagens as organizers and nucleators. Curr Opin Cell Biol 20:495–501.
147. Yurchenco PD, Patton BL. (2009) Developmental and pathogenic mechanisms of basement membrane assembly. Curr Pharm Des 15:1277–1294.
148. Antonara S, Ristow L, Coburn J. (2011) Adhesion mechanisms of *Borrelia burgdorferi*. The Prokaryotes 35–49.
149. Ebady R, Niddam AF, Boczula AE, Kim YR, Gupta N, Tang TT, Odisho T, Zhi H, Simmons CA, Skare JT, Moriarty TJ. (2016) Biomechanics of *Borrelia burgdorferi* vascular interactions. Cell Rep 16:2593–2604.
150. Lin Y-P, Tan X, Caine JA, Castellanos M, Chaconas G, Coburn J, Leong JM. (2020) Strain-specific joint invasion and colonization by Lyme disease spirochetes is promoted by outer surface protein C. PLOS Pathog 16:e1008516.
151. Coburn J, Garcia B, Hu LT, Jewett MW, Kraiczy P, Norris SJ, Skare J. (2021) Lyme disease pathogenesis. Curr Issues Mol Biol 42:473–518.
152. Weidensdorfer M, Ishikawa M, Hori K, Linke D, Djahanschiri B, Iruegas R, Ebersberger I, Riedel-Christ S, Enders G, Leukert L, Kraiczy P, Rothweiler F, Cinatl J, Berger J, Hipp K, Kempf VAJ, Göttig S. (2019) The *Acinetobacter* trimeric autotransporter adhesin Ata controls key virulence traits of *Acinetobacter baumannii*.

Virulence 10:68–81.

153. Obino D, Duménil G. (2019) The many faces of bacterium-endothelium interactions during systemic infections. Microbiol Spectr 7:69–81.
154. Ma Y, Sturrock A, Weis JJ. (1991) Intracellular localization of *Borrelia burgdorferi* within human endothelial cells. Infect Immun 59:671–678.
155. Yuste RA, Muenkel M, Axarlis K, Gómez Benito MJ, Reuss A, Blacker G, Tal MC, Kraiczy P, Bastounis EE. (2022) *Borrelia burgdorferi* modulates the physical forces and immunity signaling in endothelial cells. iScience 25:104793.
156. Krachler AM, Orth K. (2013) Targeting the bacteria-host interface: strategies in anti-adhesion therapy. Virulence 4:284–294.
157. Mühlen S, Dersch P. (2015) Anti-virulence strategies to target bacterial infections. Curr Top Microbiol Immunol 398:147–183.
158. Guo S, Zahiri H, Stevens C, Spaanderman DC, Milroy L-G, Ottmann C, Brunsveld L, Voets IK, Davies PL. (2021) Molecular basis for inhibition of adhesin-mediated bacterial-host interactions through a peptide-binding domain. Cell Rep 37:110002.
159. Jiang X, Abgottspon D, Kleeb S, Rabbani S, Scharenberg M, Wittwer M, Haug M, Schwardt O, Ernst B. (2012) Antiadhesion therapy for urinary tract infections—A balanced PK/PD profile proved to be key for success. J Med Chem 55:4700–4713.
160. Krachler AM, Ham H, Orth K. (2012) Turnabout is fair play: use of the bacterial Multivalent Adhesion Molecule 7 as an antimicrobial agent. Virulence 3:68–71.
161. Huebinger RM, Stones DH, de Souza Santos M, Carlson DL, Song J, Vaz DP, Keen E, Wolf SE, Orth K, Krachler AM. (2016) Targeting bacterial adherence inhibits multidrug-resistant *Pseudomonas aeruginosa* infection following burn injury. Sci Rep 6:39341.
162. Hawley CA, Watson CA, Orth K, Krachler AM. (2013) A MAM7 peptide-based inhibitor of *Staphylococcus aureus* adhesion does not interfere with *in vitro* host cell function. PLoS One 8:e81216.